

Philipps



Universität  
Marburg

# Regulation of peptidoglycan biosynthesis in *Hyphomonas neptunium*

Dissertation

zur Erlangung des Doktorgrades  
der Naturwissenschaften  
(Dr. rer. nat.)

dem

Fachbereich Biologie  
der Philipps-Universität Marburg

von

**Sabine Roskopf**

aus Rodgau

Marburg, August 2018

Die Untersuchungen zur vorliegenden Arbeit wurden von Juni 2015 bis Juni 2018 an der Philipps-Universität Marburg unter der Leitung von Professor Dr. Martin Thanbichler durchgeführt.

Vom Fachbereich Biologie der Philipps-Universität Marburg (HKZ: 1180)  
als Dissertation angenommen am 25.10.2018

Erstgutachter: Prof. Dr. Martin Thanbichler

Zweitgutachter: Prof. Dr. Peter Graumann

Tag der mündlichen Prüfung: 06.11.2018

Die während der Promotion erzielten Ergebnisse sind zum Teil in folgenden Originalpublikationen veröffentlicht:

Cserti, E., **Roskopf, S.**, Chang, Y. W., Eischeuer, S., Selter, L., Shi, J., Regh, C., Koert, U., Jensen, G. J., Thanbichler, M. (2017) Dynamics of the peptidoglycan biosynthetic machinery in the stalked budding bacterium *Hyphomonas neptunium*. Mol Microbiol **103**, 875-895

**Roskopf, S.**, Cserti, E., Thanbichler, M. Conserved mechanism of amidase activation in the budding  $\alpha$ -proteobacterium *Hyphomonas neptunium* (in Vorbereitung)



## Abstract

The spatial and temporal regulation of peptidoglycan biosynthesis and its role in cell morphology has been studied intensively in well-characterized model organisms such as *Escherichia coli*, *Bacillus subtilis*, and *Caulobacter crescentus*, which divide either by symmetric or asymmetric binary fission. To broaden our knowledge of the mechanisms governing bacterial morphogenesis, we started to investigate the dimorphic marine  $\alpha$ -proteobacterium *Hyphomonas neptunium* as a new model organism. This Gram-negative species is characterized by a unique mode of proliferation, whereby the new offspring is generated by the formation of a bud at the tip of a stalk that emanates from the mother cell body.

The main focus of our previous studies was the identification of cell wall biosynthetic enzymes and regulatory factors that are critically involved in stalk and bud biogenesis. These studies revealed that peptidoglycan biosynthesis in *H. neptunium* is a complex process mediated by an intricate interplay of various factors. Among the open questions, it is still unknown how the generation of the daughter cell is regulated and how the mother cell orchestrates the localization of peptidoglycan remodeling enzymes at specific site of action during the cell cycle. Consequently, that includes the initial localization of enzymes at the stalked pole. At a certain point, they have to diffuse through the stalk into the growing bud. There, they center at the junction between the bud and the stalk to separate the mother cell from the bud.

The main goal of the present study our current research is a deeper and more thorough characterization of previously investigated peptidoglycan remodeling enzymes, and especially the lytic enzymes, that cleave the peptidoglycan mesh. We particularly focused on two classes, the M23 metallopeptidases and the amidases. In doing so, we comprehensively analyzed the six M23 endopeptidases of *H. neptunium* with localization studies and genetic approaches. Our results revealed a high degree of redundancy among these enzymes, which combined with the absence of a distinct localization pattern, indicated a generalized role in cell wall maintenance. We also investigated the role of the only amidase in *H. neptunium* in cell separation and bud formation. A deletion of the amidase gene led to an aberrant morphology and a mild chaining phenotype. Importantly, we showed that one of the M23 endopeptidases (LmdE) acts as a regulator of AmiC. Using biochemical approaches, we proved an interaction between AmiC and LmdE, where LmdE stimulates the catalytic activity of AmiC and thus regulates peptidoglycan hydrolysis. A further crucial player in this system is the inner membrane-embedded FtsEX complex. A deletion of the whole complex resulted in cells with very elongated and misshapen stalks. Probably, FtsEX plays a role in the regulation of amidase activity by interacting with LmdE. These results are similar between  $\alpha$ - and  $\gamma$ -proteobacteria indicating that the mechanism of amidase regulation is conserved.

A further goal of our work was the identification of novel factors that are specifically involved in the regulation of budding in *H. neptunium*. To this end, we started to establish a transposon mutagenesis system to identify all essential genes in this species. In the future, we will be able to investigate these novel factors and their contribution to cell morphology.

Taken together, these results provide insight into the mechanisms of morphogenesis in stalked budding bacteria, thus setting the stage for an in-depth analysis of the regulatory

mechanisms that control the spatiotemporal dynamics of the peptidoglycan biosynthetic machinery in these organisms.

## Zusammenfassung

Die räumliche und zeitliche Regulation der Peptidoglycan-Biosynthese und ihre Rolle für die Zellmorphologie wurde bisher nur in wenigen gut charakterisierten Modellorganismen, wie *Escherichia coli*, *Bacillus subtilis* und *Caulobacter crescentus* untersucht. Diese Bakterien teilen sich entweder durch symmetrische oder asymmetrische Zweiteilung. Um unsere Kenntnisse über die Mechanismen der bakteriellen Morphogenese zu erweitern, haben wir begonnen das dimorphe marine  $\alpha$ -Proteobakterium *Hyphomonas neptunium* zu analysieren und als neuen Modellorganismus zu etablieren. Diese Gram-negative Spezies zeigt ein einzigartiges Vermehrungsverfahren, bei dem eine neue Tochterzelle an der Spitze eines Stiels gebildet wird, der aus dem Zellkörper der Mutterzelle wächst.

In vorausgegangen Studien lag unser Hauptfokus auf der Identifikation von Zellwand-synthetisierenden Enzymen und regulatorischen Faktoren, die in die Stiel- und Tochterzellbiogenese involviert sind. Diese Untersuchungen zeigten, dass die Peptidoglycan-Biosynthese von *H. neptunium* einen komplexen Prozess darstellt, der das Zusammenspiel vieler verschiedener Faktoren erfordert. Wie die Entstehung der Tochterzelle im Detail funktioniert oder Peptidoglycan remodelierende Enzyme während des Zellzyklus lokalisiert werden, ist bisher noch nicht bekannt. Zu Beginn der Proliferation werden sie am gestielten Pol, später aber in der Tochterzelle benötigt.

Das Hauptziel der vorliegenden Arbeit ist die detaillierte Charakterisierung schon bekannter Peptidoglycan-Biosyntheseenzyme. Dies involviert vor allem eine genauere Analyse der hydrolytischen Enzyme, die Peptidoglycan spalten. Wir betrachten hier zwei Klassen von Hydrolasen im Detail, die M23-Endopeptidasen und die Amidasen. Sechs M23-Endopeptidasen werden im Genom von *H. neptunium* codiert. In Lokalisations- und Deletionsstudien haben wir sie umfassend analysiert und konnten eine hohe Redundanz der Enzyme zeigen. Sie weisen eine diffuse Verteilung im ganzen Zellkörper auf, was auf eine Funktion bei der Erhaltung der Zellform nahelegt. Weiterhin untersuchten wir die Rolle der einzigen Amidase (AmiC) auf die Zellseparierung und Tochterzellbildung. Eine Deletion des Amidase-Genes *amiC* veränderte die Morphologie und führte zu einem leicht kettenartigen Phänotyp. Wir konnten zeigen, dass eine der M23-Endopeptidasen (LmdE) als Regulator der Amidase AmiC fungiert. In biochemischen Untersuchungen bewiesen wir eine Bindung und Interaktion von LmdE mit AmiC. LmdE stimuliert die katalytische Aktivität von AmiC und reguliert daher die Peptidoglycan-Hydrolyse. Eine weitere wichtige Komponente in diesem System ist der membranintegrale FtsEX-Komplex. Die Deletion des gesamten Komplexes resultierte in Zellen mit sehr langen und deformierten Stielen. FtsEX spielt wahrscheinlich eine Rolle in der Amidaseregulation, indem es mit LmdE interagiert. Diese Resultate sind ähnlich zwischen  $\gamma$ - und knospenden  $\alpha$ -Proteobakterien und deuten auf einen konservierten Mechanismus der Amidaseaktivierung hin.

Ein weiteres wichtiges Ziel unserer Arbeit war die Identifikation von neuen Faktoren, die in die Regulierung der Teilung von *H. neptunium* involviert sind. Daher haben wir angefangen, ein Transposon-Mutagenesesystem zu etablieren, mit dem alle essentiellen Gene identifiziert werden können. Zukünftig werden wir in der Lage sein, unbekannte Faktoren zu untersuchen und ihren Beitrag zur Morphogenese zu beleuchten.

Zusammen genommen zeigen diese Resultate tiefen Einblicke in die Mechanismen der Morphogenese in gestielten knospenden Bakterien. Sie stellen eine Plattform bereit für eine

eingehende Analyse der regulatorischen Mechanismen, die der räumlichen und zeitlichen Dynamiken der Peptidoglycan-Biosynthese zu Grunde liegen.



## Abbreviations

APS	ammonium persulfate
ASM	Artificial Salt Medium
BLI	bio-layer interferometry
bp	base pair(s)
BSA	bovine serum albumin
Co-IP	Co-immunoprecipitation
CV	column volume
DAP	diaminopimelic acid
DAPI	4',6-diamidino-2-phenylindole
DIC	differential interference contrast
DMSO	dimethyl sulfoxide
DNA	deoxyribonucleic acid
dNTPs	deoxyribonucleoside triphosphate
EDTA	ethylenediaminetetraacetic acid
ddH <sub>2</sub> O	double de-ionized water
GlcNAc	N-acetylglucosamine
GTase	glycosyltransferase
h	hour
HADA	7-hydroxycoumarin-3-carboxylic acid-amino-D-alanine
His <sub>6</sub>	hexahistidine
IPTG	isopropyl- $\beta$ -D-thiogalactopyranoside
kDa	kilo Dalton
Kan	Kanamycin
Lmds	LytM domain-containing proteins
LPP	lipoprotein
LPS	lipopolysaccharide
MB	marine broth
min	minute
MurNAc	N-acetylmuramic acid
OD <sub>600</sub>	optical density at 600 nm
PBP	penicillin-binding protein
PG	peptidoglycan
PMSF	phenylmethanesulfonyl fluoride
Rif	Rifampicin
rpm	revolutions per minute
RT	room temperature
SAP	shrimp alkaline phosphatase
SDS	sodium dodecyl sulfate
sec	second
SUMO	small ubiquitin-related modifier
TBST	phosphate-buffered saline with Tween 20
TEMED	N, N, N', N'-tetramethylethylenediamine
TFA	trifluoroacetic
TGase	transglycosylase

## Abbreviations

---

TPase	transpeptidase
Tris-HCl	Tris(hydroxymethyl)aminomethane hydrochloride
v/v	volume per volume
w/v	weight per volume
WT	wild type
x g	multiple of acceleration of gravity

## Table of Contents

Abstract.....	V
Zusammenfassung.....	VII
Abbreviations.....	IX
Table of Contents.....	XI
1. Introduction.....	1
1.1 The bacterial envelope .....	1
1.2 Structure and biosynthesis of peptidoglycan.....	1
1.2.1 PG synthases .....	5
1.3 PG lytic enzymes and their regulators.....	6
1.3.1 Endopeptidases.....	6
1.3.2 Amidases.....	7
1.3.3 Carboxypeptidases .....	9
1.4 Cell growth and division .....	9
1.5 Alternative growth modes in bacteria .....	11
1.6 <i>Hyphomonas neptunium</i> as a model organism for stalked budding bacteria .....	13
1.7 PG biosynthesis and growth of <i>H. neptunium</i> .....	15
1.8 Aim of study.....	16
2. Results .....	18
2.1 PG remodeling enzymes.....	18
2.1.1 M23 endopeptidases of <i>H. neptunium</i> .....	18
2.1.2 Analysis of their localization.....	21
2.1.3 The single amidase of <i>H. neptunium</i> .....	23
2.1.4 AmiC is a periplasmic amidase .....	25
2.1.5 The connection between AmiC and the M23 endopeptidases.....	26
2.1.6 AmiC-mCherry localization in the $\Delta$ <i>lmdE</i> mutant.....	28
2.2 The FtsEX complex of <i>H. neptunium</i> .....	29
2.2.1 AmiC-mCherry localization in the $\Delta$ <i>ftsEX</i> mutant .....	31
2.3 Protein purification and in vitro assays.....	32
2.3.1 The role of LmdE in AmiC activation.....	33
2.3.2 LmdA is an active endopeptidase .....	36
2.3.3 AmiC and LmdE physically interact.....	36
2.4 Carboxypeptidases of <i>H. neptunium</i> .....	40

2.4.1	Deletion studies of the three carboxypeptidases .....	40
2.4.2	The localization of Dacl.....	41
2.5	Transposon mutagenesis in <i>H. neptunium</i> .....	42
3.	Discussion.....	46
3.1	Role of PG remodeling enzymes.....	46
3.2	Mode of amidase activation.....	48
3.3	Function of the FtsEX complex.....	51
3.4	Identification of essential genes and novel factors.....	51
3.5	Concluding remarks and future perspectives.....	52
4.	Material and Methods.....	54
4.1	Materials .....	54
4.1.1	Chemicals and enzymes .....	54
4.1.2	Media .....	54
4.1.3	Buffer and solutions .....	56
4.1.4	Kits.....	56
4.1.5	Oligonucleotides and plasmids.....	56
4.2	Microbiological and cell biological methods .....	56
4.2.1	Cultivation of <i>E. coli</i> .....	56
4.2.2	Cultivation of <i>H. neptunium</i> .....	56
4.2.3	Storage of bacteria.....	57
4.2.4	Determination of cell density .....	57
4.2.5	Growth curves.....	57
4.2.6	Biofilm assay.....	57
4.2.7	Preparation of competent <i>E. coli</i> cells .....	57
4.2.8	Transformation of competent cells.....	58
4.2.9	Conjugation of <i>H. neptunium</i> .....	58
4.3	Microscopic methods.....	59
4.3.1	Nucleoid staining.....	59
4.3.2	Visualization of nascent peptidoglycan .....	59
4.4	Molecular biology methods.....	60
4.4.1	Isolation of bacterial DNA.....	60
4.4.2	Polymerase chain reaction (PCR) .....	60
4.4.3	Colony PCR .....	60
4.4.4	Determination of the quality and purity of DNA .....	61

---

4.4.5	Agarose gel electrophoresis .....	61
4.4.6	Restriction and ligation of DNA fragments and Gibson assembly.....	62
4.4.7	Isolation of plasmid DNA and sequencing.....	63
4.4.8	Generation of markerless deletions and insertion in <i>H. neptunium</i> .....	63
4.4.9	Construction of plasmids .....	63
4.5	Biochemical methods.....	66
4.5.1	SDS polyacrylamide gel electrophoresis (SDS-PAGE) .....	66
4.5.2	Immunoblot analysis .....	67
4.5.3	Protein fractionation.....	67
4.5.4	Co-immunoprecipitation and mass-spectroscopy.....	68
4.5.5	Protein purification .....	69
4.5.6	Dye-release assay for PG hydrolysis .....	70
4.5.7	Bio-layer interferometry (BLI).....	70
4.6	Transposon mutagenesis in <i>H. neptunium</i> .....	71
4.7	Bioinformatic methods .....	72
5.	Appendix.....	73
5.1	Supplement figures.....	73
5.2	Supplemental tables .....	78
6.	References .....	86
	Acknowledgements.....	98
	Curriculum Vitae.....	99
	Einverständniserklärung.....	100



# 1. INTRODUCTION

## 1.1 The bacterial envelope

The bacterial envelope is crucial for cell shape maintenance, withstanding the turgor pressure, and cell division. The cell wall has to expand but also be cleaved to separate the daughter cell. The structure of the cell envelope of a typical Gram-negative bacterium is the following: outer membrane, periplasm with peptidoglycan (PG), and inner membrane (cytoplasmic membrane) (Silhavy *et al.*, 2010). The latter is built of a lipid bilayer with phospholipids. The outer membrane is a special feature of Gram-negative bacteria and represents an asymmetric lipid bilayer. Its outer layer consists of lipopolysaccharides (LPS) and the inner layer of phospholipids (Kamio & Nikaido, 1976). The LPS is composed of Lipid A, core oligosaccharide and the O-antigen (Kamio & Nikaido, 1976). It is responsible for the immune response in host cells and the causative agent of septic shock (Miller *et al.*, 2005). Its location at the cell surface and its physicochemical properties make LPS primarily responsible for the barrier function of the outer membrane, which is crucial for the survival of many Gram-negative bacteria in different environments (Ruiz *et al.*, 2009). This barrier is the reason why it has been so difficult to develop antibiotics against these organisms (Delcour, 2009).

## 1.2 Structure and biosynthesis of peptidoglycan

PG (also called murein) plays a fundamental role for the structure of the cell envelope and is located in the periplasm. The PG sacculus can be isolated as a whole net-like heteropolymer and observed by light microscopy (Silhavy *et al.*, 2010). The rigidity and stiffness of PG is responsible for the cell shape of bacteria. Without it, they would lose their characteristic form and become spheroplasts (Silhavy *et al.*, 2010). Gram-negative bacteria have a relatively thin PG layer, whereas Gram-positive bacteria have a thick layer up to 100 nm (Silhavy *et al.*, 2010). Gram-positive bacteria do not possess an outer membrane, and their PG is anchored to the cytoplasmic membrane via lipoteichoic acids (Neuhaus & Baddiley, 2003). The PG of Gram-negative bacteria is anchored to the outer membrane by lipoproteins, also called Braun's lipoproteins (Lpp), which are important for the stability of the cell envelope. In detail, they are attached to the outer membrane by their N-terminal lipid residue and are among the most abundant proteins in the  $\gamma$ -proteobacterium *Escherichia coli* (Braun & Wolff, 1970).

Pores (porines) exist in the outer membrane, which let pass globular proteins with a molecular size of up to 24 kDa, but once the PG net is expanded in living cells, proteins up to 100 kDa may also pass through the structure (Demchick & Koch, 1996; Vazquez-Laslop *et al.*, 2001).

PG is composed of long glycan strands with alternating N-acetylglucosamine (GlnNAc) and N-acetylmuramic acid (MurNAc) moieties (Figure 1), connected via  $\beta$ -1,4-glycosidic bonds

and further cross-linked by their peptide side chains (Schleifer & Kandler, 1972). These peptides side are connected to MurNAc by an amide bond and they contain D-amino acids beside the normal L-amino acids. Their biosynthesis occurs as a pentapeptide with the typical structure of L-alanine–D-glutamic acid–*meso*-diaminopimelic acid (m-DAP)–D-alanine–D-alanine (Figure 1A) (Vollmer & Bertsche, 2008). Isolated PG of some species only shows a small amount of pentapeptides because they are degraded to tetra-, tri- or dipeptides. The chemical structure of the murein subunits is similar in the majority of Gram-negative and some Gram-positive bacteria, while most Gram-positive bacteria have L-lysine instead of m-DAP in their peptide stem (Figure 1B) (Schleifer & Kandler, 1972). Moreover, the chains of Gram-positive bacteria are connected by an interpeptide bridge made of glycine residues that varies in length (Royet & Dziarski, 2007).

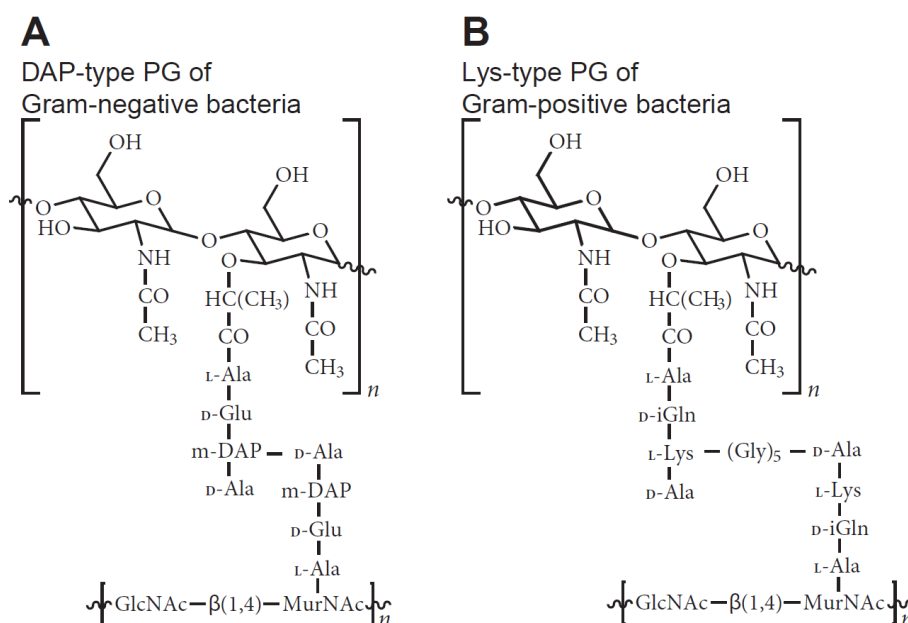


**Figure 1: Structure of PG subunits. (A)** Structure of DAP-type PG of Gram-negative bacteria with the characteristic m-DAP at the third amino acid. **(B)** Structure of Lys-type PG of Gram-positive bacteria with the characteristic L-Lys at the third amino acid and the interpeptide bridge. Areas marked with [ ] show the glycan strands, which are connected via β-1,4-glycosidic bonds. They are cross-linked by peptide side chains. Abbreviations: GlcNAc: N-acetylglucosamine; MurNAc: N-acetylmuramic acid; Ala: alanine; Glu: glutamic acid, m-DAP: *meso*-diaminopimelic acid; iGln: isoglutamine; Lys: lysine. Adapted from Royet and Dziarski (2007).

The cross-linked peptides are mainly responsible for the net-like structure of PG. In *E. coli* and other Gram-negative bacteria they can amount up to 40 – 60% of all peptides depending on the growth conditions (Glauner *et al.*, 1988; Quintela *et al.*, 1995). The majority of the cross-links belong to the DD-type, which is the connection between the carboxyl group of D-alanine (position 4) of one peptide and the amino group of m-DAP (position 3) of another peptide (Figure 1A) (Glauner *et al.*, 1988). In fewer cases, cross-links of the LD-type exist where m-DAP residues of two peptides are connected by L,D-transpeptidases (LDTs) (Vollmer & Bertsche, 2008). Analyses of the composition of PG clearly revealed a heterogeneous structure, since it consists of more than 50 different types of subunits, which differ in length (di-, tri-, tetra- and pentapeptides), in the type of cross-linkage (DD or LD) and the presence of D-alanine or glycine at position 4 or 5 (Glauner *et al.*, 1988).



PG biosynthesis takes place in two different cellular compartments. The precursor molecules (lipid I and lipid II) are synthesized in the cytoplasm and flipped across to the cytoplasmic membrane to the periplasm, where the extension of the PG polymer takes place (Figure 2) (Vollmer & Bertsche, 2008). Amino sugars are the key intermediates of the precursor molecules, since they are converted to GlcNAc and attached to uridine diphosphate (UDP) to produce UDP-GlcNAc. In a further step, UDP-GlcNAc is transformed into UDP-MurNAc. This reaction is catalyzed by MurA and MurB using phosphoenolpyruvate and NADPH. The peptide side chains are successively elongated by the addition of L-alanine, D-glutamic acid, m-DAP and the dipeptide D-alanine–D-alanine. This process is catalyzed by ATP-dependent ligases (MurCDEF and DdlA; Figure 2). The extraordinary D-amino acids are synthesized by racemases from L-amino acid precursors (Alr, DadX and Murl; Figure 2) (Vollmer & Bertsche, 2008). The resulting UDP-MurNAc subunit is attached to bactoprenyl-P (undecaprenyl-P) by the enzyme MraY, generating lipid I. The addition of UDP-GlcNAc to lipid I by a transferase (MurG) then leads to the generation of lipid II (van Heijenoort, 2001). Afterwards, lipid II is flipped across the cytoplasmic membrane. Previously, studies have shown and suspected that integral membrane proteins of the SEDS (shape, elongation, division, and sporulation) family, namely FtsW and RodA, are the flippases of the PG precursor in *E. coli* (Ikeda *et al.*, 1989; Mohammadi *et al.*, 2011). However, additional work revealed that the polytopic membrane protein MurJ is actually required for lipid II transport (Ruiz, 2008; Sham *et al.*, 2014). This was again called into question by a recent study, in which the interaction of MurJ with lipid II could not be observed, whereas a connection between FtsW, PBP1B and lipid II was clearly shown (Leclercq *et al.*, 2017). In the Gram-positive *Bacillus subtilis*, MurJ and the novel flippase Amj were shown to flip lipid II (Meeske *et al.*, 2015).

The extension of the PG sacculus net takes place at the periplasmic site of the cytoplasmic membrane, where lipid II is polymerized and the new glycan strands are integrated into the PG meshwork. This process involves glycosyltransferases (GTases) that polymerize the glycan strands and transpeptidases (TPases) that cross-link the peptides (Figure 2) (Typas *et al.*, 2012). Lipid II functions as a substrate for GTases to elongate the glycan strands. The new glycosidic bond is made between the C1 of the incorporated MurNAc and the C4 of the GlcNAc of Lipid II (van Heijenoort, 2001; Ward & Perkins, 1973). Additionally, the D-alanine (position 4) of the donor peptide is connected to m-DAP of the acceptor peptide (position 3) in the TPase reaction. The energy for this reaction is gained by the cleavage of the D-ala–D-ala bond of the pentapeptide, that functions as a donor (Terrak *et al.*, 1999).

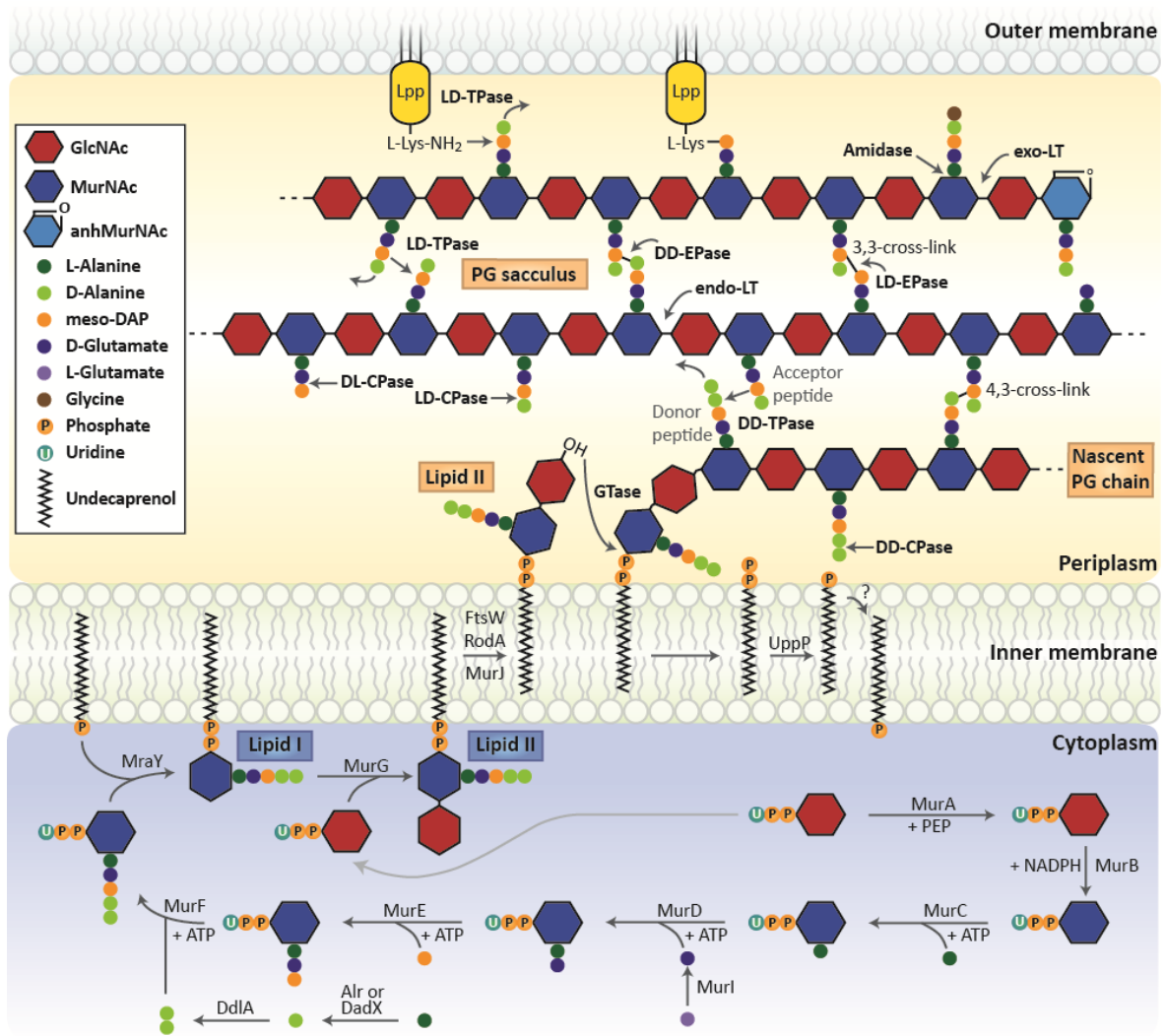


**Figure 2: Structure and biosynthesis of the peptidoglycan with its remodeling enzymes in *E. coli*.** Shown is the synthesis and attachment of new PG subunits into the existing PG meshwork. All known synthetic and hydrolytic enzymes are indicated. The PG precursor lipid I and lipid II is synthesized in the cytoplasm and linked to undecaprenol before being flipped into the periplasm. FtsW, RodA or MurJ might function as a flippase. The polymerization of the glycan chain is catalyzed by glycosyltransferases (GTase), whilst transpeptidases (TPase) cross-link the stem peptide by a 4,3-crosslink to the established PG layer. LD-transpeptidases catalyze the formation of 3,3-crosslinks between stem peptides and attach the PG strands to Lpp, which anchors the PG meshwork to the outer membrane. The stem peptides are clipped by DD-, LD-, and DL-carboxypeptidases (CPases), and cross-links are cleaved by DD- and LD-endopeptidases (EPases). Amidases remove the complete stem peptide from the MurNAc. The glycan backbone is cleaved by *exo*- or *endo*-specific lytic transglycosylases (LTs), generating 1,6-anhydro-N-acetylmuramic acid (anhMurNAc) residues at the terminal end of PG strands. Abbreviations: Alr, Ala racemase, biosynthetic; DadX, Ala racemase, catabolic; DdIA, D-ala-D-ala ligase A; GlcNAc: N-acetylglucosamine; MurNAc: N-acetylmuramic acid; meso-DAP: *meso*-diaminopimelic acid; MraY: UDP-MurNAc-pentapeptide phosphotransferase; MurA: UDP-GlcNAc enolpyruvyl transferase; MurB: UDP-MurNAc dehydrogenase; MurC: UDP-MurNAc-L-Ala ligase; MurD: UDP-MurNAc-L-Ala-D-Glu ligase; MurE: UDP-MurNAc-L-Ala-D-Glu-meso-DAP ligase; MurF: UDP-MurNAc-tripeptide-D-alanyl-D-ala ligase; MurG: UDP-GlcNAc-undecaprenoyl-pyrophosphoryl-MurNAc-pentapeptide transferase; MurI: Glu racemase; NADPH: nicotinamide adenine di-nucleotide phosphate; PEP: phosphoenolpyruvate. Adapted from Typas *et al.* (2012) and Cserti (2016).

### 1.2.1 PG synthases

The enlargement of the PG sacculus through incorporation of lipid II is catalyzed by PG synthases. Proteins with transpeptidase activity that can covalently bind penicillin are called penicillin-binding proteins (PBP) (Suginaka *et al.*, 1972). However, not all PBPs are synthases, e.g. PBP5 (see 1.3.3.). PBPs are classified into three types: bifunctional GTases-TPases (class A PBPs), monofunctional TPases (class B PBPs) and monofunctional GTases (Vollmer & Bertsche, 2008). Many known periplasmic PG synthases of *E. coli* are anchored to the cytoplasmic membrane by a short hydrophobic N-terminal transmembrane region, with their catalytic domains placed in the periplasm (Vollmer & Bertsche, 2008).

Two bifunctional PBPs (PBP1A and PBP1B) are mainly responsible for PG biosynthesis in *E. coli*, with the first one responsible for cell elongation and the second one for cell division. Lipoproteins (Lpo) that are anchored to the outer membrane and reach through the PG sacculus regulate the bifunctional PBPs. Established examples in *E. coli* are the activation of PBP1B by LpoA, and the activation of PBP1B by LpoB (Paradis-Bleau *et al.*, 2010; Typas *et al.*, 2010). Recently, the structure of LpoB was solved and revealed an N-terminal long flexible stretch that can reach throughout the periplasm and bind with its globular domain to PBP1B (Egan *et al.*, 2014). Lately, it was shown that this mode of cell wall synthase regulation is conserved in *Pseudomonas aeruginosa*, where LpoP controls PBP1B (Greene *et al.*, 2018). The third class A PBP of *E. coli* is PBP1C, whose cellular role is still unclear (Typas *et al.*, 2012). For the monofunctional TPases, two proteins are well-known and widely conserved: PBP2, which is essential for cell elongation and exhibits MreB-dependent localization, and PBP3 (FtsI), which is needed for cell division and therefore is part of the divisome (de Pedro *et al.*, 1997; Spratt, 1975; Typas *et al.*, 2012; Weiss *et al.*, 1999). MgtA functions as an additional PG synthase in *E. coli*, which localizes to the division plane and interacts with other cell division proteins, exhibiting GTase activity (Derouaux *et al.*, 2008).

In addition to the already mentioned function of the SEDS proteins FtsW and RodA in lipid II flipping, they might also possess transglycosylase activity (Cho *et al.*, 2016; Meeske *et al.*, 2016). The integral membrane protein RodA showed circumferential motion together with PBP2 in *E. coli*, showing that class A PBPs were not essential for glycan polymerization by the cell elongation machinery (Cho *et al.*, 2016). In *B. subtilis*, RodA and FtsW were identified as transglycosylases that could polymerize lipid II *in vitro* (Meeske *et al.*, 2016). Both studies revealed that SEDS family proteins are more important than previously thought and crucial for cell wall synthesis.

*C. crescentus* possesses five bifunctional PBPs, which are important for the complex cell shape of this bacterium (Strobel *et al.*, 2014; Yakhnina & Gitai, 2013). Only one of these enzymes (PbpX) is crucial for growth and normal cell morphology, while the inactivation of all five was lethal (Strobel *et al.*, 2014). Homologs of PBP2 and PBP3 were also identified and localized in *C. crescentus*. Both proteins showed an accumulation at the new cell pole at the start of the cell cycle and a signal at the division plane after the onset of constriction (Costa *et al.*, 2008; Figge *et al.*, 2004; Hocking *et al.*, 2012).

Three bifunctional PBPs (PBP1A, PBP1X and PBP1C), two monofunctional TPases (PBP2 and PBP3) and one monofunctional GTase (MgtA) exist and were identified in the budding  $\alpha$ -proteobacterium *Hyphomonas neptunium* (Cserti *et al.*, 2017). Furthermore, two L,D-

transpeptidases (LdtA and LdtB) that make 3,3-crosslinks in PG were identified (Cserti *et al.*, 2017; Magnet *et al.*, 2008). All PG synthases were analyzed in more detail, showing that PBP1A, PBP2 and PBP3 are essential for viability. In addition, PBP2 and other elongation-specific components are responsible for the elongation of *H. neptunium* (Cserti *et al.*, 2017). The role of MtgA might be redundant because a deletion had no phenotypic effect. In certain species, LDTs play an important role by cross-linking the peptide chains and they are part of the PG biosynthetic machinery. For example, previous studies have suggested that they critically contribute to cell elongation in a member of the Rhizobiales (*Agrobacterium tumefaciens*) by mediating the typical polar growth of this species (Brown *et al.*, 2012; Cameron *et al.*, 2014; Grangeon *et al.*, 2015). The LDTs of *A. tumefaciens* localize at the tip of the nascent daughter cell and produce the 3,3-crosslinks in PG (Cameron *et al.*, 2014; Grangeon *et al.*, 2015). However, the *ldt* genes of *H. neptunium* were deleted without any morphological effect (Cserti *et al.*, 2017). Thus, these synthetic LDTs are apparently dispensable for PG biosynthesis and growth of *H. neptunium*.

## 1.3 PG lytic enzymes and their regulators

PG hydrolysis is accomplished by PG lytic enzymes that cleave the covalent bonds in the PG macromolecule and produce small soluble fragments (Höltje, 1995). Cleavage of PG is necessary to gain space for the insertion of new material. In general, all PG lytic enzymes have to be strictly controlled as they can destroy the integrity of the PG meshwork. A close functional cooperation between PG synthases and hydrolases building multi enzyme complexes has been postulated (Höltje, 1998). This would ensure a coordination of the different activities, but still needs to be proven. Bacteria possess a huge variety of different lytic enzymes (three classes of them are explained in more detail in the following section 1.3.1. to 1.3.3). One class are the lytic transglycosylases (LTs), which cleave the  $\beta$ -1,4-glycosidic bonds between MurNAc and GlnNAc, thereby producing 1,6-anhydro-N-acetylmuramic acid (Figure 2) (Höltje *et al.*, 1975). Until now, seven LTs were discovered in *E. coli*. Six are membrane-bound, whereas the seventh is soluble in the periplasm (Höltje, 1998).

### 1.3.1 Endopeptidases

A separate class are the endopeptidases (EPases), which cleave the bonds between the peptide side chains and therefore separate the glycan strands (Vollmer & Bertsche, 2008). They can be subdivided according to the type of cleavage site into DD-endopeptidases (cleavage between D-amino acids) and LD-endopeptidases (cleavage between L- and D-amino acids/m-DAP) (Smith *et al.*, 2000). The endopeptidases that possess characteristic lysostaphin-like metalloproteases (LytM factors) are grouped into the family of M23 zinc-metalloproteases (Firczuk & Bochtler, 2007). These proteins are homologs of lysostaphin, a well-characterized zinc-metalloprotease that cleaves the unique pentaglycine cross-links found in the PG of *Staphylococcus aureus* (Browder *et al.*, 1965). They are generally found in bacteriophages, Gram-positive and Gram-negative bacteria (Ercoli *et al.*, 2015). The catalytic domain of LytM factors includes the typical M23 metalloprotease metal binding site with two conserved motifs, HxxxD and HxH, to complex the zinc ion ( $Zn^{2+}$ ) (Bochtler *et al.*,

2004). *E. coli* harbors two DD-endopeptidases (PBP4 or PBP7), which are also termed as low-molecular weight PBPs, and several others (Spr, YdhO and YebA) (Kishida *et al.*, 2006; Singh *et al.*, 2012; Singh *et al.*, 2015; Vollmer & Bertsche, 2008). In the human pathogen *Helicobacter pylori*, three endopeptidase homologs are required for the helical cell shape (Sycuro *et al.*, 2010). Their deletion led to an increase in PG cross-linking (Sycuro *et al.*, 2010). A second human pathogen, *Haemophilus influenzae*, also possesses three endopeptidase homologs (YebA, EnvC and NlpD), which are crucial for outer membrane composition and cell separation (Ercoli *et al.*, 2015). However, only YebA seems to be an active enzyme that can cleave PG (Ercoli *et al.*, 2015).

### 1.3.2 Amidases

Another important group of PG hydrolases are the amidases, which cleave the bond between the glycan strands and the peptides chains (Figure 2). Five amidases (AmiA, AmiB, AmiC, AmiD and AmpD) have been found and analyzed in *E. coli* (Bernhardt & de Boer, 2003; Heidrich *et al.*, 2001; Jacobs *et al.*, 1995; Uehara & Park, 2007). The soluble periplasmic proteins AmiA, AmiB and AmiC are crucial for cell separation at the division site and are characterized by a C-terminal Ami\_3 domain (Heidrich *et al.*, 2001; Korndörfer *et al.*, 2006). AmiC localizes to the division plane and participates in the separation of *E. coli* cells, whereas AmiA shows a diffuse distribution (Bernhardt & de Boer, 2003). AmiD is a lipoprotein anchored to the outer membrane that does not participate in cell separation (Uehara & Park, 2007). Finally, AmpD is a cytoplasmic enzyme that specifically cleaves the anhMurNAc-L-alanine bond of PG to recycle the cell wall components (Uehara & Park, 2007). The amidase homolog CwIM from *Mycobacterium tuberculosis* is also cytoplasmic and controls cell wall metabolism in response to starvation (Boutte *et al.*, 2016).

Regulatory proteins that influence the activity of the amidases have been discovered. They are endopeptidases of the family of M23 zinc-metallopeptidases (Firczuk & Bochtler, 2007). However, these M23 endopeptidases that activate the amidases of *E. coli* have been found to possess no catalytic activity because they miss specific catalytic amino acid residues in the conserved motif (Uehara *et al.*, 2009). Instead, the endopeptidase homolog NlpD regulates AmiC, whereas EnvC regulates AmiA and AmiB by stimulating their activity (Figure 3) (Uehara *et al.*, 2010; Yang *et al.*, 2012). EnvC possesses two coiled-coil domains, NlpD a LysM domain (Peters *et al.*, 2013; Uehara *et al.*, 2009). NlpD and EnvC localize earlier to the divisome than the amidases and require the activity of PBP3 (Peters *et al.*, 2011). They bind to their cognate amidase by an unknown mechanism and induce a conformational change that stimulates amidase activity. In detail, an inhibitory  $\alpha$ -helix that blocks the catalytic center under “off” conditions (Figure 3A), is released and PG cleavage occurs (Figure 3B) (Yang *et al.*, 2012).

In addition, an inner membrane-embedded complex was shown to be involved in this process through interaction with EnvC (Yang *et al.*, 2012). This complex consists of the cytoplasmic inner membrane attached FtsE (ATP-binding protein) and the inner membrane protein FtsX (ABC transporter permease) (de Leeuw *et al.*, 1999; Schmidt *et al.*, 2004). The complex shows characteristics of an ATP-binding cassette (ABC)-type transporter, but a transport of a substrate has never been proven (de Leeuw *et al.*, 1999). FtsE and FtsX are widely conserved among Gram-negative and Gram-positive bacteria (Arends *et al.*, 2009). The FtsEX complex is not essential, since *E. coli* cells can survive a deletion of *ftsEX* if high

salt medium is provided (Schmidt *et al.*, 2004; Yang *et al.*, 2011). In contrast, when FtsX or FtsEX were overproduced, cells showed filamentation that led to cell death (de Leeuw *et al.*, 1999). Both FtsE and FtsX localize to the division site and the localization of FtsX is dependent on FtsZ, FtsA, and ZipA, suggesting that the complex is directly involved in cell division (Schmidt *et al.*, 2004). Furthermore, FtsE and FtsZ interacted in coimmunoprecipitation experiments independent of FtsX (Corbin *et al.*, 2007). When FtsE was mutated in the ATP-binding site, Z-ring constriction and subsequent cell division was affected (Arends *et al.*, 2009). FtsEX interacts also with another cell division component, the actin-related FtsA, and regulates the assembly of the cell division machinery (Du *et al.*, 2016). The importance of the FtsEX complex was also shown in other bacteria such as *Streptococcus pneumoniae*, where FtsEX mediate PG hydrolysis by the hydrolase PcsB (Bajaj *et al.*, 2016; Bartual *et al.*, 2014; Sham *et al.*, 2011).

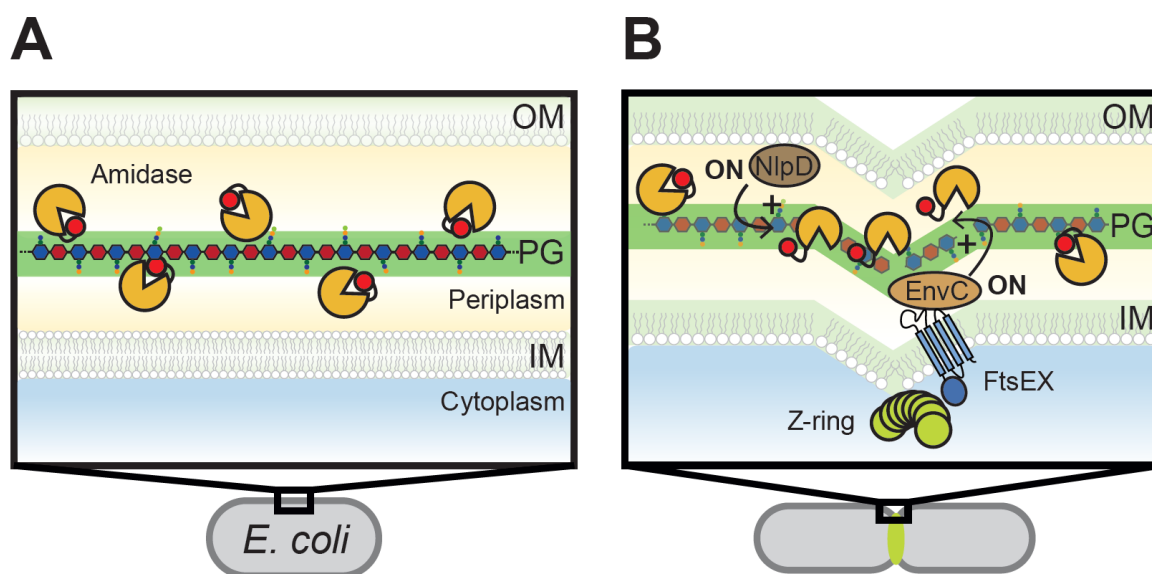


**Figure 3: Conformational control of amidase activity during the cell cycle in *E. coli*.** (A) Periplasmic amidases (light orange pac-men) are inhibited by their regulatory helix (dark red circles) at early stages in the cell cycle. (B) FtsEX and EnvC are recruited to the Z-ring early during the cell cycle. NlpD, AmiB and AmiC are recruited to the septal ring when constriction is initiated. Both amidase activators stimulate the activity of their cognate amidase via the release of the regulatory helix from their active site (Peters *et al.*, 2011). Abbreviations: OM: outer membrane; PG: peptidoglycan; IM: inner membrane. Adapted from Yang *et al.* (2012).

The current activation model implies that FtsE hydrolysis of ATP leads to a conformational change in FtsX. The membrane topology of FtsX was previously determined, showing four transmembrane segments and a relatively large periplasmic loop between segment 1 and 2 (Arends *et al.*, 2009). Subsequently, ATP hydrolysis could lead to a different fold of this loop domain resulting in an interaction with the coiled-coil domains of EnvC (Figure 3B). The latter might be activated, binding with its LytM domain to the amidase and consequently activates AmiA and AmiB (Peters *et al.*, 2013; Yang *et al.*, 2011).

A similar mechanism was found in *B. subtilis*, where the FtsEX complex is required for the activity of the endopeptidase CwIO (Meisner *et al.*, 2013). Mutants that cannot hydrolyze ATP any more were not able to stimulate CwIO (Meisner *et al.*, 2013). The pathogen *Vibrio cholerae* only possesses one amidase, AmiB, which has both an AMIN and LysM domains to bind to PG (Bateman & Bycroft, 2000; Möll *et al.*, 2014). Two catalytically inactive

endopeptidases (EnvC and NlpD) were discovered as redundant activators for AmiB and additionally showed interaction with FtsX (Möll *et al.*, 2014). Moreover, in the opportunistic pathogen *P. aeruginosa*, which also belongs to the  $\gamma$ -proteobacteria, the amidase AmiB and the three LytM proteins were investigated (Scheurwater *et al.*, 2007). They play an important role in cell separation, envelope integrity, and antibiotic resistance (Yakhnina *et al.*, 2015). The endopeptidase NlpD of the pathogen *Neisseria gonorrhoeae* can hydrolyze and bind PG but also potentiates the activity of AmiC (Stohl *et al.*, 2016). Even in the cyanobacterium *Anabaena* sp. PCC 7120, a LytM protein seems to control the activity of an AmiC-type cell wall hydrolase (AmiC1) (Bornikoel *et al.*, 2018). AmiC1 is needed to make nanopores in the septal wall to generate cell-cell junctions that facilitate the communication of adjacent cells (Berendt *et al.*, 2012). Apparently, the mechanism of amidase activation and regulation is more widely conserved than previously thought.

Recent work in *C. crescentus* revealed that only the deletion of *ftsE*, but not *ftsX*, was possible, resulting in cells with thin connections between their cell bodies (Meier *et al.*, 2017). Hence, the whole FtsEX complex seems to be important for cell constriction and separation (Meier *et al.*, 2017). In addition, and similarly to the *E. coli* model, two LytM factors (DipM and LdpF) with degenerate catalytic domains might act as regulatory hubs that, during cell constriction and fission regulate the activity of multiple autolytic enzymes (Zielińska *et al.*, 2017). Unlike in *E. coli*, only one amidase is present in *C. crescentus* and its activity is crucial for its localization (Dubey & Priyadarshini, 2018; Möll *et al.*, 2010).

### 1.3.3 Carboxypeptidases

The fourth class of PG lytic enzymes are the carboxypeptidases (CPases), which remove the last amino acid (mainly D-alanine) from the peptide side chains (Figure 2). They can be subdivided according to the type of cleavage site into DD-carboxypeptidases (cleavage between D-amino acids) and LD-carboxypeptidases (cleavage between L- and D-amino acids/m-DAP). Since CPases can also bind penicillin, they were named low-molecular weight PBPs (Tipper & Strominger, 1965). *E. coli* possesses at least four CPases such as PBP5 and PBP6 (Vollmer *et al.*, 2008). Recent studies showed that PBP6b of *E. coli* was more active at acidic pH, revealing that CPases might become important under varying environmental conditions (Peters *et al.*, 2016). PBP5 localized to the lateral cell wall and the division site and a deletion of *dacA* (PBP5) increased the frequency of branched cells (Potluri *et al.*, 2012). Three potential CPases were identified in *H. neptunium*. They show high redundancy since single deletions could be generated and their effect on growth and morphology was minimal (Cserti *et al.*, 2017).

## 1.4 Cell growth and division

The growth of a bacterial cell can be divided into two distinct stages: elongation and division. In both stages, the PG biosynthetic machinery has to be orchestrated and regulated in a precise way to ensure proper cell shape (Kysela *et al.*, 2016; Typas *et al.*, 2012). Multi-enzyme complexes perform the two synthetic processes: the elongasome and the divisome (Figure 4). The elongasome (also called Rod complex) synthesizes new PG along the lateral cell wall to drive cell elongation, while the divisome generates PG during cytokinesis

making the nascent cell poles (Mattei *et al.*, 2010). Most rod-shaped bacteria possess an elongasome that is controlled by the actin homolog MreB (Daniel & Errington, 2003; Jones *et al.*, 2001; van den Ent *et al.*, 2001). MreB is tethered to the inner leaflet of the cytoplasmic membrane, probably with the aid of the inner membrane protein RodZ (Figure 4A) (Alyahya *et al.*, 2009; Bendezu *et al.*, 2009; Morgenstein *et al.*, 2015; Shiomi *et al.*, 2008). MreB forms patch- or arc-like structures within a cell and interacts with RodA and the conserved inner-membrane or soluble periplasmic proteins MreC and MreD (de Pedro *et al.*, 2001; Dominguez-Escobar *et al.*, 2011; Ishino *et al.*, 1986; Kruse *et al.*, 2005; van den Ent *et al.*, 2006; van Teeffelen *et al.*, 2011; von Olshausen *et al.*, 2013). Furthermore, these elongasome-specific proteins interact with the PG synthases PBP1A and PBP2 (Mohammadi *et al.*, 2007; Typas *et al.*, 2012). PBP1A is regulated by its cognate outer membrane-tethered lipoprotein LpoA (Figure 4A) (Jean *et al.*, 2014).

Later in the cell cycle, the divisome of *E. coli*, which is an envelope-spanning multiprotein complex, takes over the action for constriction of the cell at the division site (Lutkenhaus *et al.*, 2012). PG synthases and hydrolases cluster in this complex, which is controlled by the tubulin homolog FtsZ (filamentation temperature sensitive) (Typas *et al.*, 2012). The process of assembly (and the corresponding cell division proteins) can be roughly divided into an early and a late stage (Aarsman *et al.*, 2005). ZipA and FtsA, which are essential for Z ring stability, localize at an early stage together with ZapA and FtsEX (Arends *et al.*, 2009; Corbin *et al.*, 2007; Haney *et al.*, 2001; Pichoff & Lutkenhaus, 2005). Recent work has suggested that filaments of FtsZ and FtsA treadmill around the division ring and thereby move the PG synthesis complex (Bisson-Filho *et al.*, 2017; Yang *et al.*, 2017). At the late stage, the essential proteins FtsK, FtsQBL, FtsW, FtsN and FtsI (PBP3) are recruited to the division plane to generate a mature divisome (Figure 4B) (Aarsman *et al.*, 2005; Weiss *et al.*, 1999). Unlike reported in previous studies, the elongasome-specific TPase PBP2 might stay at the division site and colocalize with FtsI (van der Ploeg *et al.*, 2013). FtsN is important for septal PG synthesis and constriction by interacting especially with FtsA (Weiss, 2015). It can bind to PG via its bacterial-specific sporulation-related (SPOR) domain (Yahashiri *et al.*, 2015). PBP1B and its cognate outer membrane-tethered lipoprotein LpoB also localize to the division site in a late stage as well as amidases and their regulators (EnvC and NlpD), as existing PG bonds must be cleaved to generate new ones (Bernhardt & de Boer, 2003; Egan *et al.*, 2014; Peters *et al.*, 2011). In addition, other hydrolases such as lytic transglycosylase or CPases localize at a late stage of division (Romeis & Holtje, 1994; Vollmer *et al.*, 1999).

Finally, members of the Tol-Pal complex localize to the division plane (Figure 4B) (Gerding *et al.*, 2007). The envelope-spanning Tol-Pal proteins are involved in the invagination and integrity of the outer membrane and are well-conserved in Gram-negative bacteria (Typas *et al.*, 2010). The complex consists of the inner membrane proteins TolA, TolQ and TolR, the periplasmic protein TolB and the outer membrane-anchored Pal (Cascales *et al.*, 2001; Lazzaroni *et al.*, 1999; Sturgis, 2001). However, the Tol-Pal complex is not essential in *E. coli* (Cascales & Lloubes, 2004; Typas *et al.*, 2010). By contrast, Tol-Pal proteins are essential in the  $\alpha$ -proteobacteria *C. crescentus* (Yeh *et al.*, 2010) and *H. neptunium* (unpublished data).

In contrast to the linear assembly of the divisome in *E. coli*, a series of seven functional modules are recruited in *C. crescentus* (Goley *et al.*, 2011). While nearly all investigations have focused on the assembly of the divisome, its disassembly is hardly understood. The



disassembly of the proteins is crucial, because they have to be degraded or recycled for the next cell division. In a recent study, the disassembly process in *E. coli* was shown to occur in at least five steps (Söderström *et al.*, 2016). The process starts with FtsZ leaving the former division site and ends with the disassembly of FtsN, hence it follows a first-in, first-out mechanism (Söderström *et al.*, 2016).

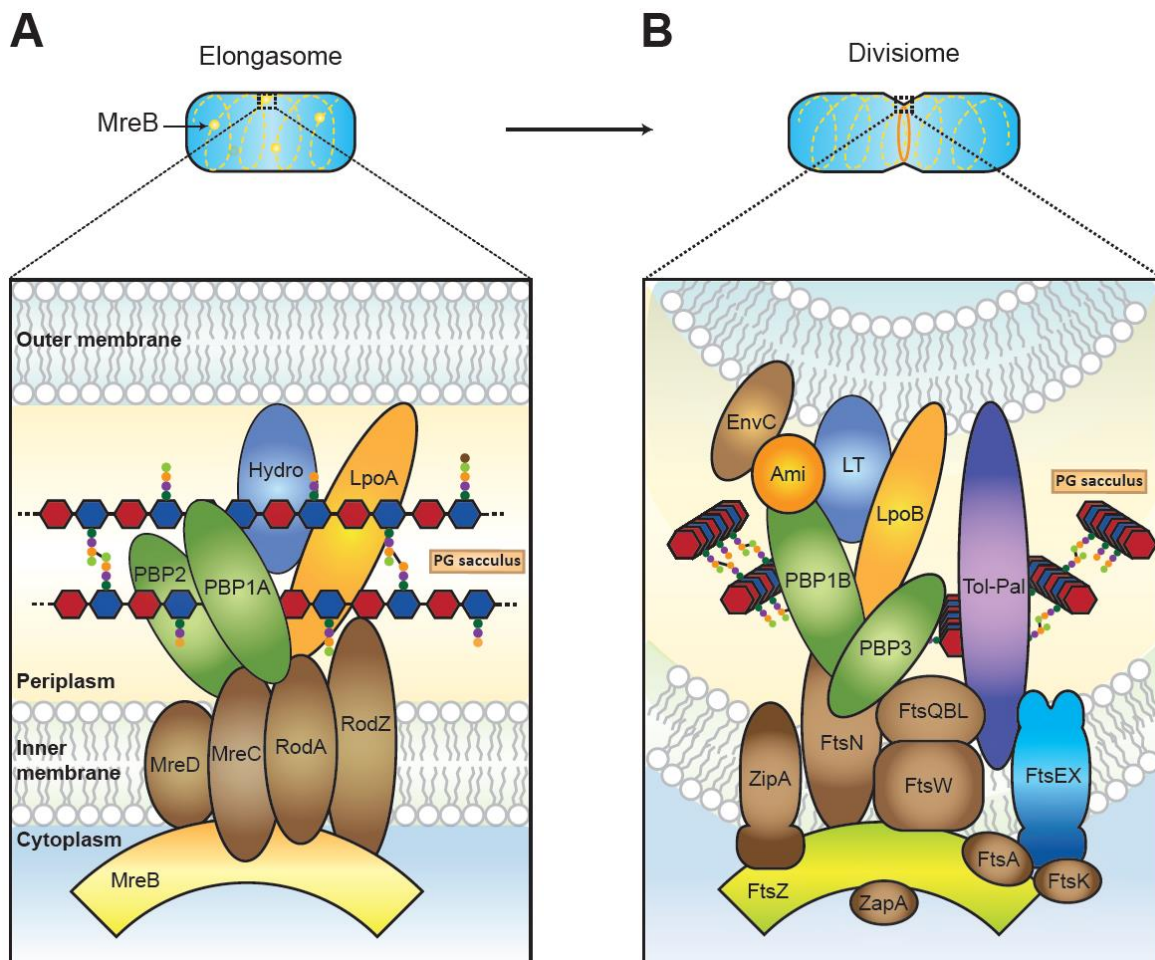


**Figure 4: Structure of the elongasome and the divisome in *E. coli*.** Different PG biosynthetic complexes are active at different stages of the cell cycle. **(A)** MreB and associated membrane proteins (MreCD and RodAZ) control or position the PG synthases PBP1A and PBP2 as well as still-unknown hydrolases (Hydro) during lateral elongation. **(B)** FtsZ guides the PG remodeling complex. The first components of the divisome were already assembled (FtsA, ZipA, ZapA, FtsEX, FtsK). The mature divisome contains essential, inner membrane-localized cell division proteins, the PG synthases PBP1B and PBP3, amidases (Ami) with their activators (EnvC), lytic transglycosylase (LT) as well as proteins of the Tol–Pal complex for constriction of the outer membrane. The activity of the PBPs is regulated in part by outer membrane-anchored lipoproteins such as LpoA and LpoB. Adapted from Typas *et al.* (2012) and Cserti (2016).

## 1.5 Alternative growth modes in bacteria

The interplay between PG synthesis and hydrolysis must be strictly regulated in space and time to ensure correct cell morphology (Höltje, 1998). Most rod-shaped bacteria (e.g. *E. coli* and *B. subtilis*) show symmetric cell wall synthesis and therefore produce two equally sized daughter cells, with an old and a new pole (de Pedro *et al.*, 1997; Stewart *et al.*, 2005). They first incorporate PG in a dispersed manner along the cell cylinder, whereas zonal PG

insertion occurs at the septum during cytokinesis (Figure 5) (Monahan *et al.*, 2014). The so far described *E. coli* and *B. subtilis* possess MreB to guide their PG biosynthesis machinery (Errington, 2015). Bacteria that lack MreB have an alternative way of PG incorporation (Kysela *et al.*, 2013). For example, the Actinobacteria (e.g. *Corynebacterium* and *Mycobacterium*) has the cell polarity factor DivIVA, which orchestrates PG remodeling enzymes and results in polar growth (Flardh, 2003; Joyce *et al.*, 2012; Letek *et al.*, 2009).

The diversity of the  $\alpha$ -proteobacteria in terms of growth and cell division is even higher (Brown *et al.*, 2011; Cameron *et al.*, 2015). Polar growth was observed in the rhizobial species *A. tumefaciens*, which grows exclusively at one pole (Brown *et al.*, 2012; Cameron *et al.*, 2014). Another alternative growth mode is budding, where daughter cells are produced from new cell material at one pole of the cell, e.g. in members of the *Rhizobiaceae* and *Brucellaceae* (Figure 5) (Hirsch, 1974). *C. crescentus* performs a further type of polar growth: it generates a cellular extension at one cell pole (Figure 5 and 6B; for details see 1.6.) (Wagner & Brun, 2007). Finally, members of the family *Hyphomonadaceae* perform budding through the formation of a polar stalk whose tip transforms into a new daughter cell (Jung *et al.*, 2015; Moore, 1981; Whittenbury & Dow, 1977). Strikingly, in recent years, bacterial symbionts have been identified that position the Z ring and divide in a longitudinal way (Leisch *et al.*, 2012). FtsZ and MreB in these species remain parallel to the long axis during the whole cell cycle (Pende *et al.*, 2018).

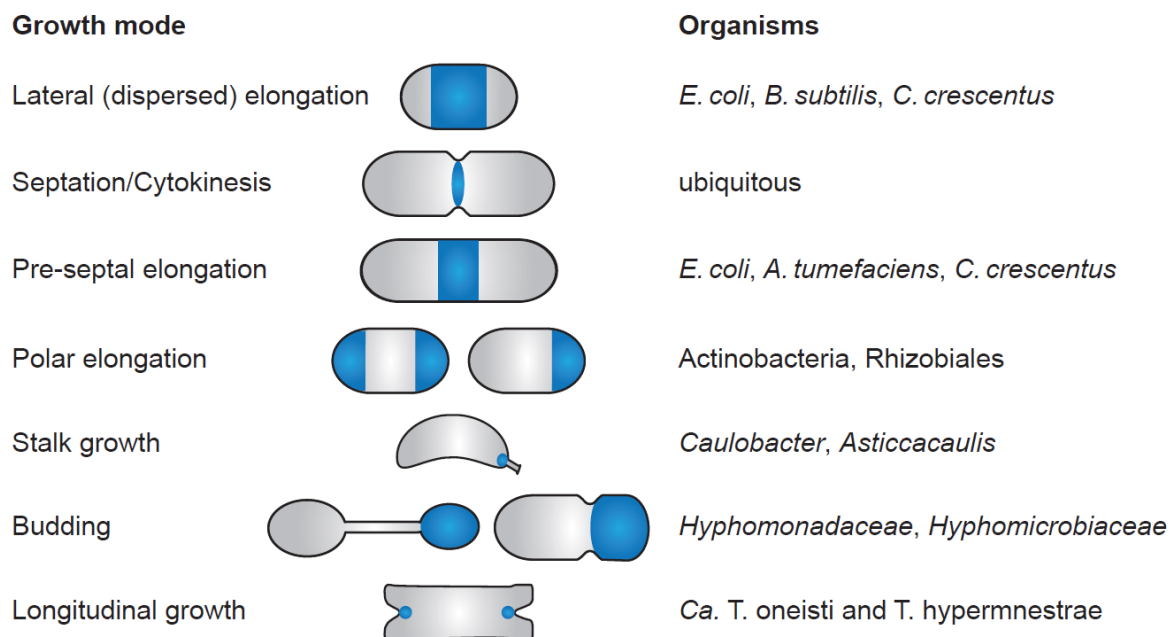


**Figure 5: Growth modes in rod-shaped bacteria.** The various growth regions of different bacterial species are schematically depicted in blue. Abbreviations: *Ca. T. oneisti*: *Candidatus* Thiosymbion oneisti; *Ca. T. hypermnestrae*: *Candidatus* Thiosymbion hypermnestrae. Adapted from Randich and Brun (2015) and Cserti (2016).

## 1.6 *Hyphomonas neptunium* as a model organism for stalked budding bacteria

The marine Gram-negative  $\alpha$ -proteobacterium *H. neptunium* has been isolated from the harbor of Barcelona (Spain) in 1964. Initially, it was classified as a member of the genus *Hyphomicrobium* due to its morphology (Leifson, 1964). A *H. neptunium* mother cell (stalked cell) has a very different morphology in comparison to a daughter cell (swarmer cell), which emanates by budding (Figure 6A). Swarmer cells have a polar flagellum and are motile, while mother cells are immotile and have a stalk at one pole (Leifson, 1964). This stalk (prosthecium) is an extension of the cell envelope that is composed of an inner membrane, the cell wall and an outer membrane.

*H. neptunium* is a mesophilic organism that can grow over a wide range of temperatures (22 – 37°C) and pH values (Havenner *et al.*, 1979). The organism is not osmophilic nor halophilic, which is striking for a marine bacterium (Leifson, 1964). Therefore, growth only occurs at salt concentrations between 1 – 5% (Havenner *et al.*, 1979). *H. neptunium* is a primary colonizer of marine surfaces and produces biofilms (Baier *et al.*, 1983). In 1984, a DNA-DNA hybridization analysis suggested a close relationship of *H. neptunium* to *Hyphomonas polymorpha*. In addition, *H. neptunium* and *H. polymorpha* cannot use C1 compounds as carbon and energy source (Baier *et al.*, 1983). Instead, they use amino acids and proteins as carbon sources under laboratory conditions (Havenner *et al.*, 1979). This caused a reclassification of *H. neptunium* into the genus *Hyphomonas* (Moore *et al.*, 1984). Genomic analysis showed the existence of genes for glycolysis and pentose phosphate pathway (genome: 3,705,021 bp) (Badger *et al.*, 2006). Nevertheless, *H. neptunium* is a non-saccharolytic organism and cannot use sugars as sole carbon and energy source (Leifson, 1964). Further analysis of the 16S rRNA classified *H. neptunium* into the order Rhodobacterales (Badger *et al.*, 2005). However, additional studies of the 23S rRNA and conserved-protein alignments suggested a close relationship to the order Caulobacterales. An important member of this group is *C. crescentus*, which serves as a model organism for asymmetric cell division, differentiation and cell cycle regulation (Brun & Janakiraman, 2000). A comparison of the genomes of both bacteria discovered many similarities in the gene repertoire of this two species (Badger *et al.*, 2006).

*H. neptunium* and *C. crescentus* both belong to the dimorphic, prosthecate bacteria (DPB) and reproduce by asymmetric binary fission or budding, respectively. The type of reproduction, where a bud grows at a stalked mother cell, was termed budding (even though budding does not require a stalk). Budding is not bacteria-specific, because unicellular and multicellular eukaryotes, e.g. sponges, also reproduce in this way (Barton, 1950). The Gram-negative  $\alpha$ -proteobacterium *C. crescentus* has the shape of a crescent rod and is ubiquitously distributed in fresh water. It belongs to the family of *Caulobacteraceae*, firstly described in 1935 (Henrici & Johnson, 1935). The swarmer cells shed their flagellum to enter into the S phase (Figure 6C), where a stalk emerges at the formerly flagellated pole (Curtis & Brun, 2010). This stalk is used to attach to surfaces in their aquatic environment by the production of a holdfast (Ong *et al.*, 1990; Tsang *et al.*, 2006). However, it is not needed for reproduction and free of ribosomes, DNA and the majority of cytoplasmic proteins (Ireland *et al.*, 2002; Poindexter & Cohenbazire, 1964; Tsang *et al.*, 2006). Additionally, it shows discoid structures (cross-bands) that physiologically separate the stalk from the cell body (Jones & Schmidt, 1973; Schlimpert *et al.*, 2012; Schmidt, 1973). In

parallel to stalk biosynthesis, the cell initiates chromosome replication and elongation of the cell body. Before entering the G2 phase, cells invaginate the cell envelope and separate the two daughter cells (Figure 6C), which differ considerable in their physiology and morphology. The stalked cell can directly start a new division cycle. The freely moving swarmer cell has to speed its flagellum and differentiate into a stalked cell before it begins the next division cycle.

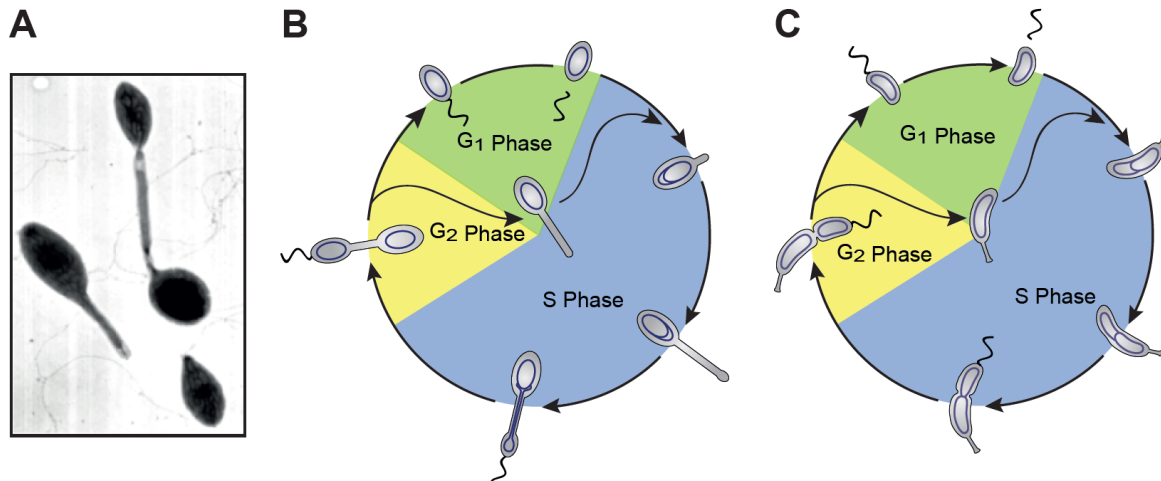


**Figure 6: *H. neptunium* and its cell cycle.** (A) Electron microscopy image of *H. neptunium* cells in three morphological states. Depicted are a swarmer cell (bottom right), a stalked cell (left) and a budding cell (mother cell, stalk and daughter cell; top right). Adapted from Wagner and Brun (2007). The three phases of the cell cycle of (B) *H. neptunium* and (C) *C. crescentus* with their characteristic cell shapes are shown (courtesy of M. Thanbichler).

Genome analysis of *H. neptunium* and *C. crescentus* revealed a common set of 1835 genes, which points to a close relationship (Badger *et al.*, 2006). This is evident by a vast similarity in the outer membrane proteins, e.g. TonB-dependent receptors and lipoproteins (Badger *et al.*, 2006). Despite these similarities, the two species differ significantly in the type of reproduction and the progression of their cell cycle. Nevertheless, both produce a stalked mother cell and a polarly flagellated daughter cell (swarmer cell). Figure 6B and 6C displays the cell cycles of *H. neptunium* and *C. crescentus*, where swarmer cells are not able to reproduce their genome and are arrested in an eukaryotic-like G1 phase. Additionally, only one replication occurs per cell cycle in the stalked cells (Iba *et al.*, 1977; Wali *et al.*, 1980).

The G1 phase of the cell cycle of *H. neptunium* is very similar to the one of *C. crescentus*. A swarmer cell has to shed its flagellum to enter into the S phase (Figure 6B). The cell develops a stalk, which is an extension of the cell envelope, opposite the former flagellated pole (Wali *et al.*, 1980; Weiner & Blackman, 1973). This stalk is a reproductive, not compartmentalized structure that contains cytoplasmic components (Conti & Hirsch, 1965). Exopolysaccharides (biological glue) are segregated at the non-stalked pole to attach the cell to the substrate (Hirsch, 1974). At the tip of the stalk the new bud emerges and grows in size. Components of the growing bud (such as proteins and DNA) must be transported through the stalk, and when the bud reaches a certain size and has developed a flagellum, cell division occurs at the junction between the bud and stalk (hereafter referred as the bud neck; Figure 6B) (Hirsch, 1974). The mother cell can directly undergo another round of cell

division, whereas the motile swarmer cell must first differentiate into a stalked cell (Wali *et al.*, 1980; Weiner & Blackman, 1973).

*H. neptunium* is not the only budding  $\alpha$ -proteobacterium analyzed in more detail. Further examples are *Rhodocrobium vanniellii* and *Rhodocrobium vulgare* (Babudieri, 1950; Duchow & Douglas, 1949). However, the molecular mechanism that underlies the budding process is not understood in any species.

## 1.7 PG biosynthesis and growth of *H. neptunium*

PG biosynthesis and bud formation in *H. neptunium* are complex processes, that are still poorly understood (Cserti *et al.*, 2017). Therefore, in previous studies, we aimed to analyze how *H. neptunium* grows and synthesizes its stalk (Cserti *et al.*, 2017). Three hypotheses were possible: First, the stalk grows through insertion of new PG at the stalk base. Second, the whole structure is elongated and third, growth takes place at the distal end of the stalk. Other  $\alpha$ -proteobacteria, such as *C. crescentus* and *Asticcacaulis excentricus*, grow their stalk from its base (Aaron *et al.*, 2007; Jiang *et al.*, 2014).

To visualize nascent PG that is incorporated into the cell wall in a growing bacterium, the fluorophore-conjugated D-alanine analog HADA was used (Kuru *et al.*, 2012). HADA is incorporated at the 5<sup>th</sup> (or the 4<sup>th</sup>) position in peptide side chains, thereby making regions of new PG synthesis visible (Kuru *et al.*, 2012). Swarmer cells showed a diffuse distribution of the signal indicating that PG was synthesized all over the cell body (Figure 7A). An intense focus appeared at the stalked pole when cells started to produce their stalk. This signal stayed at the stalked pole as long as the stalk grew in length, showing that it was synthesized from its base. Generation of the bud at the tip of the stalk led to a short shift of the signal into the stalk, resulting from a transition from zonal growth at the base to dispersed growth in the bud (Figure 7B).

As soon as the bud was produced, PG synthesis was mainly restricted to this compartment, accompanied by a strong HADA signal (Figure 7A and C). Shortly after the formation of the bud, a weak signal appeared in the rest of the cell body of the mother cell (Figure 7A). As the daughter cell grew in size, HADA incorporation was also visible at the bud neck in addition to the signal in the cell body, indicating that the separation of the bud is initiated. Taken together, this showed intensive PG biosynthesis in newly forming cellular compartments in *H. neptunium*. Furthermore, cells switch from dispersed to zonal growth in a cell-cycle dependent manner (Figure 7C) (Cserti *et al.*, 2017).

The budding mechanism is an interesting way to proliferate. In the past, it was unclear how many reproductive cycles a *H. neptunium* mother cell can undergo. For example, *C. crescentus* cells divide up to 100 times and continuously produce daughter cells (Ackermann *et al.*, 2003). Previous studies suggested that stalked budding members of the family *Hyphomicrobiaceae* can divide less than ten times (Moore, 1981; Whittenbury & Dow, 1977). However, our experiments revealed that *H. neptunium* can generate at least 30 offspring without the loss of viability (Cserti, 2016). A great advantage of budding is that every motile daughter cell will get the newly generated chromosome and new cell wall components. In addition, the competition for resources is diminished for the daughter cell.



Like *E. coli*, *H. neptunium* possesses a large set of PG remodeling enzymes to ensure PG remodeling, especially during budding. Previous bioinformatic analysis revealed that *H. neptunium* harbors six metallopeptidases (LmdA-F), three carboxypeptidases (DacBHL), five glycosyl hydrolases (MltA, MltB, GplA, RlpA and SlfA) but only one amidase (AmiC) (Cserti *et al.*, 2017). This diversity of different lytic enzymes makes a high redundancy likely. A previous study has started to investigate these enzymes but did not characterized them in detail (Cserti *et al.*, 2017).

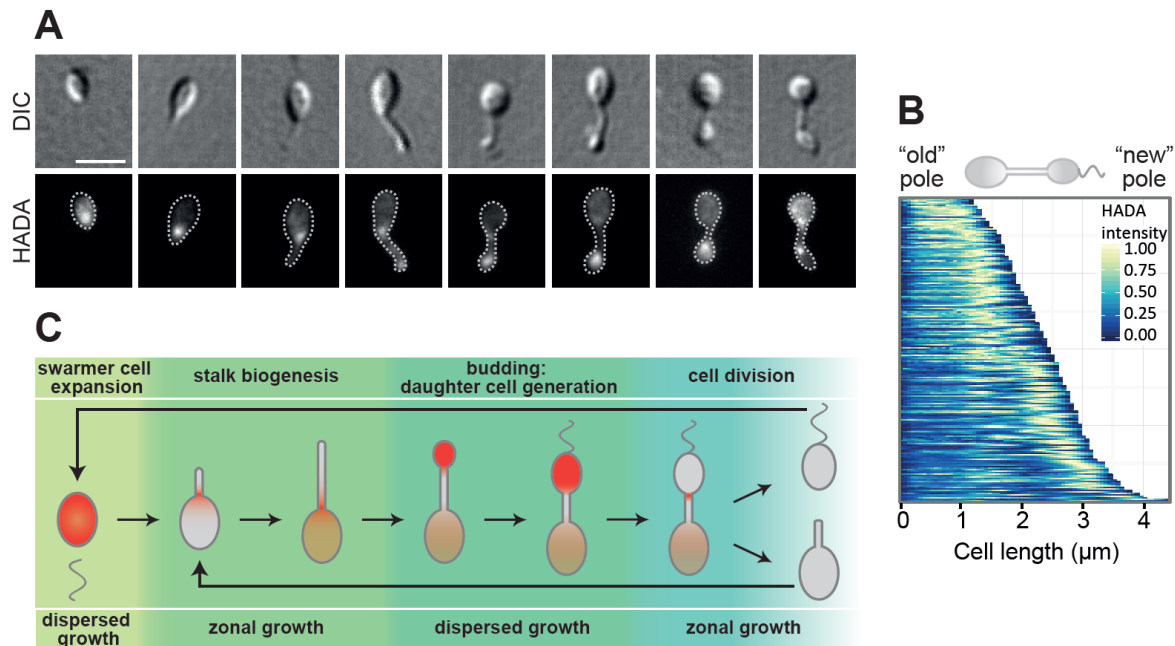


**Figure 7: The growth of *H. neptunium* is characterized by distinct growth phases. (A)** Cell growth occurs at four distinct locations in *H. neptunium*. Wild type cells were grown to exponential phase in MB medium, pulse-labelled with HADA, and imaged by DIC and fluorescence microscopy. Scale bar: 2 μm. **(B)** PG incorporation in *H. neptunium*. Demograph of new PG insertion based on images from (A); n = 207. **(C)** Model of distinct PG incorporation in *H. neptunium*. In the first phase, the swarmer cells enlarge their cell body (PG incorporation is represented in red) before stalk biogenesis is initiated. In the second phase, the stalk is elongated from the base of the mother cell body. Once the stalk has reached a critical length, the new daughter cell is generated at the tip of the stalk (third phase). In the last growth phase, the initiation of cell division between the new daughter cell and the stalk occurs. After cell division, the motile swarmer cell has to increase in size before it can further differentiate, whilst the stalked mother cell immediately reinitiates stalk biosynthesis at the stalked pole. Adapted from E. Cserti (2016) and Cserti *et al.* (2017).

## 1.8 Aim of study

The spatial and temporal regulation of PG biosynthesis and its role in cell morphogenesis has been studied intensively in well-characterized model organisms such as *E. coli*, *B. subtilis*, and *C. crescentus*, i.g., organisms that divide either by symmetric or asymmetric binary fission. However, our knowledge of budding and polarly growing bacteria is very limited due to the lack of genetic tool to analyze these organisms. To broaden our understanding of the mechanisms governing bacterial morphogenesis, we have started to investigate the dimorphic marine  $\alpha$ -proteobacterium *H. neptunium* as a new model organism (Jung *et al.*, 2015).

How the generation of the daughter cell is spatiotemporally regulated, is not known. The aim of this study is to analyze how the *H. neptunium* cell orchestrates PG remodeling enzymes at the site of action during the cell cycle. Our focus lies on the identification of regulators of the enzymes involved in PG remodeling and, a more detailed functional characterization of these proteins. This especially involves a closer analysis of hydrolytic enzymes, which cleave PG at the division site to separate the mother cell from the daughter cell. In detail, we focus on endopeptidases and amidases to analyze their potential redundancy by performing deletion and epistatic studies. Moreover, we test if the mechanism of amidase regulation by inactive endopeptidases is conserved in budding  $\alpha$ -proteobacteria by testing their binding and interaction behavior. We also start to investigate the role of the membrane-embedded FtsEX complex and its contribution to the regulatory mechanism.

A further aim of this study is to identify novel factors that are involved in the regulation of budding in *H. neptunium*. To accomplish this, we perform a transposon mutagenesis experiment that aims to identify all essential genes of *H. neptunium*. This will give us the possibility to find novel uncharacterized factors regulating or guiding the budding process.

## 2. RESULTS

### 2.1 PG remodeling enzymes

Similar to other Gram-negative bacteria, *H. neptunium* possesses a large number of different PG synthases and lytic factors to remodel its PG. These enzymes are needed for growth, division and the maintenance of cell shape. They cleave the existing glycan strands and peptide side chains to make space for the insertion of new material (Höltje *et al.*, 1975; Vollmer & Bertsche, 2008). New lipid II units are subsequently inserted to expand the PG sacculus (Vollmer & Bertsche, 2008). The variety and diversity of lytic factors is even higher than that of PG synthases. Previous studies in *H. neptunium* have already shown the importance and the function of PG synthases, such as PBPs and transglycosylases (Cserti *et al.*, 2017). Therefore, the main focus of the current study lies on PG lytic enzymes. Similar to *E. coli*, *H. neptunium* harbors many genes encoding lytic enzymes. Among them are well-known classes such as lytic transglycosylases, endopeptidases, amidases and carboxypeptidases, which are all predicted to function in PG remodeling (Cserti *et al.*, 2017). Thus, two classes of enzymes (endopeptidases and amidases) were chosen for further in-depth studies. The analysis of these enzymes and their effect on PG biosynthesis is crucial to understand the molecular mechanisms that underlies the extraordinary reproduction mechanism of *H. neptunium*.

#### 2.1.1 M23 endopeptidases of *H. neptunium*

Six proteins harboring an M23 peptidase domain were predicted to be present in *H. neptunium*, named LmdA-F (LytM domain-containing protein A-F; Figure 8A) (Cserti *et al.*, 2017). They are characterized by a M23 peptidase (LytM) domain. Three of them (LmdABC) have a predicted transmembrane segment at the N-terminus and are thus likely to be inserted into the cytoplasmic membrane, with the catalytic domain presumably localized in the periplasm. By contrast, LmdDEF have a predicted N-terminal signal peptide, which makes it likely that these proteins are soluble and periplasmic. Additionally, LmdC and LmdE possess coiled-coil rich regions, which are known to be involved in protein-protein interactions (Figure 8A) (Lupas, 1996). LmdA-F possess the characteristic C-terminal M23 peptidase domain that should enable them to cleave the peptide side chains in PG and affect cell morphology.

Notably, an alignment of all six endopeptidase homologues revealed that one of them (LmdE) only shows a partial M23 peptidase domain motif. LmdE lacks the crucial amino acid residues (HxxxD, YxH and HxH) that bind the catalytic zinc ion in the active center (Figure 8B). A similar situation was already observed for the *E. coli* endopeptidases EnvC and NlpD, which regulate the activity of the amidases AmiA, AmiB and AmiC (Figure 3) (Uehara *et al.*, 2010; Yang *et al.*, 2012). LmdE and EnvC were aligned and revealed similarities in the amino acid composition of the M23 peptidase domain (data not shown). In addition,



EnvC possesses two coiled-coil regions, making a related function of LmdE possible. Therefore, we tested the catalytic activity of LmdE and its potential role in PG remodeling.

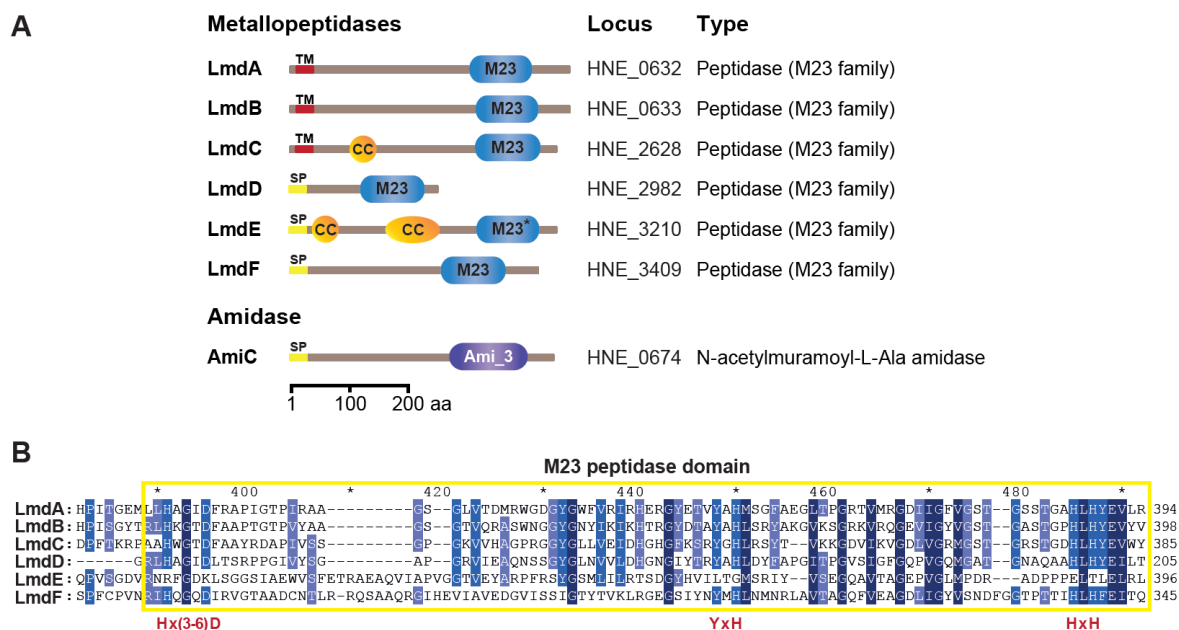


**Figure 8: Graphical representation of proteins with a putative role in PG hydrolysis of *H. neptunium*.** (A) Domains have been identified using the Pfam database (Bateman *et al.*, 2004; Finn *et al.*, 2010). The SMART database was used to depict the proteins (Letunic *et al.*, 2009; Schultz *et al.*, 1998). Abbreviations: LmdA-F (LytM domain containing protein A-F); TM: transmembrane segment; SP: signal peptide; CC: coiled-coil domain; M23: M23 peptidase domain; M23\*: inactive peptidase domain; Ami\_3: amidase\_3 domain; aa: amino acids. (B) Alignment of all M23 peptidases in *H. neptunium* reveal that the peptidase domain is not conserved in all Lmd peptidases. LytM (M23) domains are highlighted by a yellow frame and the LytM signature motive is depicted in red below. Residues in dark blue color are highly conserved, blue indicates average conservation, and light blue indicates low conservation of residues across the aligned homologs. The alignment was generated with Clustal Omega (06.2016) (<http://www.ebi.ac.uk/Tools/msa/clustalo/>).

First, deletion studies were performed to better understand the contribution of the M23 endopeptidases to cell morphogenesis. Five of them could be deleted in previous experiments (Cserti *et al.*, 2017). We were able to generate all single deletions except that for *lmdC*, which turned out to be essential. Multiple attempts to delete or deplete *lmdC* have been unsuccessful so far. The deletion of *lmdA*, *lmdB*, *lmdD* and *lmdF* had no visible effect on the cell morphology as the mutants looked like wild type (Figure 9A). The only exception was the *lmdE* mutant, which showed a significant elongation of the cell body and specifically, the stalk (Figure 9A). The cell length of all generated strains was measured to quantify the phenotype, and the results were represented as a box plot (Figure 9B). We managed to complement the  $\Delta$ *lmdE* phenotype by introducing an inducible copy of *lmdE* (Figure S1A). Cells restored wild-type morphology already after 2 h of induction and cell length returned back to normal (Figure S1B). We also tested if the single deletions have a positive or negative effect on cell growth. All strains showed normal growth in comparison to the wild type (Figure S4A and Table S1). In summary, only the  $\Delta$ *lmdE* mutant showed a significant difference in cell length in comparison to wild-type cells.

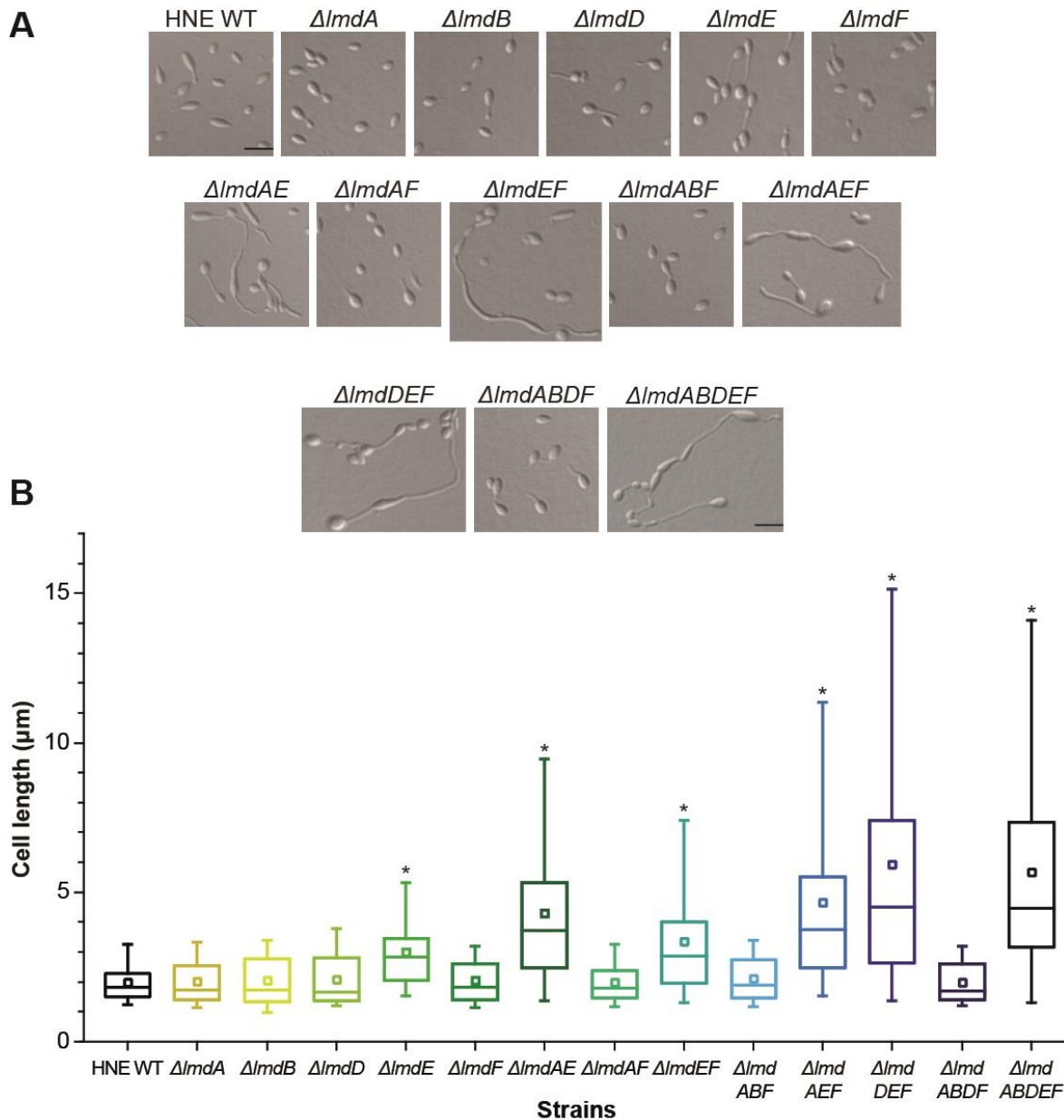


**Figure 9: Multiple deletions of M23 endopeptidases have a strong effect on the cell length of *H. neptunium*.** (A) Phenotype of the wild type (HNE WT), the single deletion mutants, the double deletion mutants SR34 ( $\Delta lmdAF$ ), and SR35 ( $\Delta lmdEF$ ), the triple deletion mutants SR41 ( $\Delta lmdABF$ ), SR40 ( $\Delta lmdDEF$ ), and SR78 ( $\Delta lmdAEF$ ), the quadruple deletion mutant SR45 ( $\Delta lmdABDF$ ), and the quintuple deletion strain SR51 ( $\Delta lmdABDEF$ ). EC36 ( $\Delta lmdA$ ), EC38 ( $\Delta lmdD$ ), EC39 ( $\Delta lmdE$ ), EC53 ( $\Delta lmdB$ ) and EC90 ( $\Delta lmdF$ ) were generated by E. Cserti (Cserti *et al.*, 2017). Cells were either grown in MB medium or ASM at 28°C (shaking at 210 rpm) to the exponential phase and analyzed microscopically. Scale bar: 3  $\mu$ m. (B) Cell lengths of the indicated strains. Cells were grown as described in (A). The distribution of cell length is shown as a box plot. The box shows the 2<sup>nd</sup> and 3<sup>rd</sup> quartile of the values. The small square marks the mean value. The median is depicted by the line in the box (50% of values). The whiskers mark the 5<sup>th</sup> and 95<sup>th</sup> percentile. Asterisks indicate a *p*-value of < 0.0001 (*t*-test). Quantifications are based on 300 cells for the wild-type strain and 200 cells for each mutant strain.

The absence of single endopeptidases did not lead to changes in cell morphology (with one exception), showing the high redundancy of these enzymes. Therefore, we generated double, triple, quadruple and quintuple deletion mutants to test for synthetic phenotypes. The double deletion  $\Delta lmdAF$  strain showed a wild-type phenotype (Figure 9A). Additional

deletion of *lmdB* or *lmdBD* did not lead to a different phenotype. This again suggests a high redundancy of the M23 endopeptidases in *H. neptunium*, since four of them can be inactivated without any effect. However, the situation was different when *LmdE* was missing. A double deletion of *lmdEF* and *lmdAE* led to cells with clearly elongated and misshapen stalks (Figure 9A). This observation was also reflected in a larger cell length (up to 10  $\mu\text{m}$ ) in comparison to wild-type cells (up to 3  $\mu\text{m}$ ) or the single *lmdE* deletion (Figure 9B). The defects in cell morphology were even more severe when *lmdAEF* or *lmdDEF* were deleted. Mutant cells were not able to divide in a correct way and often formed misshapen cell bodies within the stalk (Figure 9A). The  $\Delta$ *lmdDEF* mutant generated the longest cells of all M23 endopeptidase mutants (Figure 9B). The additional deletion of *lmdAB* to create the quintuple deletion mutant ( $\Delta$ *lmdABDEF*) did not further aggravate the morphological defects, as increase the cell length. To validate that the phenotype of the  $\Delta$ *lmdABDEF* mutant was only dependent on the deletion of *lmdE*, we performed a complementation experiment. The *lmdE* gene was induced in the  $\Delta$ *lmdABDEF* mutant that led to a fast recovery of the morphology to wild-type levels (Figure S1C). Cells were no longer elongated and showed normal cell length (Figure S1D). The uninduced strain nearly restored the wild-type cell length due to the leakiness of the promoter. Furthermore, we analyzed if the multiple deletions generated have a negative effect on the growth behavior. Cells grew normally under the tested conditions and did not show any major differences compared to the wild-type strain (Figure S4B and Table S1). Collectively, our deletion studies confirmed the high redundancy of M23 endopeptidases in *H. neptunium* and point to a major role of *LmdE*, beside *LmdC*, in stalk biosynthesis and division. Once we combined the *lmdE* deletion with deletions of *lmdA*, *lmdF*, *lmdAF*, *lmdDF* or *lmdABDF* we observed an additive phenotype, suggesting that they act in different pathways.

### 2.1.2 Analysis of their localization

The localization pattern of all *Lmd* proteins was analyzed to determine if any of them accumulates at the major sites of PG biosynthesis. For this purpose, natively expressed C-terminal mCherry fusions were generated, but several of them showed stability problems or could not be generated at all. This phenomenon was already known from studies of the M23 endopeptidases *LdpA-F* in *C. crescentus* (Zielińska *et al.*, 2017). However, in *H. neptunium*, we managed to generate strains expressing *lmdA-mCherry*, *lmdB-mCherry*, *lmdD-mCherry* and *lmdF-mCherry* fusions from the respective native promoters. They were analyzed microscopically and the subcellular distribution of the fluorescently labeled proteins were depicted in demographs (Figure 10).

*LmdA-mCherry* localized in the whole cell body (Figure 10A). The fusion protein was largely stable in a Western Blot analysis and only a minor signal of cleaved mCherry was detected (Figure S2A). The only fully stable fusion was the one of *LmdB*. The fusion protein was observed in the whole cell body and in the stalk. The localization pattern can be clearly seen in the demograph (Figure 10B). The localization of *LmdC* was not possible because a native C-terminal fusion did not integrate into the genome and the inducible C-terminal fusion was diffused in the cells and completely unstable (Kanngießner, 2016). In a third attempt, we tried to generate an inducible *LmdC<sup>N</sup>* fusion, where we used the N-terminal region of *LmdC* (1 – 270 bp) lacking the M23 domain fused to the mCherry tag. However, only a weak fluorescence signal was observed due to the instability of the fusion protein (data not

shown). In contrast, LmdD-m-Cherry could be localized in the cell body and occasionally at the stalked pole (Figure 10C). However, Western Blot analysis showed low protein production and protein instability as well (Figure S2A).

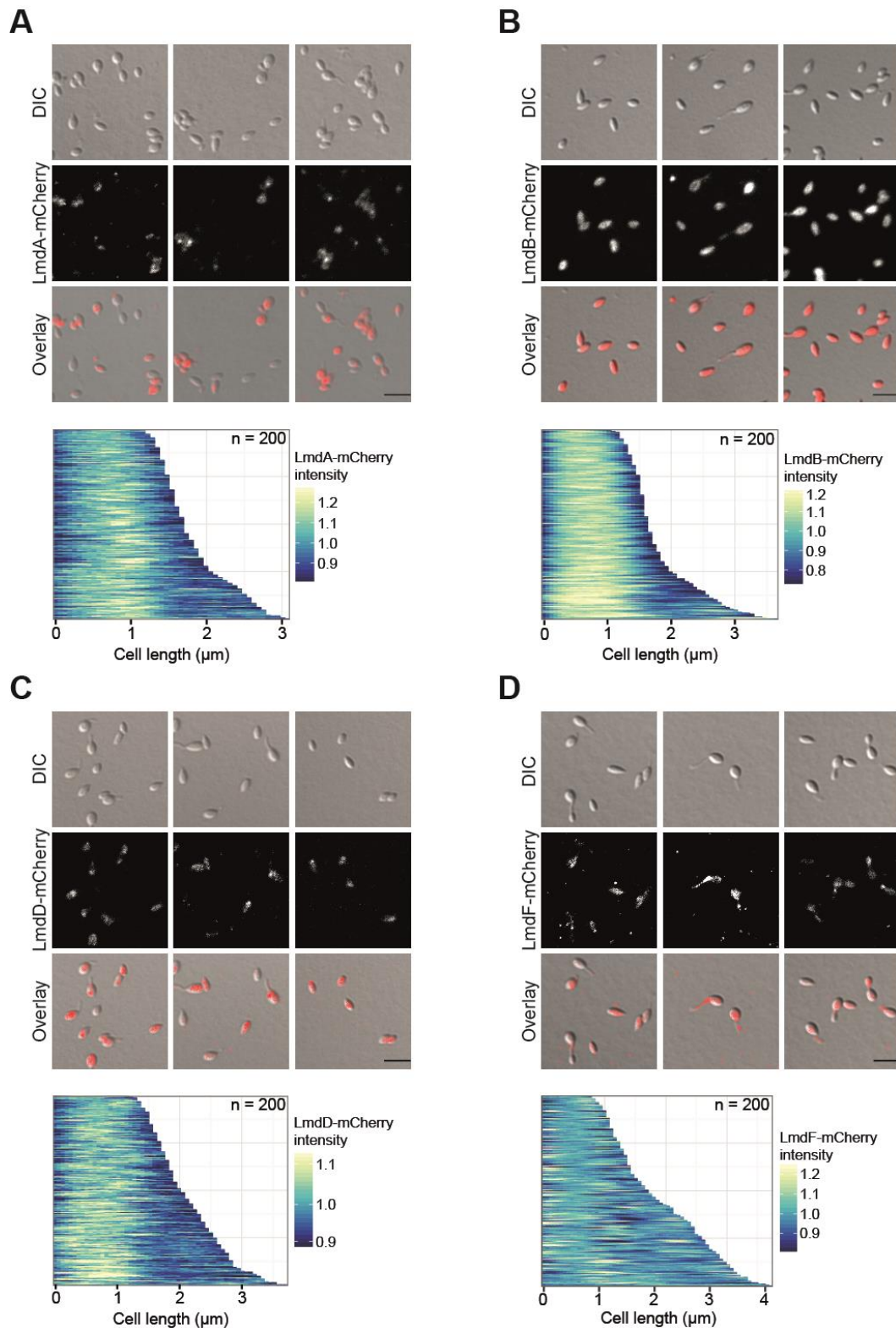


**Figure 10: M23 endopeptidases show distinct localization patterns in *H. neptunium*.** (A) LmdA-mCherry localizes in the whole cell body. SR61 (*lmdA-mCherry*) was grown to exponential phase in ASM and imaged by DIC and fluorescence microscopy. Scale bar: 3  $\mu\text{m}$ . LmdA-mCherry fluorescence intensity in SR61 cells depicted in a demograph below (based on images from A). (B) LmdB-mCherry localizes in the whole cell body and the stalk. SR24 (*lmdB-mCherry*) was grown to

**Figure 10 (continued):** exponential phase in ASM and imaged by DIC and fluorescence microscopy. Scale bar: 3  $\mu\text{m}$ . LmdB-mCherry fluorescence intensity in SR24 cells depicted in a demograph below (based on images from B). **(C)** LmdD-mCherry shows a diffuse pattern in the cell body. SR58 (*lmdD-mCherry*) was grown to exponential phase in ASM and imaged by DIC and fluorescence microscopy. Scale bar: 3  $\mu\text{m}$ . LmdD-mCherry fluorescence intensity in SR58 cells depicted in a demograph below (based on images from C). **(D)** LmdF-mCherry localizes in the cell body and the stalk. SR26 (*lmdF-mCherry*) was grown to exponential phase in ASM and imaged by DIC and fluorescence microscopy. Scale bar: 3  $\mu\text{m}$ . LmdF-mCherry fluorescence intensity in SR26 cells depicted in a demograph below (based on images from D).

The localization of LmdE was not possible at all. In different attempts, alleles encoding an N-terminal, a C-terminal or a sandwich (after P128) fusion were generated and integrated downstream of the native promoter. None of the fusions was stable in a Western Blot analysis, and all of them yielded a diffuse fluorescence distribution (data not shown). In addition, the strain harboring the sandwich fusion displayed the phenotype of the  $\Delta\text{lmdE}$  mutant, suggesting that the mCherry tag interfered with the fold of the protein (data not shown). In contrast, LmdF-mCherry was largely stable in a Western Blot analysis, and only a faint signal was detected for cleaved mCherry (Figure S2A). However, the signal for the full-length protein was higher (>100 kDa) than expected (72 kDa). Even though the signal was not strong, localization was observed in the cell body, the stalk and occasionally at the stalked pole (Figure 10D). The gene expression levels of all six endopeptidases were analyzed in a comparative RNA sequencing analysis to see if this could be a reason for the low protein production (Jung, 2016). For this, the RPKM values (Reads Per Kilobase per Million reads) were compared. Indeed, *lmdA* and *lmdD* showed the lowest gene expression of all endopeptidases, explaining the faint protein signals in the Western Blot analysis. In contrast to this, *lmdB*, *lmdE* and *lmdF* showed medium expression levels. Finally, *lmdC* had the highest RPKM value (17x more than *lmdA* and *lmdD*) of the endopeptidase genes. Taken together, M23 endopeptidases localized mainly in the cell body of *H. neptunium* and infrequently at the stalk pole or in the stalk. Our results further confirmed the instability of the fluorescently tagged forms that was already known from previous studies in *C. crescentus* with the same class of proteins (Zielińska *et al.*, 2017).

### 2.1.3 The single amidase of *H. neptunium*

Amidases have a crucial function during cell division and growth as they remove the peptide side chains from the glycan strands by splitting the amide bond and thus allow the separation of the daughter cell PG layers during cell constriction (Heidrich *et al.*, 2001). The genome of *H. neptunium* only codes for one putative amidase (*HNE\_0674*) with a predicted characteristic amidase\_3 domain (Figure 8A). The presence of a single amidase gene is a common feature of  $\alpha$ -proteobacteria, whereas  $\gamma$ -proteobacteria often possess three or more members of this family (Möll *et al.*, 2014). Based on its domain structure, HNE\_0674 (hereafter named AmiC or AimC<sub>HNE</sub>) is a homolog of the *E. coli* amidase AmiC. AmiC<sub>EC</sub> is a soluble periplasmic protein that localizes at the division side (Bernhardt & de Boer, 2003). The prediction for AmiC<sub>HNE</sub> is also soluble and periplasmic.

First, we generated a strain lacking the *amiC* gene and analyzed the resulting phenotype (Cserti *et al.*, 2017). It turned out that AmiC is not essential, but the *amiC* deletion strain showed severe cell division defects, which manifested in elongated and misshapen stalks



(Figure 11A) and occasional cell chaining. Overall, the mutant cells were significantly longer than wild-type cells (Figure 11B). This indicates that AmiC may play a crucial role during cell division and bud formation in *H. neptunium*. A complementation study was performed to validate that the phenotype of the  $\Delta amiC$  mutant is only due to the inactivation of AmiC and, the induction of the native AmiC for several hours restored the wild-type phenotype (Figure S3A). Measurements of the cell lengths confirmed that the complementation was fully successful (Figure S3C).

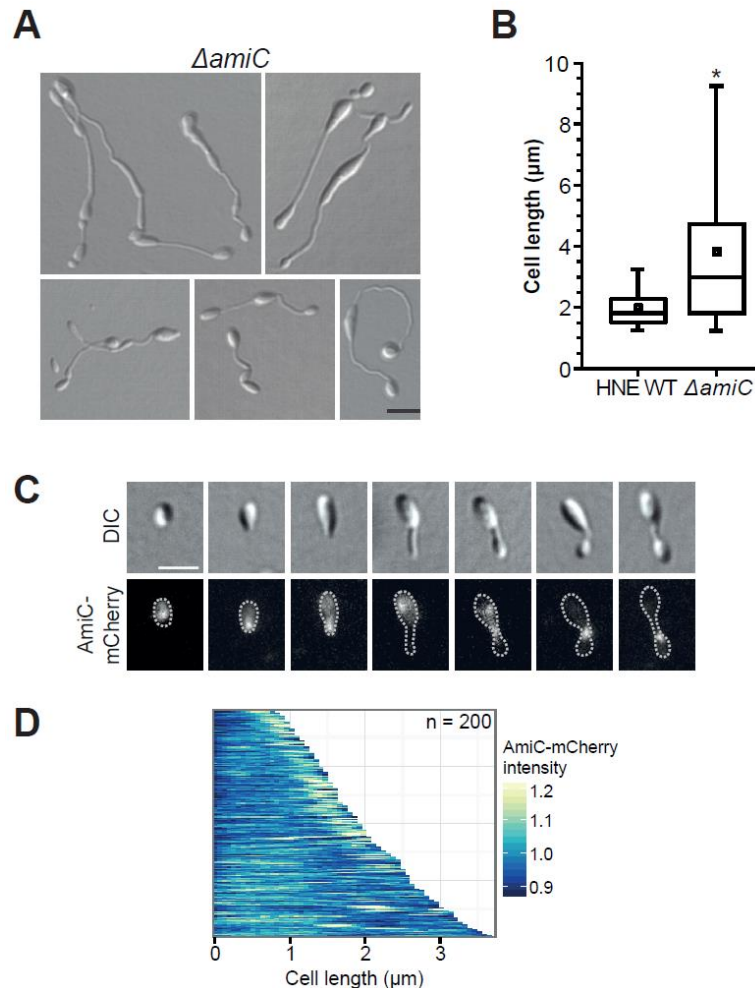


**Figure 11: The amidase AmiC plays an important role in the division of *H. neptunium*.** (A) The  $\Delta amiC$  mutant shows cells with elongated stalks that have a severe defect in cell separation. SR18 ( $\Delta amiC$ ) was grown in ASM at 28°C (shaking at 210 rpm) to the exponential phase and analyzed microscopically. Scale bar: 3  $\mu\text{m}$  (B) Distribution of cell lengths in population of SR18 cells. Cells were grown as described before. The distribution of cell length is shown as a box plot (explanation see Figure 9). Asterisk indicates a  $p$ -value of  $< 0.0001$  ( $t$ -test). (C) AmiC-mCherry localizes to the stalked pole and the division plane. EC70 ( $P_{Cu}::P_{Cu}\text{-}amiC\text{-}mCherry$ ) was grown to exponential phase in MB medium, induced for 24 h with 300 mM  $\text{CuSO}_4$ , and imaged by DIC and fluorescence microscopy. Scale bar: 2  $\mu\text{m}$ . (D) AmiC-mCherry fluorescence intensity in EC70 cells depicted in a demograph (based on images from C). C and D are adapted from Cserti *et al.* (2017).

Secondly, we generated an inducible AmiC-mCherry fusion that localized to the stalked pole in swarmer cells (Figure 11C) (Cserti *et al.*, 2017). The signal remained at the stalked pole until the bud was formed following a transition into the nascent bud. At the end of the cell cycle AmiC localized to the future division site, where it is presumably needed to separate the bud from the mother cell. This localization pattern is less obvious in the demograph due

to the short time AmiC stays at the division plane as a late cell division protein (Figure 11D). The weak background signal in the cell body might be due to partial instability of the fusion protein, as observed in a Western Blot analysis (Figure S2B). In conclusion, the single amidase of *H. neptunium* is crucial for proper cell shape and, based on the deletion phenotype and the localization it exhibits, it is probably involved in cell division.

#### 2.1.4 AmiC is a periplasmic amidase

According to bioinformatic data, AmiC is predicted to be a soluble periplasmic protein. To verify the periplasmic localization of AmiC, we performed protein fractionation experiments. Since antibodies against AmiC were not available, we used the strain SR23 (*amiC-mCherry*) and detected the fusion protein with an antibody against mCherry. This was possible due to the high stability of the fusion protein (Figure S2B). The fractionation showed that AmiC was exclusively detected in the soluble fraction of *H. neptunium* cells (Figure 12A). In a control sample the soluble cytoplasmic master regulator CtrA was detected, showing that the fractionation was successfully (Figure S3D). To further investigate the localization of AmiC, the protein was localized in a heterologous system. An inducible AmiC-mCherry fusion was visualized in *E. coli* cells (Figure 12B). The protein could be detected best after 3 and 4 h of induction and showed a periplasmic localization, as indicated by strong fluorescence signal along the cell periphery. This further suggests that AmiC localizes in the periplasm. An interesting side effect is the steady fitness of the *E. coli* cells. They did not lyse due to cleavage of PG, which shows that AmiC<sub>HNE</sub> is not active in this heterologous system.

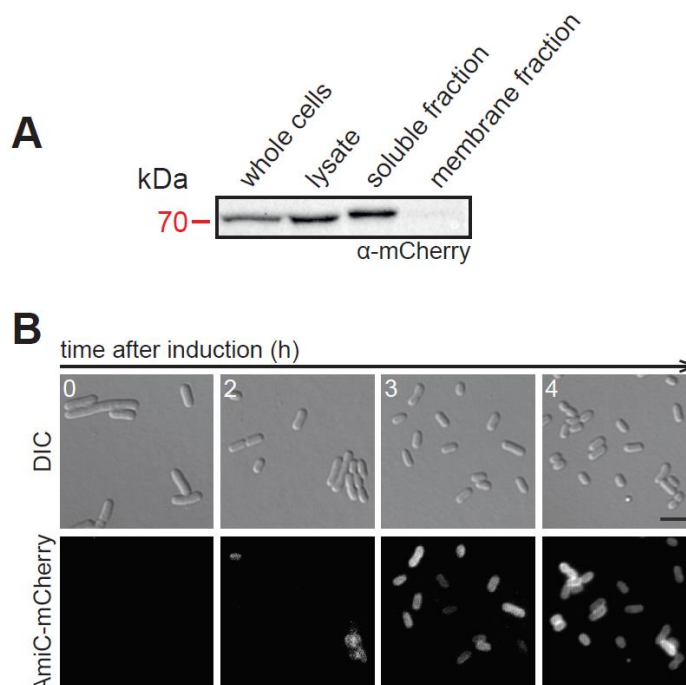


**Figure 12: AmiC is a periplasmic amidase. (A)** AmiC-mCherry is exclusively found in the soluble fraction. Whole cell lysate of strain SR23 (*amiC-mCherry*) of *H. neptunium* was fractionated by ultracentrifugation into membrane fraction and soluble fraction followed by immunoblot analysis with an anti-mCherry antibody. **(B)** AmiC-mCherry shows a periplasmic pattern in *E. coli*. Cells of SR59 *E. coli* BL21(DE3) bearing the plasmid pSR61 (*P<sub>ara</sub>-amiC-mCherry*) were grown in LB to exponential phase, induced with 0.02% arabinose and analyzed with DIC and fluorescence microscopy. Scale bar: 3 μm.

### 2.1.5 The connection between AmiC and the M23 endopeptidases

To further investigate if the M23 endopeptidases and the amidase interact and even act in the same pathway, we performed epistasis experiments. This would mainly address the question of how redundant certain gene combinations are and reveal potential synthetic sickness or lethality. Specifically, a deletion of the *amiC* gene was combined with deletions of various M23 endopeptidase genes to see if a combination of mutations results in a more severe phenotype than the single *amiC* deletion.

First, we generated a strain lacking the *amiC* gene as well as either the *lmdE* or *lmdF* gene and analyzed the resulting phenotype. The cell length of both strains did not differ from that of the  $\Delta amiC$  mutant (Figure 13B). However, the cell shapes of the  $\Delta amiC \Delta lmdE$  and the  $\Delta amiC \Delta lmdF$  mutants were slightly different (Figure 13A). Both mutants showed swellings within their stalks, which was not observed that frequently in  $\Delta amiC$  cells. Secondly, a strain lacking the *amiC* gene and both *lmdE* and *lmdF* gene displayed elongated stalks (Figure 13A). Surprisingly, the phenotype was less severe, resulting in a shorter cell length than the  $\Delta amiC \Delta lmdE$  mutant. Next, we decided to delete *lmdA* in the  $\Delta amiC$  mutant because the  $\Delta lmdAE$  mutant had the strongest phenotype of all double deletions (Figure 9). As supposed, a  $\Delta amiC \Delta lmdA$  double deletion leads to a drastic phenotypic defects. The cells were not able to correctly divide and therefore reached cell length up to nearly 20  $\mu\text{m}$  (Figure 13B). In addition, we further checked for an additive effect by deletion *lmdF* in the  $\Delta amiC \Delta lmdA$  double mutant. The resulting  $\Delta amiC \Delta lmdAF$  triple mutant displayed the most severe morphological defect and the longest cells of all strains generated. Single cells up to 24  $\mu\text{m}$  were observed, which mostly consist of one extremely long stalk, sometimes interrupted by deformed cell bodies (Figure 13A). Finally, we created a strain were *amiC* and all M23 endopeptidase genes (except *lmdC*) were deleted. The cells were viable but elongated showing again the redundancy of those classes of enzymes (Figure 13A). The cell length was in the same range as the  $\Delta amiC \Delta lmdA$  mutant.

In addition, we performed growth experiments to check for growth defects of the generated mutants. Even though, the deletion of *amiC* strongly affects the cell morphology, it did not change its growth behavior (Figure S4C and Table S1). Under normal growth conditions wild-type cells of *H. neptunium* form a biofilm. However, biofilms formation was abolished in all tested strains and none displayed an obvious growth defect (Figure S4C and Table S1).

Taken together, the combination of the  $\Delta amiC$  mutation with the deletion of specific M23 endopeptidase genes seems to severely affect cell division and bud synthesis. *H. neptunium* cells are not able to separate their cell bodies anymore and therefore continue with stalk elongation. However, this elongation is not endless. As suggested, the  $\Delta amiC \Delta lmdE/F$  mutant did not show any additive effect, proposing an interaction in the same pathway.



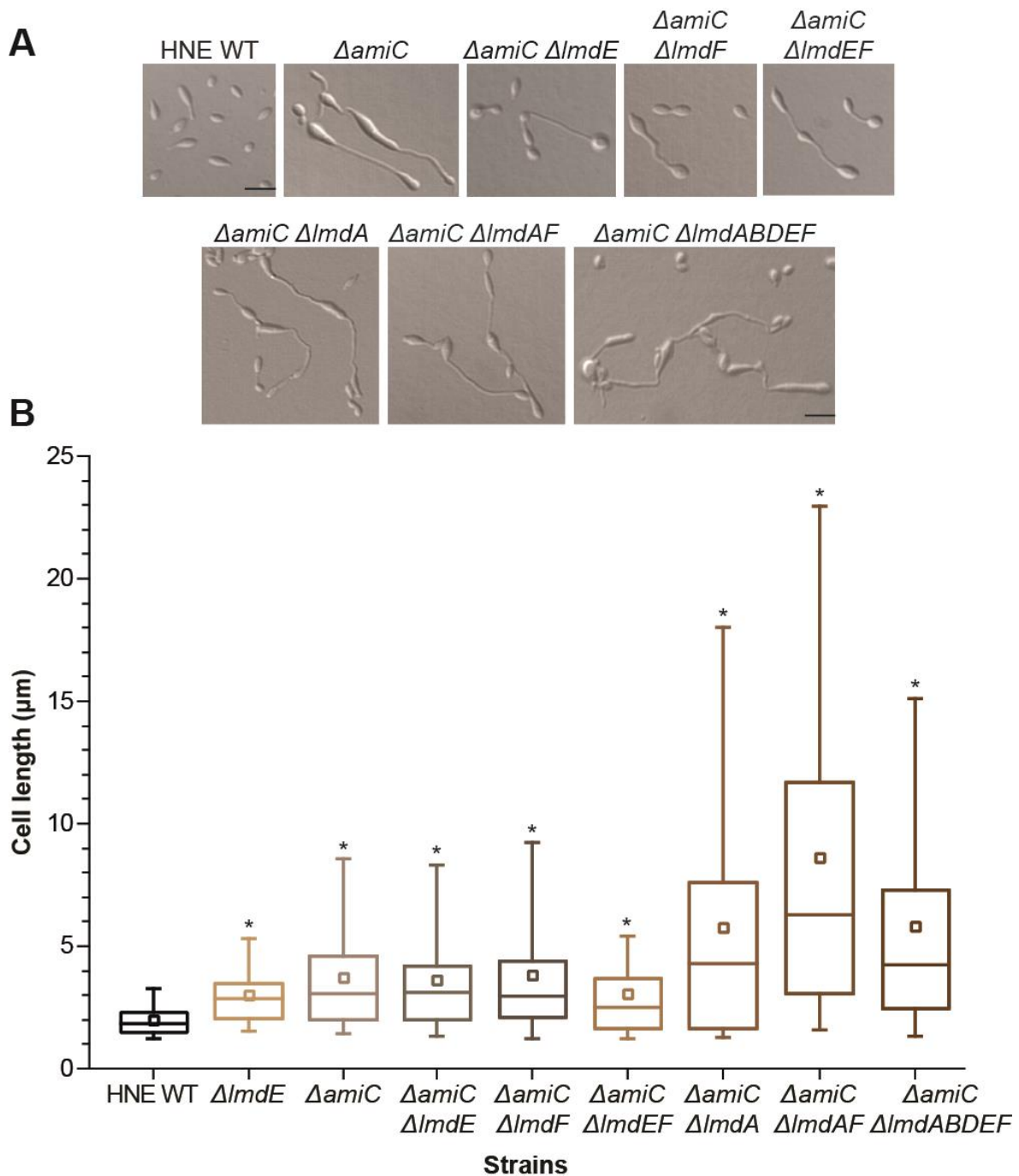


**Figure 13: Influence of the amidase AmiC and the M23 endopeptidases on the cell length and division of *H. neptunium*.** (A) Phenotype of the wild type (HNE WT), the single mutants EC39 ( $\Delta lmdE$ ) and SR18 ( $\Delta amiC$ ), the double mutants SR36 ( $\Delta amiC \Delta lmdE$ ), SR37 ( $\Delta amiC \Delta lmdF$ ) and SR47 ( $\Delta amiC \Delta lmdA$ ) and the triple mutants SR42 ( $\Delta amiC \Delta lmdAF$ ), SR55 ( $\Delta amiC \Delta lmdEF$ ) and SR60 ( $\Delta amiC \Delta lmdABDEF$ ). Cells were either grown in MB medium or ASM at 28°C (shaking at 210 rpm) to the exponential phase and analyzed microscopically. Scale bar: 3  $\mu$ m. (B) Cell lengths of the indicated strains. Cells were grown as described in (A). The distribution of cell lengths is shown as a box plot (explanation see Figure 9). Asterisks indicate a  $p$ -value of < 0.0001 ( $t$ -test).

An elegant method to identify interaction partners of any protein of interest is co-immunoprecipitation (Co-IP) followed by mass spectrometric analysis, because this allows the identification of novel and unknown binding partners. To identify potential interaction partners of AmiC, Co-IP analysis was performed (in collaboration with Dr. Timo Glatter,

Max-Planck-Institut, Marburg). Since antibodies against AmiC are currently not available, we used the stable AmiC-mCherry fusion (SR23) and antibodies against the mCherry protein. Transient protein-protein interactions were stabilized by cross-linking with paraformaldehyde prior to Co-IP followed by mass spectrometric analysis and the experiment was done in triplicates. Several proteins were detected that were specifically enriched on the anti-RFP beads. Among them were AmiC and the mCherry protein, showing that both were binding to the anti-RFP beads. In Table S2, we summarized the most significantly enriched genes, which are interesting candidate interactors of AmiC. They were sorted according to their index values, which gives the relative protein abundance in comparison to the wild type cells (control sample). All identified proteins have a predicted localization in the periplasm and are either membrane-integral or soluble. Beside well-known proteins such as FtsQ and MreC, we also found the previously investigated PBP1X and RlpA (Cserti *et al.*, 2017). RlpA of *P. aeruginosa* has a function in daughter cell separation and rod shape (Jorgenson *et al.*, 2014). However, it is dispensable for growth and morphology in *H. neptunium* (Cserti, 2016). Another interesting candidate is CpoB (*HNE\_0156*), which is a component of the Tol-Pal complex (Gerding *et al.*, 2007). In *E. coli*, CpoB (coordinator of PG synthesis and outer membrane constriction, associated with PBP1B) interacts with PBP1B-LpoB and TolA at the onset of constriction (Gray *et al.*, 2015). CpoB of *H. neptunium* is an essential protein (unpublished data). However, the majority of identified genes are uncharacterized proteins with conserved domains of unknown function (Table S2). Future investigations have to show if these putative candidates interact or influence AmiC.

### 2.1.6 AmiC-mCherry localization in the $\Delta$ *lmdE* mutant

As we previously showed in our epistasis experiments, the simultaneous deletion of  $\Delta$ *amiC* and  $\Delta$ *lmdE* did not lead to an additive phenotype, suggesting that both proteins act in the same pathway. However, the likelihood that AmiC and LmdE operate in the same pathway does not reveal how they interact. One possibility is that LmdE activates AmiC. Another option is that LmdE helps AmiC to localize to the site where PG hydrolysis occurs. The latter hypothesis was tested by localization experiments. An inducible AmiC-mCherry fusion protein was introduced into the *lmdE* mutant and analyzed by fluorescence microscopy. As expected, no fluorescence was observed at the onset of induction (Figure 14A). After the fusion protein had been produced for several hours, a diffuse distribution was visible in the cell body and the stalk. A clear focus of AmiC-mCherry at the future stalked pole was occasionally visible but a signal at the division plane could not be detected during the course of the experiment. In confirmation, a diffuse pattern can be seen in the demograph as well (Figure 14B). Western blot analysis showed a high stability of the fusion protein (Figure S2B). In essence, this suggests that AmiC does not localize in the normal way once LmdE is missing. However, a definitive interpretation of these results is difficult due to a weak fluorescence signal and the elongated and misshapen cells.

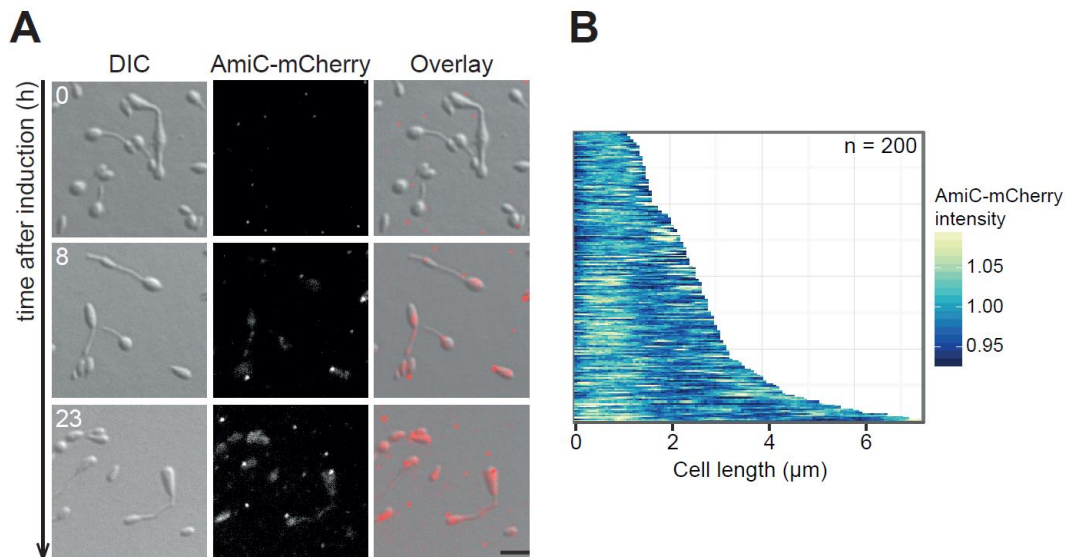


**Figure 14: Deletion of *lmdE* affects the localization pattern of AmiC-mCherry.** (A) AmiC-mCherry localizes throughout the cell body of the *H. neptunium*  $\Delta lmdE$  mutant. SR71 ( $\Delta lmdE$   $P_{Cu}::P_{Cu-amiC-mCherry}$ ) was grown to exponential phase in ASM, induced with 300  $\mu\text{M}$   $\text{CuSO}_4$  and imaged by DIC and fluorescence microscopy. Scale bar: 3  $\mu\text{m}$ . (B) Distribution of AmiC-mCherry fluorescence in cells of SR71 strain, shown in a demograph (based on images from A).

## 2.2 The FtsEX complex of *H. neptunium*

In  $\gamma$ -proteobacteria, such as *E. coli*, the inactive endopeptidases EnvC and NlpD activate the amidases AmiA, AmiB, and AmiC in the periplasm (Uehara *et al.*, 2010). In addition, the inner membrane-embedded FtsEX complex was showed to be involved in this process by interacting with EnvC (Yang *et al.*, 2012). The current model implies that FtsE hydrolyzes ATP, leading to a conformational change in FtsX. Subsequently, the interaction of a periplasmic loop of FtsX with EnvC activates the latter, which then in turn activates AmiA and AmiB (Yang *et al.*, 2011). *E. coli* cells can survive a deletion of *ftsEX* if high-salt medium is provided (Schmidt *et al.*, 2004; Yang *et al.*, 2011). In contrast, in *C. crescentus* only the deletion of *ftsE* was possible, resulting in cells with thin tubular connections between their cell bodies (Meier *et al.*, 2017). Therefore, we were particularly interested in the FtsEX complex of *H. neptunium* and its potential role in cell separation.

Bioinformatic analysis resulted in the identification of an operon where *HNE\_3390* was predicted as a cell division ATP-binding protein and *HNE\_3391* as a permease protein. The smaller gene, *HNE\_3390*, was named *ftsE* and its product contained of a single predicted ABC-transporter domain (Figure 15A). A cytoplasmic localization is likely due to the lack of a signal sequence. *HNE\_3391*, which only consists of transmembrane segments, was named FtsX. Like for FtsX<sub>EC</sub>, a larger periplasmic loop domain is predicted for FtsX<sub>HNE</sub>.

In a first attempt, we tried to delete the *ftsEX* operon of *H. neptunium*. Even though we did not obtain many positive clones, we manage to delete both genes. The knockout of *ftsEX* severely affected the morphology of the resulting cells. Stalks were highly elongated and showed misshapen cell bodies within the stalk structure (Figure 15B). Some stalks appeared thinner than normal ones. Measurements of the cell length indicated significant differences in comparison to the wild type (Figure 15C). A complementation experiment

revealed that the observed phenotype is exclusively due to the deletion of *ftsEX*. When native FtsEX was induced for 21 h in the  $\Delta$ *ftsEX* mutant, cells showed normal cell shape and length (Figure 15C and D).

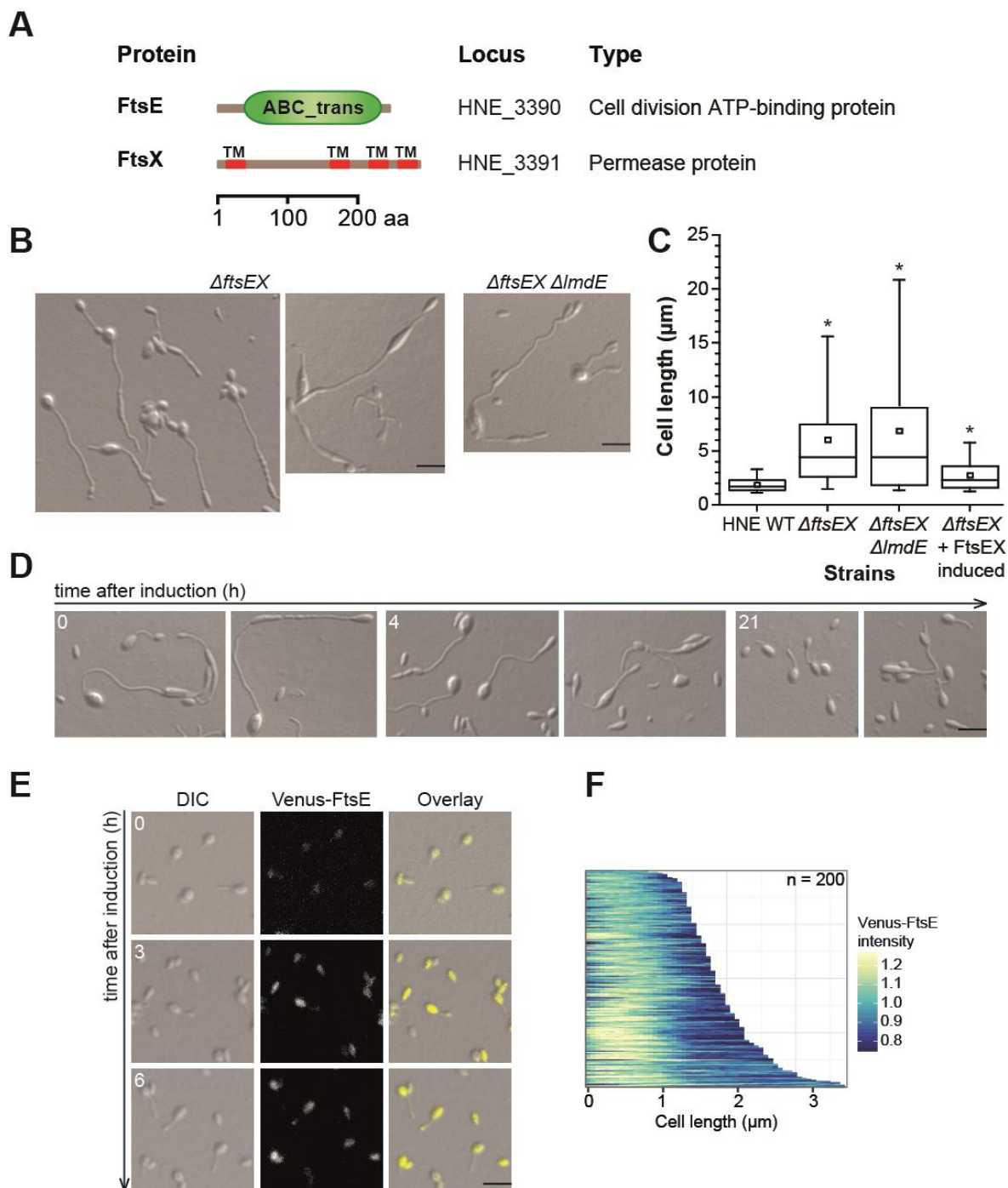


**Figure 15: The FtsEX complex is involved in cell separation.** (A) Graphical representation of the FtsE and FtsX proteins of *H. neptunium*. Domains were identified using the Pfam database (Bateman et al., 2004; Finn et al., 2010). The SMART database was used to depict the proteins (Letunic et al., 2009; Schultz et al., 1998). Abbreviations: TM: transmembrane segment; ABC\_trans: ABC transporter; aa: amino acids. (B) Deletion of *ftsEX* and combined deletion of *ftsEX* and *lmdE* causes severe morphological defects with highly elongated stalks. Phenotype of the double deletion strain SR64 ( $\Delta$ *ftsEX*) and the triple deletion strain SR80 ( $\Delta$ *ftsEX*  $\Delta$ *lmdE*). Cells were grown in ASM at 28°C (shaking at 210 rpm) to the exponential phase and analyzed microscopically. Scale bar: 3  $\mu$ m. (C) Cell lengths of the indicated strains. Cells were grown as described in (B). The distribution of cell lengths is shown as a box plot (explanation see Figure 9). Asterisks indicate a *p*-value of < 0.001 (*t*-test).

**Figure 15 (continued): (D)** Complementation of the  $\Delta ftsEX$  mutant with native FtsEX restores the wild-type morphology. SR76 ( $\Delta ftsEX P_{Cu}::P_{Cu}-ftsEX$ ) was grown to exponential phase in ASM, induced for 21 h with 300  $\mu$ M  $CuSO_4$  and imaged by DIC microscopy. Scale bar: 3  $\mu$ m. **(E)** Venus-FtsE shows a diffuse localization pattern. JZ12 ( $P_{Zn}::P_{Zn}-venus-ftsE$ ) was grown to exponential phase in ASM, induced for 6 h with 300  $\mu$ M  $ZnSO_4$  and imaged by DIC and fluorescence microscopy. Scale bar: 3  $\mu$ m. **(F)** Venus-FtsE fluorescence intensity in JZ12 cells depicted in a demograph (based on images from D).

In a further attempt, FtsE was localized to test if its localization pattern was similar to that of AmiC. To this end, an inducible *venus-ftsE* version was introduced into the wild type of *H. neptunium*. The fusion protein was fully stable (Figure S2C) (Zimmer, 2013). Fluorescence was observed throughout the cell body and the bud (Figure 15E), and foci at the stalked pole or at the division plane were not observed. Possibly, the expression level of *venus-ftsE* and the right time point during the cell cycle is crucial to see the localization to the sites of PG remodeling. The Venus-FtsE fluorescence intensity, depicted in a demograph, confirmed a strong signal in the cell body (Figure 15F). In short, the FtsEX complex is not essential in *H. neptunium*, though important for normal cell shape and division.

However, the question if LmdE and FtsEX interact or reside in the same pathway was not answered. To this end, we again performed an epistasis experiment, deleted *lmdE* in the  $\Delta ftsEX$  mutant, and tested for synthetic lethality. Interestingly, the resulting strain SR80 ( $\Delta ftsEX \Delta lmdE$ ) was viable but showed a highly aberrant morphology similar to the *ftsEX* double mutant (Figure 15B). Cells exhibited severely elongated stalks and some cell bodies were rounder or more misshapen than normal ones. The cell length was slightly increased in comparison to the  $\Delta ftsEX$  mutant (Figure 15C). However, the median was nearly identical. The growth behavior and rate of the  $\Delta ftsEX$  and  $\Delta ftsEX \Delta lmdE$  strains was determined (Figure S4D and Table S1). Both strains form the highest amount of biofilm ever detected for a *H. neptunium* strain. Hence, the number of planktonic cells was low (and the measured  $OD_{580}$  values were low), since cells formed a biofilm. Conclusively, the results suggested that LmdE and FtsEX act in the same pathway, since additive effects were not observed.

### 2.2.1 AmiC-mCherry localization in the $\Delta ftsEX$ mutant

It is still unclear if FtsEX regulates LmdE. One possibility is that the periplasmic loop of FtsX stimulates/activates LmdE, which in turn relays the activation to AmiC. Another option is that the FtsEX complex helps LmdE to localize and thus subsequently localizes AmiC. The second hypothesis was investigated by a localization experiment. An inducible AmiC-mCherry fusion protein was introduced into the  $\Delta ftsEX$  mutant and analyzed by fluorescence microscopy. As expected, cells were not fluorescent before induction (Figure 16A). After the production of AmiC-mCherry for several hours, a diffuse distribution was observed in the cell body and discontinuous in the stalk. A clear focus of the fusion protein at the stalked pole or at the division plane was not visible during the course of the experiment. In addition, the diffuse distribution can be seen in the demograph (Figure 16B). This pattern is not due to protein degradation since Western blot analysis confirmed the stability of the fusion protein (Figure S2B). In summary, those results indicate that AmiC does not localize in the normal way once FtsEX is missing. However, it is difficult to draw definitive conclusions from these results due to the elongated and misshapen stalks.

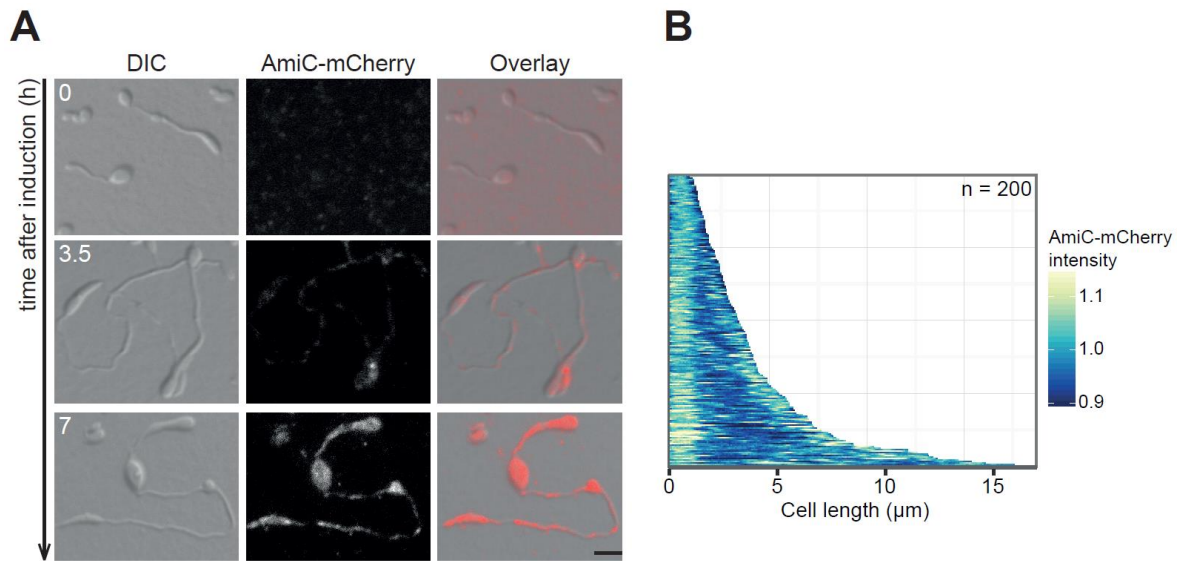


**Figure 16: Deletion of *ftsEX* affects the localization pattern of AmiC-mCherry.** (A) AmiC-mCherry localizes in the whole cell body of *H. neptunium*  $\Delta$ *ftsEX*. SR72 ( $\Delta$ *ftsEX*  $P_{Cu}::P_{Cu}$ -*amiC-mCherry*) was grown to exponential phase in ASM, induced with 300  $\mu$ M  $CuSO_4$  and imaged by DIC and fluorescence microscopy. Scale bar: 3  $\mu$ m. (B) AmiC-mCherry fluorescence intensity in SR72 cells is depicted in a demograph (based on images from A).

## 2.3 Protein purification and in vitro assays

So far, we concentrated on the *in vivo* characterization of AmiC, FtsEX and the M23 endopeptidases. To further analyze the potential interaction of the key proteins AmiC and LmdE, we started to perform *in vitro* biochemical experiments. To this end, we purified certain proteins. All proteins were His-SUMO-tagged and purified by Ni-affinity chromatography (see Material and Methods 4.5.5.). In a second step, the His-SUMO (small ubiquitin-related modifier) tag was successfully cleaved using the specific His-Ulp1 (SUMO protease 1) (Malakhov *et al.*, 2004). First, AmiC and LmdE were purified, followed by a second M23 endopeptidase LmdA (Figure 17) and LmdA, a putatively active endopeptidase, served as a control enzyme. Next, a catalytically inactive version of AmiC was generated and purified. The glutamate residue in the active center at position 370 (E370) was replaced by alanine (AmiC<sup>E370A</sup>). This mutation should repress the proton transfer from the substrate and prevent AmiC to hydrolyze PG (Christianson *et al.*, 1989; Rocaboy *et al.*, 2013). To analyze which domain of LmdE might interact with AmiC, the protein was divided into two parts. The larger coiled-coil domain (LmdE<sup>CC</sup>) and the smaller M23 peptidase domain (LmdE<sup>M23</sup>) of LmdE were separately purified (Figure 17). Finally, the predicted periplasmic loop of FtsX was purified (FtsX<sup>Loop1</sup>) to test if this loop domain could stimulate or repress the activity of LmdE.



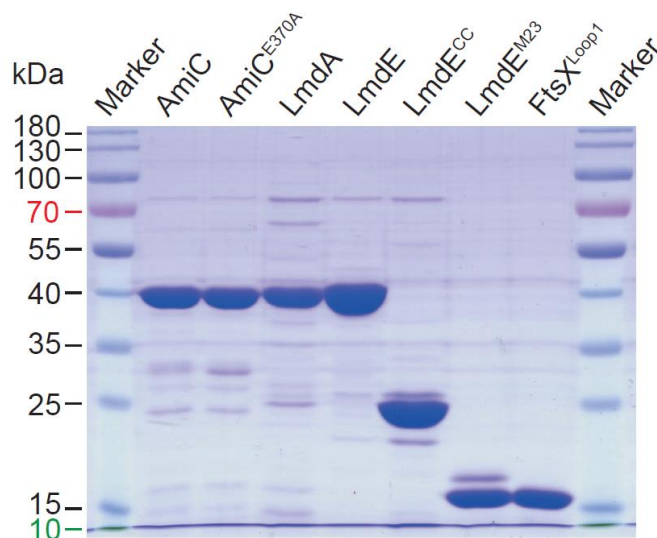


**Figure 17: Purified proteins or protein domains used for *in vitro* assays.** 5  $\mu$ g of each sample was loaded. Proteins (AmiC, AmiC<sup>E370A</sup>, LmdA and LmdE) and protein domains (LmdE<sup>CC</sup>, LmdE<sup>M23</sup> and FtsX<sup>Loop1</sup>) were purified and analyzed by SDS-PAGE as described in Material and Methods (4.5.5.).

### 2.3.1 The role of LmdE in AmiC activation

Amidases are important enzymes for cell division in *E. coli* and many other bacteria. However, they are redundant and in *E. coli* only a triple deletion caused a severe phenotype (Heidrich *et al.*, 2001). The activation of these amidases is dependent on the action of the catalytically inactive M23 endopeptidases EnvC and NlpD, which lack critical residues in their peptide active sites (Uehara *et al.*, 2009). The binding of these inactive enzymes to their cognate amidase stimulates and activates the amidases, leading to PG hydrolysis. So far, this mechanism was mainly observed in  $\gamma$ -proteobacteria.

It was unknown whether the AmiC of *H. neptunium* is stimulated or activated by other regulatory proteins or enzymes. A structural model of AmiC clearly showed the presence of an inhibitory helix covering the predicted active site of the protein (data not shown; modelled with *E. coli* AmiC as template), suggesting a similar mode of activation. These results also indicate that the M23 endopeptidase LmdE with its predicted partial M23 peptidase motif might be a promising candidate to regulate AmiC. We already showed that the two proteins likely act in the same pathway (2.1.5). For the first time, this could reveal a conserved mechanism of activation between  $\alpha$ - and  $\gamma$ -proteobacteria.

Enzymes of interest can be tested for their ability to hydrolyze PG with a dye-release assay (Uehara *et al.*, 2010; Zhou *et al.*, 1988). We labeled PG sacculi with Remazol Brilliant Blue (RBB), which binds to the hydroxyl groups of sugars and therefore to the glycan backbone (Stamm, 1963). A mixture of the enzymes of interest and sacculi were incubated for a specific time, heat-inactivated and pelleted afterwards. Bound RBB would pellet with the sacculi, whereas released dye would remain in the supernatant and color it blue. Thus, a release of the dye is equivalent to the release of PG fragments from the intact sacculi, indicating hydrolysis and therefore catalytic activity of the tested enzyme. Finally, dye-release was analyzed by measuring the absorption of the supernatant and visually by color change.

Several attempts to purify the PG of *H. neptunium* were unsuccessful (data not shown). Therefore, we decided to use PG sacculi of wild-type *C. crescentus*, since the PG composition of both species is very similar (Cserti *et al.*, 2017). Subsequently, these RBB-labeled PG sacculi were incubated with the protein(s) of interest (4  $\mu$ M). Buffer with PG sacculi served as a negative control in which no PG hydrolysis occurred. Mixtures containing lysozyme were used as a positive control because this enzyme cleaves the glycan backbone between the MurNAc and GlcNAc. When lysozyme was incubated with RBB-labeled PG sacculi a high absorption was observed ( $>0.16$  units) and the supernatant turned blue (Figure 18A). Both observations showed the reliability of the assay for the detection of PG hydrolysis.

Next, either AmiC or LmdE were incubated together with PG sacculi. No dye-release was observed (Figure 18A). Nevertheless, the absorption value obtained with AmiC was slightly increased in comparison to the negative control, pointing to a weak basal activity. LmdE alone was not active. However, a significant increase in dye-release was measured when AmiC and LmdE were incubated together. This was confirmed by a clear color change (Figure 18A). To rule out the possibility that the two proteins act not in accordance but successively, e.g. by LmdE processing PG to make it accessible to AmiC, we performed a control experiment. For this purpose, we incubated RBB-labeled PG sacculi with AmiC and LmdE in a sequential manner. First, AmiC was added, incubated and heat-inactivated, then LmdE was added, incubated and heat-inactivated. The experiment was then also performed in the inverse order. The values obtained, were similar to the ones of the single AmiC sample (data not shown). Thus, the presence and interaction of both enzymes is crucial for their reaction.

Afterwards, we tested FtsX<sup>Loop1</sup> for an enhancing or repressing effect on the AmiC-LmdE interaction. No difference was observed and the reaction occurred as effectively as before (Figure 18A). This could suggest that either the full-length FtsX is needed for an interaction that the protein domain did not adopt the active conformation required for stimulation or that FtsX does not stimulate LmdE. Finally, we analyzed the inactive variant of AmiC. Incubation of AmiC<sup>E370A</sup> with RBB-labeled PG sacculi did not lead to cleavage of PG. Even the basal weak activity seen before was completely abolished. As expected, the addition of LmdE did not stimulate the reaction and lead to PG lysis (Figure 18A). Moreover, we tried to complement the  $\Delta$ amiC mutant by introducing an inducible *amiC*<sup>E370A</sup> allele to test if the present of a catalytically inactive AmiC variant was sufficient for a normal wild-type morphology. AmiC<sup>E370A</sup> was not able *in vivo* to restore the wild-type phenotype and cells still showed the characteristic  $\Delta$ amiC morphology (Figure S3B). This observation was additionally verified by cell length measurements (Figure S3B).

Taken together, these results suggest that both AmiC and LmdE are needed to successfully hydrolyze PG. LmdE is indeed an inactive M23 endopeptidase and only the active version of AmiC (not the inactive AmiC<sup>E370A</sup>) could hydrolyze PG. The precise function of the periplasmic loop of FtsX is not solved, yet. Thus, in *H. neptunium* the catalytically inactive LmdE is needed for the activity of AmiC.



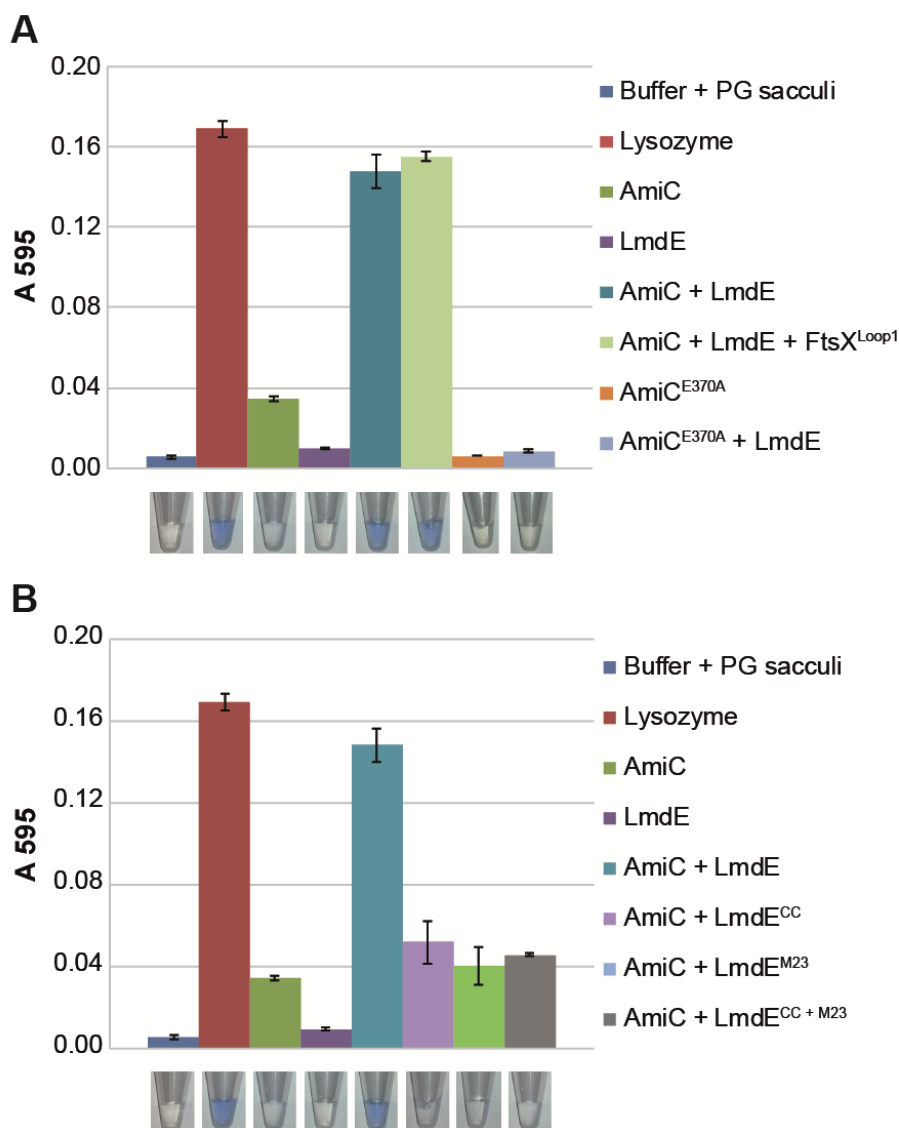


**Figure 18: The catalytically inactive endopeptidase LmdE stimulates the activity of the amidase AmiC *in vitro*.** (A) Dye-release assay for PG hydrolysis. RBB-labelled PG sacculi were incubated with the indicated proteins (4  $\mu$ M each) for 2 h at 37°C. Undigested PG was pelleted and the absorbance of the supernatant was measured at 595 nm. Reactions were performed in triplicate and the error bars indicate the standard deviation. Supernatants of samples are shown below. Blue color indicates the release of dye and therefore PG hydrolysis. (B) The coiled-coil and/or the M23 domain of LmdE cannot activate AmiC. The dye-release assay for PG hydrolysis was performed as in (A).

After we showed that full-length LmdE activated AmiC, we wondered which part of LmdE was responsible for the activation. Therefore, the assay was performed using the purified LmdE domains (LmdE<sup>CC</sup> and LmdE<sup>M23</sup>) instead of the full-length LmdE. Incubation of AmiC with either LmdE<sup>CC</sup> or LmdE<sup>M23</sup> did not lead to PG hydrolysis (Figure 18B). Even though the measured values were higher than the ones obtained with the negative control, they were in the range of the AmiC sample. Subsequently, LmdE<sup>CC</sup> and LmdE<sup>M23</sup> were added together to AmiC and incubated. No dye-release was visible and no PG hydrolysis occurred. Although it is possible that the LmdE domains did not fold properly and therefore could not interact with the amidase, there reasons suggested that full-length LmdE is essential for the activation of AmiC.

### 2.3.2 LmdA is an active endopeptidase

The results of the dye-release assay clearly indicated that LmdE is not active as an enzyme and unable to hydrolyze PG. This was already expected based on the alignment of the M23 peptidase domains (Figure 8B). The other endopeptidases, LmdABCDF, showed a complete M23 motif and should thus cleave the stem peptides of PG. However, the question arose whether they are active on their own or if they need additional regulatory proteins for their function. Notably, the *lmdA* gene showed one of the strongest phenotypes in the performed deletion and epistatic studies. Therefore, LmdA was chosen as a representative endopeptidase and purified. LmdA was applied to RBB-labeled PG sacculi and the reaction was monitored as before (Figure 19). Dye-release was visible in the supernatant (light blue). Although, the absorbance values were not as high as for the lysozyme or AmiC with LmdE, the difference to the negative control was highly significant. This result showed that LmdA is active on its own.

Nevertheless, we incubated LmdA in the presence of LmdE to check for any stimulating or repressing effects (Figure 19). None were observed, meaning that LmdE did not affect the ability of LmdA to cleave PG at all. Next, we tried a combination of LmdA and AmiC, to test if LmdA would act in a similar way to LmdE. A minor increase in the absorbance was detected, pointing to an additive effect and AmiC was clearly not stimulated by LmdA. The increase can be explained by the weak basal activity of AmiC. Lastly, LmdA, AmiC and LmdE were incubated together to analyze the additive effect. The result was the same as without LmdA (Figure 19). Collectively, we were able to prove our hypothesis that LmdA is an active M23 endopeptidase and does not require other regulatory proteins. These results underline the specificity of the AmiC-LmdE interaction.

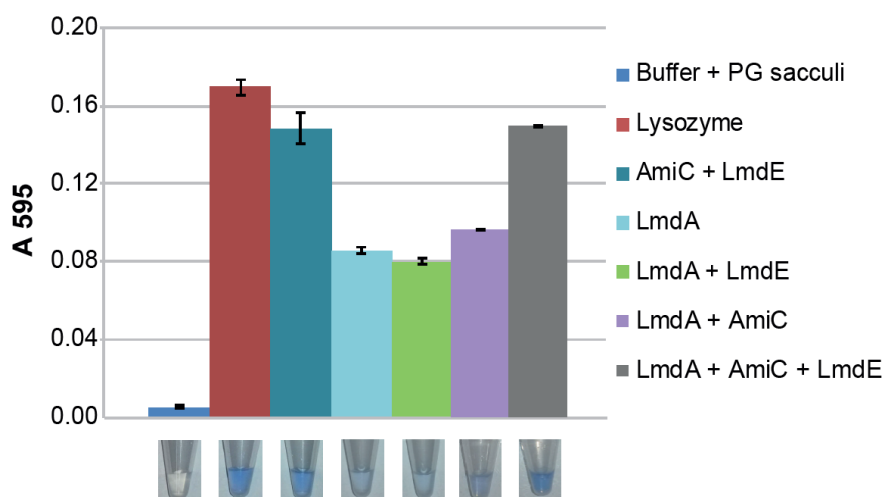


**Figure 19: The M23 endopeptidase LmdA is an active enzyme.** LmdA can hydrolyze PG and the addition of LmdE or AmiC did not influence the activity. Dye-release assay for PG hydrolysis was performed as in Figure 18.

### 2.3.3 AmiC and LmdE physically interact

AmiC and LmdE of *H. neptunium* interact to hydrolyze PG in the dye-release assay. Nevertheless, this result is not a full proof that both enzymes interact physically. Studies in *E. coli* failed to show a direct interaction using a biochemical method, since it was not easy

to prove binding of EnvC to AmiA/B based on the fact, that it should be a transient interaction. Most likely, the reaction is also transient in *H. neptunium* because cleavage of the amidase is only needed at the late stage of cell division in a short time frame.

To test AmiC for a physical interaction with LmdE *in vitro*, we used the Bio-Layer Interferometry (BLI) technology. In this assay, proteins of interest were biotinylated by incubation with NHS-PEG<sub>4</sub>-biotin. Next, the biotinylated protein was immobilized on a streptavidin biosensor, and the non-labeled analyt was flushed over the surface. Protein interactions could be detected in real time and the association and dissociation traces are recorded. Biotinylated AmiC showed a strong binding to the biosensor, whereas non-specific binding of non-labeled LmdE was barely observed (Figure S5A). We started with different concentrations of LmdE (0 – 150  $\mu$ M) and probed them against immobilized AmiC-Biotin (Figure 20). LmdE displayed binding to immobilized AmiC in a clear concentration-dependent manner (Figure 20). As expected, LmdE could be washed off in the dissociation phase (time = 150 sec), suggesting a transient and fast interaction. Taken together, these results strongly point to a physical interaction of AmiC to its catalytically inactive regulator protein LmdE.

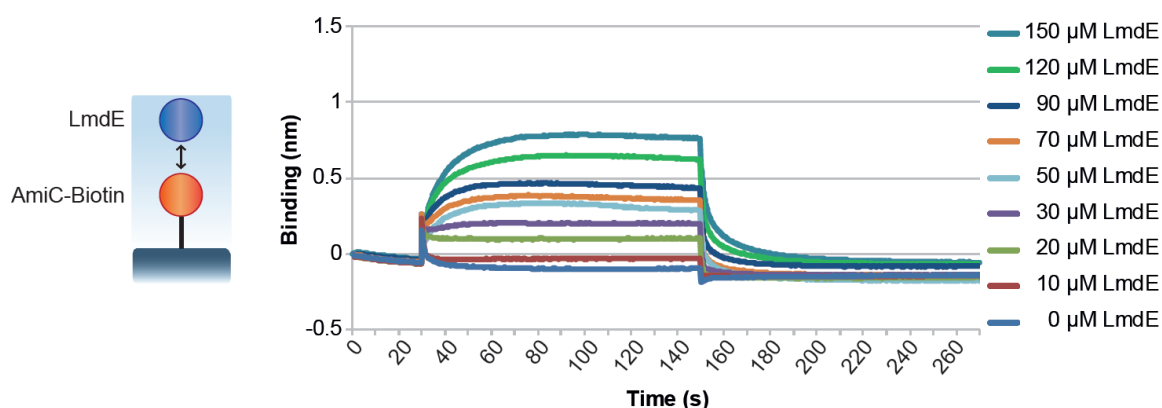


**Figure 20: LmdE binds to AmiC in a concentration-dependent way.** AmiC-Biotin (red circle) was immobilized on a streptavidin biosensor (dark blue square) and probed with LmdE (blue circle) by BLI. Binding of LmdE (0 – 150  $\mu$ M) to biotinylated AmiC (30  $\mu$ M) was recorded. The graph shows LmdE binding to AmiC (association), followed by LmdE dissociation.

Then, we tried the reaction vice versa with different concentrations of AmiC (0 – 150  $\mu$ M) and probed them against immobilized LmdE-Biotin (Figure 21). As before, biotinylated LmdE strongly bound to the biosensor, whereas non-specific binding of non-labeled AmiC was not observed (Figure S5B). Similar to the previous reaction, AmiC displayed binding to immobilized LmdE in a concentration-dependent manner (Figure 21). Surprisingly, AmiC could not be washed off completely in the dissociation phase (time = 180 sec). This would argue for a stronger and tighter interaction. Maybe the orientation of the protein on the chip is important for the binding properties. Most important, these results underline a physical interaction of AmiC with LmdE.

To validate that this interaction is specific and does not occur due to random binding of AmiC to the endopeptidases, we performed a control experiment. We biotinylated LmdA as a related M23 endopeptidase that did not stimulate AmiC activity *in vitro* and probed non-labeled AmiC. As expected, biotinylated LmdA bound to the biosensor (data not shown).

When different concentrations of AmiC were probed against immobilized LmdA-Biotin, no binding could be detected (data not shown). Thus, AmiC binds specifically to LmdE.

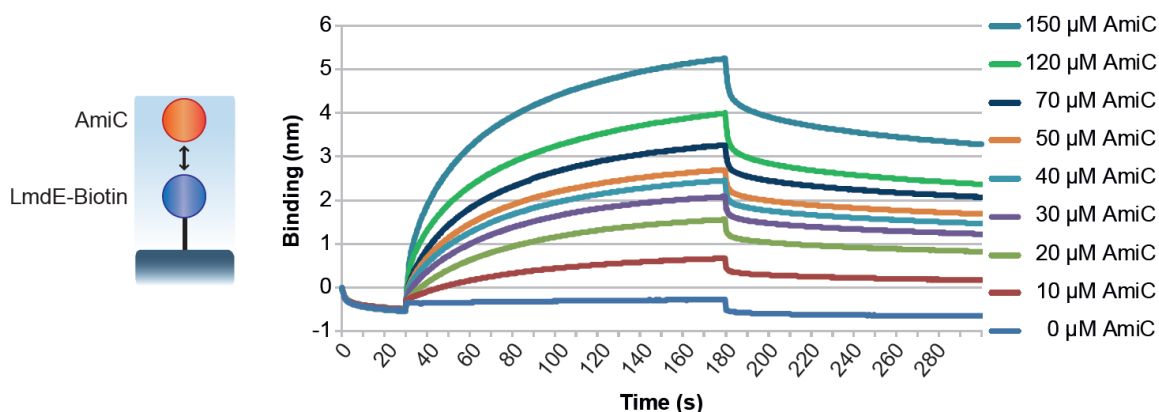


**Figure 21: AmiC binds to LmdE in a concentration-dependent way.** LmdE-Biotin (blue circle) is immobilized on a streptavidin biosensor (dark blue square) and probed with AmiC (red circle) by BLI. Binding of AmiC (0 – 150  $\mu$ M) to biotinylated LmdE (30  $\mu$ M) was monitored. The graph shows AmiC binding to LmdE (association), followed by AmiC dissociation.

After we showed that full-length LmdE binds to AmiC, we wondered which part of LmdE is responsible for this interaction. Therefore, another BLI experiment was performed as before using the purified LmdE domains (LmdE<sup>CC</sup> and LmdE<sup>M23</sup>) instead of full-length LmdE. Non-specific binding of non-labeled LmdE<sup>CC</sup> and/or LmdE<sup>M23</sup> to the sensor surface was not observed at all (Figure S5C). Two concentrations of LmdE<sup>CC</sup> (50  $\mu$ M and 100  $\mu$ M) were probed and displayed no binding to immobilized AmiC (Figure 22A). When LmdE<sup>M23</sup> was used, no binding occurred in the association phase (Figure 22B). Finally, incubation of AmiC-Biotin with both LmdE<sup>CC</sup> and LmdE<sup>M23</sup> did not lead to any interaction (Figure 22C). As speculated before, it is possible that the LmdE domains were not functional or that only the full-length protein can interact with the amidase. We also tested the reaction in an inverse way and biotinylated LmdE<sup>CC</sup> to rule out the possibility that the biotinylation of AmiC blocks the interaction. However, no binding was detected between the two proteins (data not shown).

In the dye-release assay, we showed that FtsX<sup>Loop1</sup> did not influence the reaction of AmiC and LmdE (Figure 18A). However, the interaction of the periplasmic loop domain of FtsX with EnvC of *E. coli* was shown in a bacterial two-hybrid assay (Yang *et al.*, 2011). The authors suggested that this interaction activates EnvC, which in turn activates AmiA and AmiB. We biotinylated purified FtsX<sup>Loop1</sup> and tested for binding to LmdE. The reaction was also performed vice versa using LmdE-Biotin and non-tagged FtsX<sup>Loop1</sup>. No binding was detected under the tested conditions (data not shown). Thus, either the loop domain had the wrong conformation to bind to LmdE or full-length FtsX or even the whole FtsEX complex is needed to observe an interaction.

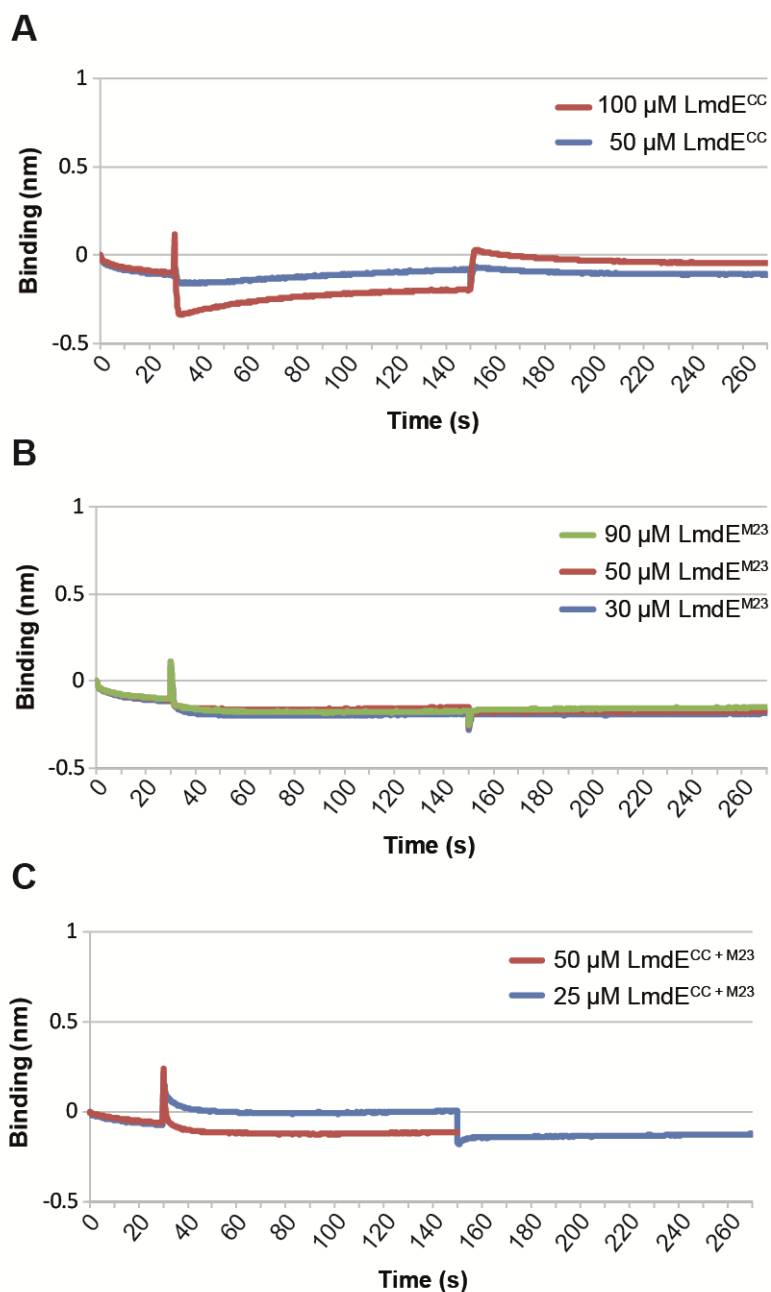


**Figure 22: Full-length LmdE is needed for binding to AmiC.** (A) Binding of LmdE<sup>CC</sup> to biotinylated AmiC (30 μM) was tested by BLI. AmiC was immobilized on a streptavidin biosensor. The graph shows LmdE<sup>CC</sup> binding to AmiC (association), followed by LmdE<sup>CC</sup> dissociation. (B) Binding of LmdE<sup>M23</sup> to biotinylated AmiC (30 μM) was tested by BLI as in (A). (C) Binding of LmdE<sup>CC+M23</sup> to biotinylated AmiC (30 μM) was tested by BLI as in (A).

## 2.4 Carboxypeptidases of *H. neptunium*

### 2.4.1 Deletion studies of the three carboxypeptidases

The main focus of this study was to analyze the role of endopeptidases and the amidase in the cell morphology of *H. neptunium*. However, other classes of PG remodeling enzymes (lytic transglycosylases, carboxypeptidases, and glycosyl hydrolases) are also involved in the regulation of cell shape. Hence, carboxypeptidases were chosen as an example and investigated in more detail. They cleave the last amino acid (e. g. D-alanine) of the peptide side chains, which are needed to cross-link PG (Glauner & Holtje, 1990). Therefore, carboxypeptidases control the degree of cross-linking. Six carboxypeptidases that belong to the class C of PBPs are known in *E. coli* (Typas *et al.*, 2012).

By contrast, *H. neptunium* only possesses three genes, which were found in a bioinformatic analysis (Cserti *et al.*, 2017; Rosskopf, 2014). They were named DacB, DacH and DacL (D-alanine-D-alanine carboxypeptidase). DacH and DacL are specific for *H. neptunium* and its relatives, whereas DacB is a close homolog of DacB from *E. coli* (Cserti *et al.*, 2017; Korat *et al.*, 1991). All three proteins have a predicted signal peptide and presumably localize in the periplasm (Figure 23A). They have a characteristic peptidase S13 or a  $\beta$ -lactamase\_2 domain. In addition, DacL possesses a PBP5\_C domain, which is distinctive for PBP5 of *E. coli*, but its precise function is unknown (Davies *et al.*, 2001).

First, deletion studies were performed to better analyze the significance of the carboxypeptidases and their contribution to cell morphology. All of them could be deleted in previous experiments and thus turned out to be dispensable (Rosskopf, 2014). The  $\Delta dacH$  and  $\Delta dacL$  mutants did not show any aberrant phenotype (Figure 23B). By contrast,  $\Delta dacB$  cells displayed elongated stalks and an increased cell length (Figure 23B and C). In a complementation experiment wild-type morphology was restored by the production of DacB in the mutant background (Figure S6). Second, we aimed to investigate the redundancy of these proteins in more detail by introducing multiple deletions. As expected, the combination of deletions in *dacH* and *dacL* had no negative effect on the cells (Figure 23B and C). Surprisingly, when we additionally deleted *dacB* in the  $\Delta dacHL$  mutant, cells looked like wild type (Figure 23C). At first glance, it is striking that a triple gene deletion causes a less severe phenotype than a single. Maybe the deletion of one gene causes a disequilibrium in the levels of other carboxypeptidases, whereas the deletion of the whole pathway is less severe because the carboxypeptidase system is redundant in *H. neptunium*.

Third, we tested if the single and multiple deletions have a positive or negative effect on cell growth. Growth experiments were performed and biofilm production was analyzed by a biofilm assay. All strains showed normal growth in comparison to wild-type cells (Figure S4D and Table S1). The  $\Delta dacB$  and  $\Delta dacH$  mutants formed more biofilm than the wild type and therefore, showed a slower growth rate. In the  $\Delta dacHL$  and  $\Delta dacBHL$  mutant no biofilm formation was detected (Table S1). Taken together, deletions of carboxypeptidase-encoding genes only mildly affected the growth of *H. neptunium*.

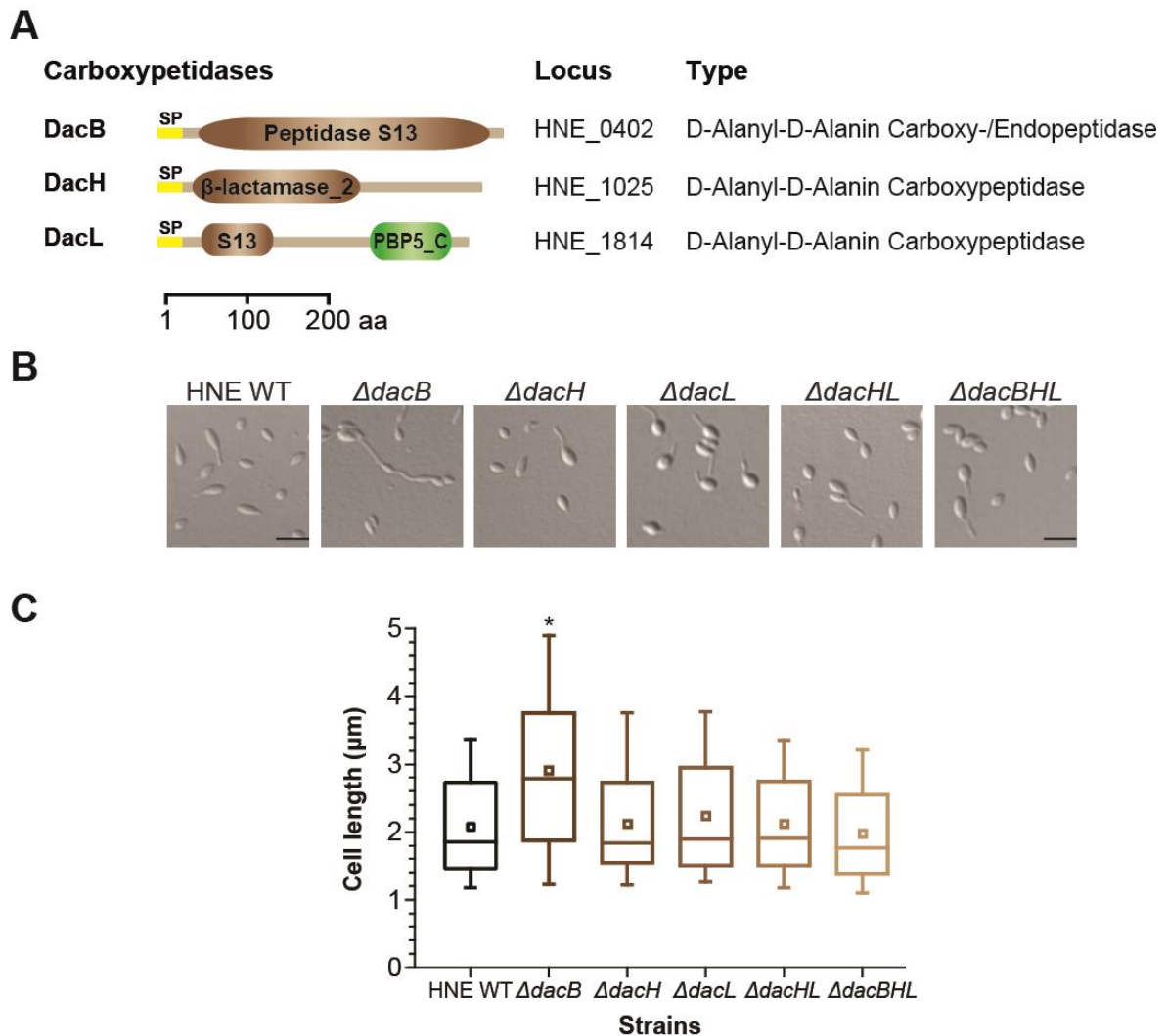


**Figure 23: Deletions of carboxypeptidases have a mild phenotypic effect. (A)** Graphical representation of proteins with a putative role in PG hydrolysis of *H. neptunium*. Domains have been identified using the Pfam database (Bateman et al., 2004; Finn et al., 2010). The SMART database was used to depict the proteins (Letunic et al., 2009; Schultz et al., 1998). Abbreviations: SP: signal peptide; S13: D-Ala-D-Ala carboxypeptidase family 3 domain; PBP5\_C: penicillin-binding protein 5 C-terminal domain; aa: amino acids. **(B)** Deletions reveal a high redundancy of carboxypeptidases. Phenotype of the wild type (HNE WT), the single deletion mutants SR11 ( $\Delta dacB$ ), SR08 ( $\Delta dach$ ), EC46 ( $\Delta dacL$ ), the double deletion mutant SR50 ( $\Delta dachL$ ) and the triple deletion mutant SR54 ( $\Delta dacBHL$ ). Cells were grown in ASM at 28°C (shaking at 210 rpm) to the exponential phase and analyzed microscopically. Scale bar: 3  $\mu\text{m}$ . **(C)** Cell lengths of the indicated strains. Cells were grown as described in (B). The distribution of cell lengths is shown as a box plot (explanation see Figure 9). Asterisk indicates a  $p$ -value of  $< 0.001$  ( $t$ -test).

#### 2.4.2 The localization of DacL

The localization pattern of all carboxypeptidases was analyzed to test if any of them localizes to the major sites of PG remodeling. To this end, natively expressed C-terminal mCherry fusions were generated. It was not possible to generate either a DacH-mCherry fusion or to produce a stable DacB-mCherry fusion protein (data not shown). However, we managed to construct a stable DacL-mCherry fusion that frequently localized to the stalk pole in swarmer cells and in a diffuse pattern in the whole cell body of swarmer and stalked



cells (Figure 24A) (Cserti *et al.*, 2017). Quantification analysis of the DacL-mCherry fluorescence intensity displayed in a demograph confirmed the localization in the whole cell body. In summary, DacL is the only carboxypeptidase that localizes to a site of PG remodeling and might have a function in the cell shape maintenance.

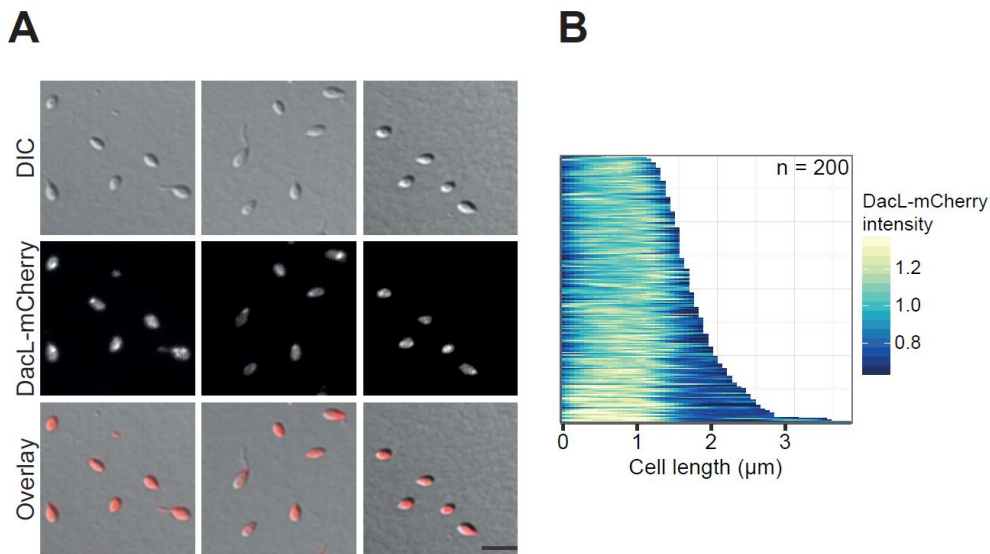


**Figure 24: DacL is the only carboxypeptidase with a distinct localization in *H. neptunium*.** (A) DacL-mCherry localizes at the stalked pole and partly in the whole cell body of *H. neptunium*. SR28 (*dacL-mCherry*) was grown to exponential phase in MB medium and imaged by DIC and fluorescence microscopy. Scale bar: 3 μm. Adapted from Roskopf (2014). (B) DacL-mCherry fluorescence intensity in SR28 cells is depicted in a demograph (based on images from A).

## 2.5 Transposon mutagenesis in *H. neptunium*

Even though the genome *H. neptunium* has already been sequenced, we do not know all essential genes (Badger *et al.*, 2005). The main reason to perform a transposon (Tn) mutagenesis experiment is the identification of novel factors, involved in the mechanisms of budding and bud separation in *H. neptunium*. Proteins or factors must exist that guide the PG remodeling enzymes (and other proteins) to the site of biosynthesis (stalked pole versus bud neck). We hypothesize that these unidentified proteins act as regulators or scaffolds. If we manage to identify these new proteins involved in the regulation of PG biosynthesis, we will be able to understand the complex budding mechanism of *H. neptunium* in depth.

A transposon (Tn or transposable element) is a DNA sequence that can change its position within a genome. The basic principle of a Tn as a mobile genetic element is its ability to randomly integrate into a genome. The Tn only requires the enzyme transposase for this step. When Tn mutagenesis is performed in a bacterium, Tns will insert in all types of genes. However, once an essential gene is affected, the bacterium cannot survive. Insertions into non-essential genes can happen multiple times, since the organism will survive the loss.



To analyze the insertions of Tns a method called transposon sequencing (TnSeq), that will reveal the insertion sites, is performed. In the corresponding experiment, the Tn, which is usually a resistance cassette (e.g. against kanamycin), only inserts once into the genome because the Tn and the *transposase* gene are located on a non-replicating delivery plasmid. Therefore, the integration of the Tn into the genome is stable, allowing Tn-specific sequencing. The outcome is a map of genes that either show insertions or not (Figure 25A). Certain genes that are not hit by the Tn can be listed as essential genes (Figure 25A, white arrows). Thus, Tn mutagenesis and TnSeq are a promising method to identify all essential genes in the genome of any organism.

By the time we started to establish the Tn mutagenesis approach, only a few Tn studies were done in  $\alpha$ -proteobacteria and none in a stalked representative (Curtis & Brun, 2014). First, we decided to use a *mariner* transposon that would serve as a mutagenic agent (Jacobson *et al.*, 1986). This element was first discovered in *Drosophila melanogaster* and inserts into TA dinucleotide target sites (Jacobson *et al.*, 1986). We performed the first test experiments with a set of pSAM-vectors carrying a *mariner* transposon. These vectors were successfully used in previous studies (Goodman *et al.*, 2009; Perry & Yost, 2014; Wiles *et al.*, 2013). Our goal was the identification of the most effective vector, which is the one with the best Tn insertion frequency (checked by colony-PCR) and the highest number of obtained clones.

The pSAM-vector is a sequence-adapted *mariner* transposon delivery vector with three major features (Goodman *et al.*, 2009). The vector contained an antibiotic resistance cassette (Kan<sup>R</sup>) flanked by Mmel-modified *mariner* inverted repeats (IRs), a multiple cloning site immediately upstream of the *himar1C9 mariner* transposase, and genes for replication in the donor strain (RP4 *oriT*) and transfer by conjugation (*oriR6K*, Figure 25B) (Goodman *et al.*, 2009; Lampe *et al.*, 1999). For the actual mutagenesis experiments we used the modified vectors pSAM-Ec and pSAM-RI, which harbor different promoters optimized for specific bacteria (Perry & Yost, 2014; Wiles *et al.*, 2013). Since pSAM-Ec harbored the *E. coli lac* promoter and pSAM-RI a *Rhizobium leguminosarum* bv. *viciae* 3841 *rpoD* promoter region (Figure 25B), we wondered how effective both promoters would be in *H. neptunium*. To address this issue, we slightly modified the pSAM-RI vector by introducing a *Hyphomonas*-specific promoter (*P<sub>HNE\_0038</sub>*). *P<sub>HNE\_0038</sub>* is the promoter for the small subunit of the ribosomal protein S16 and thus a strong constitutive promoter (Leicht, 2016). The generated vector was named pSAM-HNE (Figure 25B).

We used our set of pSAM-vectors (pSAM-Ec, pSAM-RI and pSAM-HNE) and transformed *H. neptunium* by conjugation (in collaboration with H. Wendt). After several test conjugations, we decided that pSAM-HNE was the most effective of the three vectors (data not shown). To solve the problem of *E. coli* contamination in the later conjugation steps, we used MB plates supplemented with gentamicin in addition to kanamycin. Gentamicin prevented the growth of *E. coli* but did not affect *H. neptunium* cells (data not shown).

The next problem to be solved was the low number of clones obtained in a single conjugation event. Based on previous published Tn mutagenesis approaches, we decided that we would need at least 500,000 clones to make a representative mutagenesis experiment and get a good gene coverage (e.g. 168 transposons per open reading frame) (Curtis & Brun, 2014; Langridge *et al.*, 2009). Therefore, upscaling of our standard conjugation protocol was necessary. This optimization procedure was successful after

several attempts, resulting in the use of large square plates (245 mm x 245 mm dish) with a high number of clones (>6000 clones per plate). Finally, I could perform the first round of Tn mutagenesis in *H. neptunium* and obtained approximately 800,000 clones on 50 large square plates. A company (Fasteris SA, Switzerland) performed the library preparation and TnSeq analysis. The outcome was not satisfying since many reads (>80%) did not map to the *H. neptunium* genome but to the vector (data not shown).

Alternatively, we tried a new sequencing method called Insertion sequencing (InSeq), which is based on the restriction with the MmeI enzyme and the ligation of specific adaptors for sequencing (Goodman *et al.*, 2011). After adapting the protocol for *H. neptunium*, we tried several times to get the correct PCR fragments. The right arrangement of the fragments was never observed, so that we ultimately discarded the InSeq method. Next, we tested a newly developed TnSeq protocol (A. Camilli, unpublished). It is based on a tagmentation reaction where a specific enzyme cuts the genomic DNA and randomly adds adaptors. In a first PCR amplification, a Tn- and a tagmentation-specific primer are used to generate short products. A second PCR reaction is needed to add the defined adaptors (Index1 and 2, P7 and P5) for the sequencing step (Figure 25C). The protocol was adapted for *H. neptunium*, (Figure 25C and Material and Methods 4.6.). The library preparation and the TnSeq analysis was performed using the Nextera™ DNA Library Preparation Kit FC-121-1030 (Illumina, USA). We performed the sample preparation and collaborated with Dr. J. Serrania for the TnSeq analysis (Dept. of Biology, FB17, Philipps-Universität and LOEWE Center for Synthetic Microbiology, Germany).

The results of the TnSeq analysis were carefully evaluated. All in all, we got 20,000,000 reads of which approximately 10% mapped to the genome of *H. neptunium*. The other 90% did not map at all or mapped to the vector pSAM-HNE. One explanation is that the vector integrated into the genome due to the *Hyphomonas*-specific promoter it contains. The frequency of mapped reads on the genome is depicted in Figure 25D. Transposon insertion sites are equally distributed over the whole genome. However, the coverage was not high enough to make precise statements about essential genes (Curtis & Brun, 2014; Langridge *et al.*, 2009). Additionally, large regions did not show any Tn insertions. Therefore, we decided to generate a new and larger pool of Tn mutants. We hypothesize that the created pSAM-HNE caused the problems. Hence, we performed a second round of Tn mutagenesis in *H. neptunium* and used the vector pSAM-RI, which had the second highest effectivity (data not shown). We obtained proximately 670,000 clones (in collaboration with Dr. M. van Teeseling). We again used the modified protocol from A. Camilli (unpublished) and analyzed the Tn library by TnSeq analysis. This time, we obtained 50,000,000 reads, of which approximately 0.03% mapped to the genome of *H. neptunium*. The other 99.97% mapped to the vector pSAM-RI or, for unknown reasons, did not map at all. Apparently, pSAM-RI is not fully suitable for *H. neptunium* (see Discussion 3.4.).

Taken together, our Tn mutagenesis experiment in *H. neptunium* could work in principle, since we were able to isolate thousands of Tn clones by upscaling the conjugation process. We also managed to perform library preparation and TnSeq analysis and we obtained first results. However, we have to rethink our attempt and carefully analyze the errors to finally find all essential genes of *H. neptunium* by improving presumably the efficacy of the Tn.

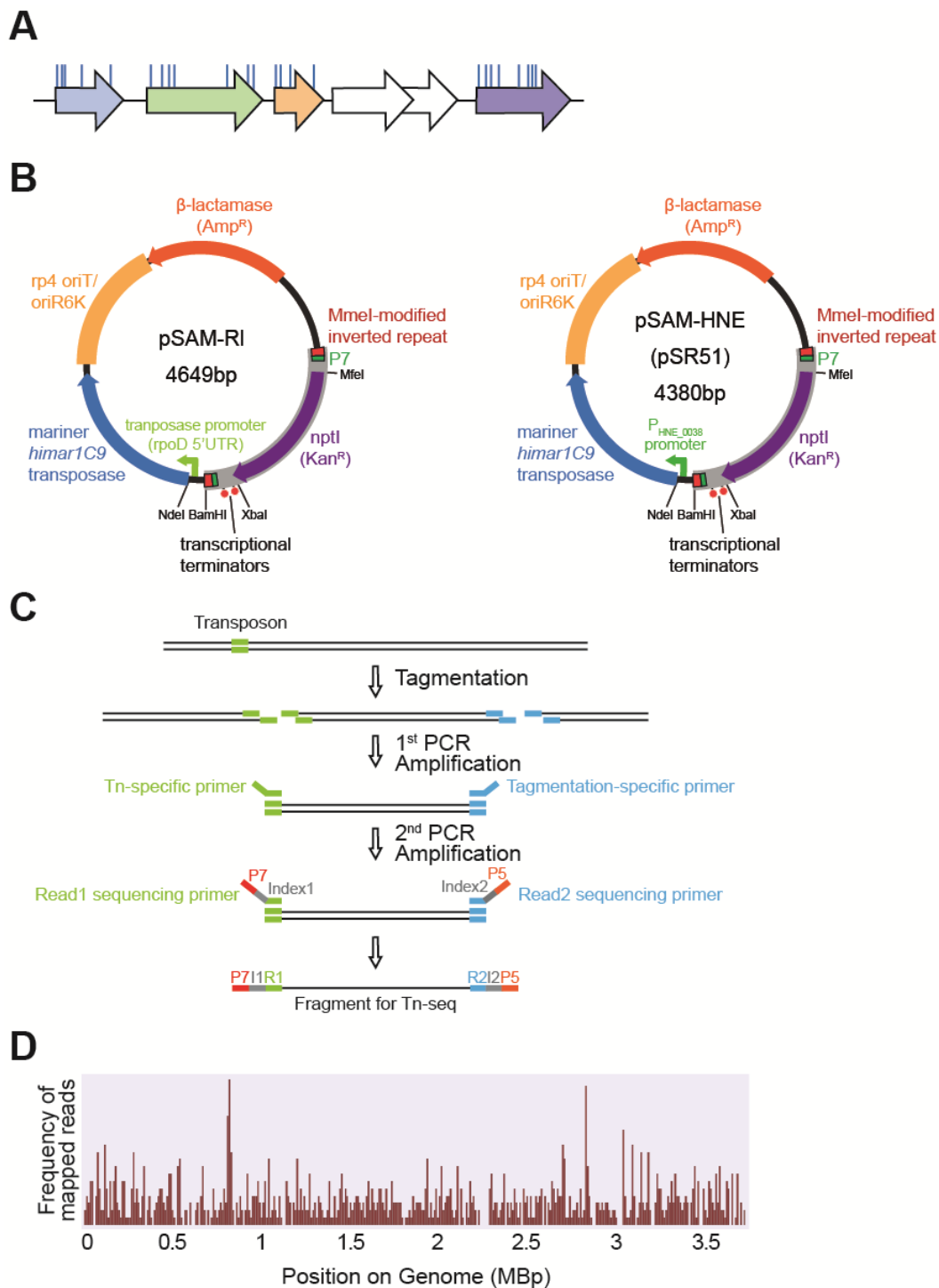


**Figure 25: Transposon mutagenesis of *H. neptunium*.** (A) Principle of transposon insertion into a genome. Several genes (colored arrows) are shown exemplarily. Blue lines indicate multiple insertion sites of the transposon. Essential genes (white arrows) do not show insertions. (B) Map of pSAM-RI plasmid. Adapted from Perry and Yost, 2014. Restriction enzymes, antibiotic markers (ampicillin,  $\beta$ -lactamase; kanamycin, *nptI*), origin of replication (*oriR6K*) and origin of transfer (*rp4-oriT*), transposase (*himar1C9*), transposase promoter (*rpoD* 5'UTR), Mm<sub>el</sub>-adapted mariner inverse repeats and transposon borne Rho-independent terminator are indicated. The modified plasmid pSAM-HNE has the same structure except for the transposase promoter that was replaced by a *Hyphomonas*-specific promoter ( $P_{HNE\_0038}$ ). (C) Schematic representation of the method used to generate fragments for the TnSeq analysis. Genomic DNA is cut by a tagmentation enzyme, and adaptors are added. In a 1<sup>st</sup> PCR, fragments are amplified using a transposon(Tn)-specific and a tagmentation-specific primer. Adaptors for Illumina<sup>®</sup> sequencing (P7-Index1 and P5-Index2) are added in a 2<sup>nd</sup> PCR reaction. (D) Transposon insertion sites in the genome of *H. neptunium* depicted as the frequency and distribution of mapped reads.

## 3. DISCUSSION

Growth and division is essential in all living organisms. Until now, studies to understand the bacterial cell division have mainly focused on well-established, rod-shaped model bacteria such as *E. coli* and *B. subtilis*. Previous work focused on the budding  $\alpha$ -proteobacterium *H. neptunium* as an alternative model system. We developed genetic tools and analyzed how *H. neptunium* grows and which enzymes are involved in this complex process (Cserti *et al.*, 2017; Jung *et al.*, 2015). In this work, we concentrate on a more detailed investigation of certain PG remodeling enzymes and their regulation. In addition, we made a first step in the identification of novel factors involved in the budding procedure.

### 3.1 Role of PG remodeling enzymes

PG synthases and hydrolases are important enzymes for all bacteria. They are needed to produce new glycan strands, cross-link the peptide side chains and cleave existing bonds to insert new material (Vollmer & Bertsche, 2008). The diversity of PG lytic enzymes is even higher than the abundance of PG synthases in most bacteria (Typas *et al.*, 2012). For example, *E. coli* possesses at least eight soluble lytic transglycosylases, four M23 EPases, four amidases and four CPases (Typas *et al.*, 2012). Previous studies show that these enzymes are highly redundant and the majority of them is dispensable under standard laboratory conditions (Egan *et al.*, 2017). However, good reasons must exist why these enzymes were maintained during evolution. We have to consider that standard laboratory conditions do not reflect the natural environment and free-living bacteria usually have to cope with pH changes, different salt conditions, nutrient limitation, and many more stresses. A recent study investigated the CPase PBP6b of *E. coli* under acidic conditions and showed that the enzyme was more active at low pH (Peters *et al.*, 2016). The authors suggested that *E. coli* maintains a redundant set of CPases for robust growth under various growth conditions (Peters *et al.*, 2016). Hence, these enzymes would be dispensable under standard laboratory conditions and nobody would consider them as crucial. However, once we observe the bacterium in its natural environment, these enzymes become significant for growth under specific conditions and suddenly fulfill a vital role.

A similar situation could apply to *H. neptunium*, which lives in a marine environment. It possesses three CPases and six EPases that are all (except of one) dispensable for normal growth (Figures 9 and 23). We were able to generate single and even multiple deletions in the respective genes. The  $\Delta lmdABDEF$  deletion strain showed a severe defect in cell morphology but was still viable. Single deletions only had a mild ( $\Delta lmdE$ ) or no effect at all. It is likely that *H. neptunium* keeps a set of PG lytic enzymes for the same reasons as *E. coli* does. Especially in marine environments, the salt concentration and the pH can radically change. Therefore, *H. neptunium* might use its lytic enzymes to adapt to the different stress conditions. The corresponding genes exhibit only low or medium expression levels, suggesting that these proteins only have a minor role under standard laboratory conditions.

However, the expression level of a gene does not necessarily correspond to its importance. For instance, *H. neptunium* needs only a few copies of transcription regulators, whereas it has hundreds copies of FtsZ and MreB. Nevertheless, we could prove that LmdA is an active endopeptidase and does not need other proteins to cleave PG (Figure 19). Since its expression is low under standard laboratory conditions, this might argue for a role under special stress conditions. In addition, the M23 endopeptidases LmdA, LmdB, LmdD and LmdF localize mainly in the cell body (Figure 10), proposing a primary role in the maintenance of the cell shape. Future experiments should investigate the effect of changing conditions (low and high salt or pH) on multiple deletion strains.

LmdE is the only EPase, where a single gene deletion had a phenotypic effect (Figure 9). Interestingly, the homolog of LmdE in *C. crescentus*, LdpF, is required for proper cell division under salt stress (Zielińska *et al.*, 2017). LdpF (like LmdE and EnvC) also possesses two coiled-coil regions and a degenerate M23 peptidase domain, suggesting that it does not actively hydrolyze PG (Zielińska *et al.*, 2017). In contrast, the deletions of multiple endopeptidase genes ( $\Delta ldpABCDE$ ) barley affected the cell morphology of *C. crescentus* (Zielińska *et al.*, 2017). These results are similar to the ones observed in the *H. neptunium*  $\Delta lmdABCDF$  mutant, suggesting a conservation of the EPase function. It remains to be clarified, if LdpF directly or indirectly stimulates the activity of AmiC in *C. crescentus* and which exact role the FtsEX complex plays. Recent work has shown that FtsEX of *C. crescentus* controls the early and late stages of cytokinesis (Meier *et al.*, 2016). A deletion of *ftsE* resulted in cells with thin connections between cell bodies, which could not separate (Meier *et al.*, 2016). Lately, several Co-IP experiments suggested an interaction of LdpF with FtsE and FtsX (A. Izquierdo Martinez, unpublished data). Further investigations have to clarify if LdpF interacts with FtsEX in a similar way as in *E. coli*. If this could be proven, it would confirm a high conservation of pathways and protein activation modes among different species of proteobacteria.

LmdC remains the only mysterious M23 endopeptidase of *H. neptunium*, as it is difficult to analyze. Several attempts to localize this protein failed because the fusions were unstable (Cserti, 2016; Kanngießler, 2016). We even tried the generation of an inducible LmdC<sup>N</sup> fusion where the 3'-end of *lmdC* was fused to the *mCherry* gene. However, the attempt resulted in instability of the protein fusion (data not shown). Additionally, neither deletion nor depletion studies have been successful so far (Kanngießler, 2016). We are especially interested in LmdC because the gene lies upstream of and overlaps with the bactofilin *bacA*, a bacteria-specific cytoskeletal element. Bactofilins are a class of cytoskeletal elements that is widespread among bacteria and characterized by a conserved bactofilin domain (Kühn *et al.*, 2010; Punta *et al.*, 2012). The bactofilins BacA and BacB of *C. crescentus* were the first ones described in detail, and both form sheet-like structures that line the cytoplasmic membrane at the stalked cell pole (Kühn *et al.*, 2010). Furthermore, they are important for the polar localization of PG synthases involved in stalk biosynthesis and thus the regulation the cell wall biosynthesis (Kühn *et al.*, 2010). The presence of a LytM factor-encoding gene overlapping with a bactofilin gene is conserved in proteobacteria such as *C. crescentus* and *H. pylori* (Kühn *et al.*, 2010; Sycuro *et al.*, 2010; Sycuro *et al.*, 2012). In *H. neptunium*, the simultaneous deletion of the *bacA* and the *lmdE* genes as well as the depletion was not possible (Cserti, 2016). All tested clones showed the wild-type phenotype after the second homologous recombination event, suggesting an essential role for both proteins (Cserti, 2016). Previous studies, have shown the importance of bactofilins for the morphology of

*H. neptunium* (Cserti, 2016). It is possible that bactofilins act as scaffolds for PG remodeling enzymes and have a crucial role in guiding these complexes. Therefore, bactofilins could mediate the localization of LmdC, or other EPases or even help to stabilize the elongasome or the divisome by anchoring the corresponding proteins to the membrane. In the future, key analyses will be the deletion of essential genes, such as *lmdC*, to reveal their role in PG remodeling. Since deletion and depletion studies are not always possible in *H. neptunium* due to the basal activity of the heavy metal-inducible promoters, we are currently establishing a technique called CRISPRi to knockdown any selected genes of interest (Harberding, 2018; Qi *et al.*, 2013).

## 3.2 Mode of amidase activation

Amidases are a crucial class of PG lytic enzymes, that cleave the peptide side chains from the glycan backbone. These periplasmic soluble enzymes are involved in cell separation at the division site (Heidrich *et al.*, 2001). Typical periplasmic amidases have an AMIN domain structure (a  $\beta$ -sandwich of two symmetrical four-stranded  $\beta$ -sheets exposing highly conserved motifs on the two outer faces) that can bind to PG (de Souza *et al.*, 2008; Rocaboy *et al.*, 2013). In *E. coli*, the catalytic C-terminal domain of AmiC shows an auto-inhibitory  $\alpha$ -helix covering the active center with the complexed zinc ion (Rocaboy *et al.*, 2013). This helix is the reason why AmiC (and amidases in general) is not active on its own and relies on special regulatory proteins.

Our protein fractionation experiment revealed that AmiC of *H. neptunium* is a soluble protein (Figure 12). Even though this is not a direct proof that AmiC is soluble in the periplasm, it is likely, since the majority of known amidases are soluble periplasmic proteins (Firczuk & Bochtler, 2007). In addition, a signal peptide and a periplasmic localization was predicted for AmiC. Moreover, the localization of AmiC<sub>HNE</sub> in the heterologous *E. coli* system gave an additional hint to a periplasmic localization (Figure 12). Hence, we assume that AmiC is located in the periplasm of *H. neptunium* and functions as a normal, active amidase.

We wanted to investigate the mode of amidase activation in *H. neptunium* in more detail. To this end, we modeled the structure of AmiC of both *H. neptunium* and *C. crescentus* and saw that the inhibitory  $\alpha$ -helix was conserved in these  $\alpha$ -proteobacteria. Thus, a similar mode of amidase activation consistent with this notion is very likely since natively AmiC<sub>HNE</sub> alone was not active in a dye-release assay (Figure 18). When LmdE was added, PG hydrolysis was observed. This strongly suggested that LmdE interacts with AmiC. We do not know which exact part of LmdE binds to the surface of AmiC. However, the coiled-coil part of LmdE might bind to the N-terminal region of AmiC and the globular M23 peptidase domain could interact with the inhibitory  $\alpha$ -helix and lead to a conformational change of AmiC that results in the displacement of the  $\alpha$ -helix.

An N-terminal AMIN domain was also visible in our model of AmiC<sub>HNE</sub>. This domain could function as a PG-binding domain, as previously shown for *E. coli* (Rocaboy *et al.*, 2013). AMIN domains are one of three types of PG-binding domains, beside SPOR and LysM domains (Bateman & Bycroft, 2000). SPOR domain-containing proteins localize to septal regions of PG in *E. coli* (Yahashiri *et al.*, 2015). We found at least two proteins with SPOR domains in *H. neptunium*, the lipoprotein RlpA and the late cell division protein FtsN (Cserti,

2016; Eisheuer, 2016). In contrast, LysM domain-containing proteins (e.g. DipM in *C. crescentus*) do not exist. In summary, *H. neptunium* only possesses a few proteins, that are able to bind to PG. However, to prove that the AMIN domain of AmiC<sub>HNE</sub> is important we can mutate or delete this part and test how this affects cell morphology. Furthermore, we will test the ability of AmiC<sub>HNE</sub> to bind to PG in a PG-binding assay. Another target is the inhibitory  $\alpha$ -helix itself, since a deletion of the  $\alpha$ -helix in AmiC<sub>EC</sub> resulted in a constantly active enzyme (Rocaboy *et al.*, 2013). Consequently, in future studies we will purify a mutant version of AmiC<sub>HNE</sub> lacking the inhibitory  $\alpha$ -helix and test for its ability to hydrolyze PG without the addition of LmdE.

In addition, we compared the structure of EnvC to a model of LmdE (Peters *et al.*, 2013). We observed a high structural similarity, where both protein folds showed long  $\alpha$ -helices in the N-terminal region that are the coiled-coil regions and a globular C-terminal M23 peptidase domain (data not shown). Thus, the structural conservation of inactive EPases seems to be high among proteobacteria and supports a functional relationship of both proteins, which we proved by dye-release assays and BLI. So far, we used purified PG sacculi of wild-type *C. crescentus* cells for all dye-release assays because several attempts to purify PG from *H. neptunium* were not successful. Even though the PG composition of both organisms is very similar, we would like to purify PG sacculi of wild-type *H. neptunium* cells to validate our results (Cserti *et al.*, 2017). To this end, we will adapt the PG isolation protocol to the requirements of the *H. neptunium* cell wall.

In our BLI experiments, AmiC and LmdE showed binding to each other in both ways (Figure 20 and 21). However, the binding intensity of the reactions was very different. We observed a transient as well as a tight interaction of both proteins depending on the reaction order. We cannot definitely say which result is more reliable, but we assume that amidase activation should occur at the late stage of cell division to cleave the PG and finally separate the daughter cells. In other words, PG remodeling has to occur at specific time points during the cell cycle to ensure correct cytokinesis. However, this does not solve the question about the tightness or weakness of the interaction. In addition, the orientation of immobilization of the biotinylated protein is crucial for the binding capability. Apparently, this orientation of the protein on the sensor chip is key for the interaction. Immobilization of AmiC might result in weak accessibility of the interaction regions on the protein surface, which does not happen in a living cell. Furthermore, biotin could block the interface between AmiC and LmdE and weaken the interaction. Maybe a third component or different buffer conditions are needed for an *in vivo*-like interaction.

To investigate which part of LmdE that binds to AmiC, we divided the protein in its two domains (LmdE<sup>CC</sup> and LmdE<sup>M23</sup>) but could not observe AmiC activation nor binding to AmiC (Figures 18 and 22). Moreover, when we incubated both protein parts together, they did not show the behavior of the full-length protein. It is possible that LmdE<sup>CC</sup> and LmdE<sup>M23</sup> are not functional to activate AmiC or misfolded. Most likely, the whole protein is needed for correct binding and activation of AmiC. Furthermore, LmdE<sup>M23</sup>, which comprises the globular M23 peptidase domain, might not have the required length, or the coiled-coil domain is necessary to change the conformation of the second domain. In the future, we can purify a larger part of LmdE<sup>M23</sup> and test the binding/stimulation of AmiC.

We observed a similar result for FtsX<sup>Loop1</sup>. This extracellular loop domain, which possesses predicted secondary structures, did not bind to LmdE nor enhance/repress AmiC activity

(Figure 18 and data not shown) (Arends *et al.*, 2009). Most likely, FtsX<sup>Loop1</sup> is not folded in a proper way or has the wrong conformation. Maybe, the right conformation only exists when the whole FtsEX complex is assembled. It has been proven that FtsE binds and hydrolyze ATP, whereas an ATP hydrolysis-deficient FtsE mutant affects cell division (Arends *et al.*, 2009; Schmidt *et al.*, 2004). Hence, the free energy gained from ATP cleavage might activate/energize the FtsX part or the loop domain leading to a conformational change that enables interaction to the coiled-coil part of LmdE and modifies the conformation of the peptidase domain. Next, the M23 domain binds to AmiC and stimulates the latter by moving the auto-inhibitory  $\alpha$ -helix away from the active center, leading to PG hydrolysis by the activated amidase. Obviously, this was not possible to test in our experiments, since we missed FtsE and full-length FtsX. Our assumption is summarized in the model of amidase activation in *H. neptunium* (Figure 26). Future studies have to address the question of which part of FtsX binds to LmdE, and which role FtsE has in the interaction. Furthermore, it remains to be clarified how crucial ATP hydrolysis might be for this process. Thus, it will be necessary to purify FtsE, FtsX or the whole complex and perform the appropriate analyses. Nevertheless, we could show for the first time that the mechanism of amidase activation is conserved in a budding  $\alpha$ -proteobacterium.

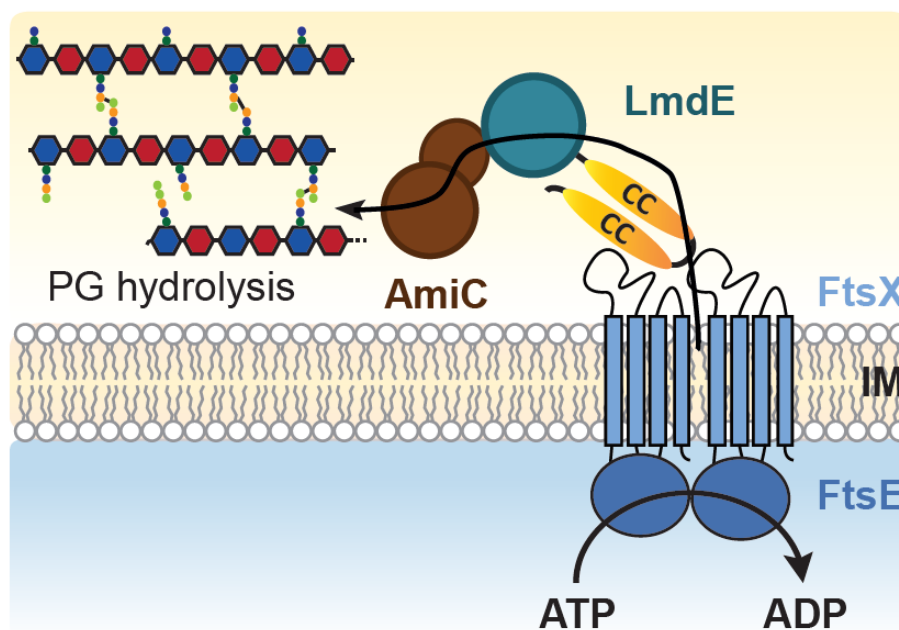


**Figure 26: The mode of amidase activation in *H. neptunium*.** The membrane-embedded FtsEX complex is energized by the hydrolysis of ATP, resulting in a conformational change in the periplasmic loop domain. Subsequently, this domain interacts with the catalytically inactive endopeptidase homolog LmdE, which then binds to the amidase AmiC. AmiC is activated and PG is cleaved. Abbreviation: IM: inner membrane.



### 3.3 Function of the FtsEX complex

The FtsEX complex is built of two proteins, that are encoded in one operon, the inner-membrane attached protein FtsE (ATP-binding protein) and the inner membrane protein FtsX (ABC transporter permease) (de Leeuw *et al.*, 1999; Schmidt *et al.*, 2004). Even though a homology to ABC transporter exists, substrate transport was never proven and the substrate-specific transmembrane channel of FtsX does not contain charged amino acids (Arends *et al.*, 2009; de Leeuw *et al.*, 1999). TM segments of most transporters normally contain charged amino acids that interact with charges on the substrate surface. Therefore, these observations suggest that FtsEX does not transport any substrate but has a function in cell division and the stability of the divisome, since it localizes to the division site (Arends *et al.*, 2009; Schmidt *et al.*, 2004).

Later, the involvement of FtsEX in the activation of amidases by EnvC was observed in *E. coli*. In the Gram-positive ovococcus *S. pneumonia*, FtsEX controls the activity of the lytic enzyme PcsB (Sham *et al.*, 2011; Yang *et al.*, 2012). PcsB has a similar domain structure as EnvC with an N-terminal coiled-coil domain and a C-terminal PG hydrolase-like domain. In contrast to EnvC, it is catalytically active, can hydrolyze PG and interacts with the extracellular loop 1 and 2 of FtsX (Bajaj *et al.*, 2016; Bartual *et al.*, 2014; Sham *et al.*, 2013). A further example was observed in the Gram-positive *B. subtilis*, where the activity of the EPase CwIO was dependent on FtsEX (Meisner *et al.*, 2013). An interaction between CwIO and FtsEX was already shown to be important for cell elongation (Dominguez-Cuevas *et al.*, 2013). A similar pathway was investigated in the human pathogen *V. cholera*. FtsX was interacting with homologs of EnvC and NlpD that for their part activate AmiB as the single amidase (Möll *et al.*, 2014).

These examples show how similar and conserved the FtsEX system is among bacteria of completely different lineages. Thus, we suggest a related and important role for the FtsEX complex in *H. neptunium* as well, although FtsEX is not essential. We think that it acts in the same pathway as LmdE because the  $\Delta ftsEX \Delta lmdE$  mutant did not show an additive phenotype (Figure 15). Therefore, it is very likely that the mechanism is also conserved in *H. neptunium* as shown in our experiments, discussed above and depicted in the model (Figure 26). This mode of amidase activation is critical for the characteristic cell shape and daughter cell separation.

### 3.4 Identification of essential genes and novel factors

We would like to identify novel factors that direct/regulate the complex process of budding. In the past, several proteins involved in the coordination of PG biosynthesis and cell shape have been identified in different organisms. For example, the scaffold-forming protein DivIVA localizes cell division proteins and has a preference for curved membranes (Lenarcic *et al.*, 2009). The membrane protein EzrA with FtsZ and PBPs could function as a key component in *B. subtilis* cell division (Cleverley & Lewis, 2015; Singh *et al.*, 2007). It influences cell wall synthesis and thereby regulates the Z-ring (Egan *et al.*, 2017). A further instance is the cell division regulator GpsB in rod-shaped and ovococoid Gram-positive

bacteria (Pinho *et al.*, 2013). GpsB coordinates PG synthesis at the side wall during elongation and at the septum during division by forming complexes with PBP2a and PBP2b (Rued *et al.*, 2017). Proteins that associate with membranes directly *in vivo* could function as assembly hubs for other factors and guide PG remodeling enzymes. Well-known representatives are FtsA and ZipA but also the recently analyzed FzIC from *C. crescentus*, which all interact with FtsZ (Meier *et al.*, 2016; Pichoff & Lutkenhaus, 2002).

*H. neptunium* must also possess proteins with the above-mentioned characteristics. We previously showed that a coiled-coil-rich protein and the already mentioned bactofilin are critical for proper cell morphology (Cserti, 2016). However, if we compare the genome of *H. neptunium* only to well-established model organisms such as *E. coli* or *B. subtilis*, we will not find factors involved in bud formation and regulation, because they do not possess such proteins. To finally identify factors that guide PG remodeling enzymes and to find all essential genes we designed and performed Tn mutagenesis (Figure 25). We used a *mariner* Tn, a *himar1C9 mariner* transposase, whose expression was driven by a *Hyphomonas*-specific promoter. We obtained proximately 800,000 clones in a first Tn mutagenesis experiment and subsequently performed TnSeq. Only 10% of all obtained reads mapped to the genome, whereas 90% did not map at all or mapped to the vector pSAM-HNE. In a second Tn mutagenesis experiment, in which we used a different vector (pSAM-RI), we observed even less mapped reads.

There are several reasons why the Tn mutagenesis approach used may not be very effective. Apparently, both vectors (pSAM-HNE and pSAM-RI) and their elements are not completely suitable for *H. neptunium*, meaning that pSAM-RI is less effective than in other  $\alpha$ -proteobacteria or pSAM-HNE could integrate into the genome due to its *Hyphomonas*-specific promoter. However, the integration of the vector in the promoter region is very unlikely, since the promoter fragment is short (90 amino acids). Secondly, the *mariner* Tn, which inserts at AT sites, might not be effective, because the genome of *H. neptunium* is GC rich (Jacobson *et al.*, 1986). This could result in Tns that do not randomly insert into the genome but integrate by recombination events. We should test if other Tn elements, such as Tn5, might be more suitable. Tn5 was already used to identify essential  $\alpha$ -proteobacterial genes (Curtis & Brun, 2014). Finally but less likely, the *rpoD* promoter region might not produce enough transposase, the enzyme is simply not active enough or degraded too fast. The change of either the promoter, the Tn or the transposase will be tested in future experiments. Once this method is established, we can mutagenesis *H. neptunium* under different conditions (e.g. salt or pH stress) or test specific mutants and compare the results to the standard wild-type conditions to analyze if certain protein become essential.

### 3.5 Concluding remarks and future perspectives

Previous studies have shown that the budding process of *H. neptunium* is more complex than originally thought (Cserti *et al.*, 2017). In this work, we investigated the role of PG remodeling enzymes in bud formation and separation. We analyzed in detail how an inactive member of the class of endopeptidases regulates an active member. We proved that the mechanism of amidase activation is conserved among different proteobacteria. For the first time, a direct interaction of an endopeptidase to its cognate amidase was observed by bio-layer interferometry. Hence, inactive endopeptidases serve as regulators for amidase

activity in a broad range of bacterial species. Integral membrane complexes might be involved in the regulation by the transfer of signals from the cytoplasm to the periplasm.

The complex budding mechanism of *H. neptunium* is still not fully understood. Future studies have to intensively search for novel factors involved in this process. A good starting point are the results obtained by the Co-IP performed with AmiC, because several uncharacterized but conserved proteins have been identified. Among them are interesting candidates for deeper analyses. The already known CpoB protein, which is part of the envelope-spanning Pol-Tal complex, could be a link between amidase regulation and outer membrane constriction. A further approach is the performance of Tn mutagenesis to find essential genes. Once we solve the current issues, this method might be a powerful tool to identify potential novel factors. Finally, we would like to reveal a connection between endopeptidases and bacteria-specific cytoskeletal elements. Those elements such as bactofilins, could guide PG remodeling enzyme or function as scaffolds.

Unravelling the exact mechanism of budding might broaden our knowledge of cell division in bacteria. This would not only expand our understanding of bud formation and separation but also underscore the diversity of proliferation modes in prokaryotes. The in-depth analysis of the budding process and its spatiotemporal regulation in *H. neptunium* will thus expand our knowledge of bacterial cell biology in general.

## 4. MATERIAL AND METHODS

### 4.1 Materials

#### 4.1.1 Chemicals and enzymes

All chemicals used in this study were obtained from Applichem (Germany), Becton Dickinson (USA), Bioline (Germany), Carl Roth (Germany), Difco (Spain), GE Healthcare (Germany), Illumina (USA), Invitrogen (Germany), Merck (Germany), PerkinElmer (USA), Peqlab (USA), Roche (Switzerland), Sigma-Aldrich (USA), Thermo Scientific (USA) and Qiagen (Germany).

The restriction enzymes were obtained from Fermentas (Germany) or New England Biolabs (NEB, USA). The shrimp alkaline phosphatase and the T4 DNA ligase were from Thermo Scientific (USA). The DNA and protein ladder were from Fermentas (Germany) or Thermo Scientific (USA). The polymerase chain reaction was either performed with KOD Hot Start DNA Polymerase (Merck, Germany) or with Biomix™ Red (Bioline, Germany).

#### 4.1.2 Media

LB, MB and ASM were used as media. Their components are listed below. All used additives are listed in Table 1.

LB medium (Luria-Bertani; Miller, 1972) for *E. coli*:

Tryptone	10 g/l
Yeast extract	5 g/l
NaCl	10 g/l

All components were dissolved in de-ionized water (dH<sub>2</sub>O). The medium was autoclaved at 121°C for 20 min. Medium additives were added after cooling to 60°C. For LB agar plates, 1.5% [w/v] agar was added prior to autoclaving.

MB medium (Marine Broth; Difco™) for *H. neptunium*:

Bacto peptone	5.0 g/l
Bacto yeast extract	1.0 g/l
Fe(III) citrate	0.10 g/l
NaCl	19.45 g/l
MgCl <sub>2</sub>	5.90 g/l
MgSO <sub>4</sub>	3.24 g/l

CaCl <sub>2</sub>	1.80 g/l
KCl	0.55 g/l
Na <sub>2</sub> CO <sub>3</sub>	0.16 g/l
KBr	0.08 g/l
SrCl <sub>2</sub>	34 mg/l
H <sub>3</sub> BO <sub>3</sub>	22 mg/l
Na-silicate	4.0 mg/l
NaF	2.4 mg/l
(NH <sub>4</sub> )NO <sub>3</sub>	1.6 mg/l
Na <sub>2</sub> HPO <sub>4</sub>	8.0 mg/l

All components were dissolved in de-ionized water (dH<sub>2</sub>O). The medium was autoclaved at 121°C for 20 min. Medium additives were added after cooling to 60°C. The medium was filter-sterilized using bottle top filters (pore size 0.2 µm, Sarstedt, Germany). For MB agar plates, 1.5% [w/v] Marin Agar (Difco™, USA) was added prior to autoclaving.

ASM (Artificial Salt Medium) for *H. neptunium*:

Bacto peptone	5 g
Yeast extract	1 g
1 M MgSO <sub>4</sub>	1 ml
1 M CaCl <sub>2</sub>	0.5 ml
Sea salt	15 g

All components were dissolved in de-ionized water (dH<sub>2</sub>O). The medium was autoclaved at 121°C for 20 min. Medium additives were added after cooling to 60°C. For ASM agar plates, 1.5% [w/v] agar was added prior to autoclaving.

**Table 1:** Used antibiotics and additives for liquid and solid media for *E. coli* and *H. neptunium*.

Additives	Organism	Liquid medium	Solid medium
Kanamycin (20 mg/ml)	<i>E. coli</i>	30 µg/ml	50 µg/ml
	<i>H. neptunium</i>	100 µg/ml	200 µg/ml
Rifampicin (10 mg/ml, in methanol)	<i>E. coli</i>	25 µg/ml	50 µg/ml
	<i>H. neptunium</i>	1 µg/ml	2 µg/ml
Ampicillin (100 mg/ml)	<i>E. coli</i>	200 µg/ml	200 µg/ml
Streptomycin (10 mg/ml)	<i>E. coli</i>	30 µg/ml	30 µg/ml
Sucrose	<i>H. neptunium</i>	3% [w/v]	3% [w/v]
DAP (60 mM)	<i>E. coli</i>	300 µM	300 µM
CuSO <sub>4</sub> (20 mM)	<i>H. neptunium</i>	300 µM	300 µM
NiCl <sub>2</sub> (1 M)	<i>H. neptunium</i>	1 mM	-
IPTG (1 M)	<i>E. coli</i>	0.5 mM	-
Glucose (40%)	<i>E. coli</i>	0.5 mM	-

### 4.1.3 Buffer and solutions

Standard buffers and solutions were prepared as described (Ausubel, 1988; Sambrook *et al.*, 1989). Special buffers and solutions are listed in the respective method section. All buffers were prepared with de-ionized water (Purelab Ultra water purification system, Elga).

### 4.1.4 Kits

The diverse kits for DNA purification and DNA extraction are listed in Table 2.

**Table 2:** Kits and their application.

Kit	Application
GenElute™ PCR Clean-Up Kit (Sigma, USA)	Purification of DNA
GenElute™ Gel Extraction Kit (Sigma, USA)	Elution of DNA from agarose gels
GenElute™ Plasmid Miniprep Kit (Sigma, USA)	Extraction of plasmid DNA
Western Lightnin™ Chemiluminescence Reagent Plus Kit (PerkinElmer, USA)	Detection of chemiluminescence
NucleoSpin® Microbial DNA	Isolation of chromosomal DNA
Nextera™ DNA Library Preparation Kit FC-121-1030	Tagmentation of DNA
Roti®-Nonoquant (Carl Roth, Germany)	Determination of protein concentrations

### 4.1.5 Oligonucleotides and plasmids

Oligonucleotides (PCR primers) for molecular cloning were designed using SnapGene® 3.2.1 (GSL Biotech LL, USA) and synthesized by Eurofins MWG Operon (Germany). A complete list of oligonucleotides (Table S6, Table S7 and Table S8) and plasmids (Table S5) used in this study can be found in the appendix.

## 4.2 Microbiological and cell biological methods

### 4.2.1 Cultivation of *E. coli*

*E. coli* was cultivated either in LB medium (shaking at 210 rpm) or on LB agar plates at 37°C. Cryo cultures or cultures from plates were used as inoculum. Liquid and solid media were supplemented with antibiotics or additives if required (Table 1).

### 4.2.2 Cultivation of *H. neptunium*

The cultivation of *H. neptunium* was achieved either in MB medium or ASM at 28°C under aerobic conditions (shaking at 210 rpm) in baffled flasks or on MB or ASM agar plates. Cryo cultures or cultures from plates were used as inoculum. Liquid and solid media were supplemented with antibiotics or additives if required (Table 1).

The purity of the cultures was regularly verified by light microscopy (Axiostar plus, Zeiss, Germany).

#### 4.2.3 Storage of bacteria

Cryo-stocks of bacteria were made for long-term storage. An overnight culture was supplemented with 10% (v/v) DMSO (dimethyl sulfoxide) and permanently stored in a special cryo tube at -80°C.

#### 4.2.4 Determination of cell density

The optical density (OD) of bacterial cultures was determined photometrically by using an Ultrospec™ 10 Cell Density Meter (GE Healthcare, Germany) at a wavelength of 600 nm. The corresponding culture medium was used as a blank.

#### 4.2.5 Growth curves

*H. neptunium* strains were grown in MB or ASM to stationary phase for 2 days, diluted 1:10, and cultivated further overnight. The main cultures were inoculated to an OD<sub>600</sub> of 0.01 in a 24-well plate (Becton Dickinson Labware, USA), incubated at 31 – 33°C shaking while cell growth was monitored at OD<sub>580</sub> for 31 h using an EPOCH 2 microplate reader (BioTek, USA). Growth rates were calculated using a modified solver spreadsheet (Huang, 2011).

#### 4.2.6 Biofilm assay

To quantify biofilm formation in *H. neptunium*, the biofilm was stained with crystal violet after a growth assay in a 24-well plate (Becton Dickinson Labware, USA). Each well of the culture plate was incubated with 70 µl of 0.5 % (w/v) crystal violet (Roth, Germany) solution for 5 min at RT. The wells were washed twice with 1 ml ddH<sub>2</sub>O for 10 min. The supernatant was carefully extracted via suction. To determine biofilm formation, the wells were incubated with 1 ml 100% ethanol for 5 min to release bound crystal violet, which was subsequently measured at a wavelength of 580 nm using an EPOCH 2 microplate reader (BioTek, USA).

#### 4.2.7 Preparation of competent *E. coli* cells

Chemically competent *E. coli* cells were prepared using the CaCl<sub>2</sub> method (Cohen *et al.*, 1972). A 10 ml LB pre-culture from *E. coli* TOP10 (Str<sup>R</sup>) was inoculated using a cryo-stock and incubated at 37°C overnight. 250 ml LB medium were inoculated with 2.5 ml of this pre-culture and incubated at 37°C until the cultures reached an OD<sub>600</sub> of 0.6. Following an incubated on ice for 10 min, cells were transferred into GSA centrifuge beakers, and harvested by centrifugation using a Sorvall GS3 rotor (Thermo Fisher, USA) at 3000 x g for 10 min at 4°C. The supernatant was discarded. The pellet was resuspended in 15 ml ice-cold 0.1 M CaCl<sub>2</sub> solution and transferred in pre-cooled SS34 tubes. The cells were then incubated on ice for 30 min and collected by centrifugation with an SS34 rotor (Thermo Fisher, USA) at 3000 x g for 10 min at 4°C. Then, the pellet was carefully resuspended in

4 ml pre-cooled 0.1 M CaCl<sub>2</sub> containing 15% [v/v] glycerol. Aliquots of 150 µl were transferred to “Safe-lock”-Eppendorf tubes, snap-frozen in liquid nitrogen (N<sub>2</sub>), and stored at -80°C.

For the generation of competent *E. coli* WM3064 cells (*dap*<sup>-</sup>), 300 µM diaminopimelic acid (DAP) was added to the LB medium.

### 4.2.8 Transformation of competent cells

#### *E. coli* TOP10

An aliquot of chemically competent *E. coli* TOP10 cells was thawed on ice and 10 µl ligation reaction (or 2 µl plasmid DNA) was added. The cells were incubated on ice for 30 min, followed by a heat shock at 42°C for 90 sec without agitation in a heat block (VWR, USA). The sample was further incubated on ice for 2 min and 500 µl LB medium was added. The cells were incubated for 1 h at 37°C. 200 µl of the suspension was plated on a LB agar plate containing the corresponding antibiotic and incubate at 37°C overnight.

#### *E. coli* WM3064

An aliquot of chemically competent *E. coli* WM3064 cells was thawed on ice and 2 µl plasmid DNA was added. The cells were incubated on ice for 30 min, followed by a heat shock at 42°C for 90 sec without agitation in a heat block (VWR, USA). The sample was further incubated on ice for 2 min and 500 µl LB medium supplemented with 300 µM DAP were added. The cells were incubated for 1 h at 37°C. 200 µl of the suspension was plated on a LB agar plate containing the corresponding antibiotic and 300 µM DAP. Plates were incubated at 37°C until single colonies appeared.

#### *E. coli* Rosetta™ (DE3)pLysS

Chemically competent *E. coli* Rosetta™ (DE3)pLysS purchased from Merck Millipore (Germany). An aliquot of 100 µl of cells was thawed on ice and 4 µl plasmid DNA was added. The cells were incubated on ice for 30 min, followed by a heat shock at 42°C for 45 sec without agitation in a heat block (VWR, USA). Afterwards, the cells were further incubated on ice for 2 min and 500 µl LB medium was added. The cells were incubated for 1 h at 37°C. 200 µl of the suspension was plated on a LB agar plate containing 200 µg/ml ampicillin and incubate at 37°C overnight.

### 4.2.9 Conjugation of *H. neptunium*

The transformation of *H. neptunium* was performed via conjugation using a suitable donor strain (*E. coli* WM3064 harboring the plasmid of interest). *H. neptunium* cells (recipient strain) were inoculated from a cryo-stock into MB medium or ASM and incubated at 28°C for two days. *E. coli* WM3064 harboring the plasmid of interest were inoculated from a cryo-stock or a fresh LB agar plate into LB medium supplemented with 300 µM DAP and antibiotic. Cells were incubated at 37°C overnight. Both cultures were harvested after they reached the stationary phase. 1 ml of *E. coli* and 2 ml of *H. neptunium* cells were centrifuged at 9000 rpm for 2 min at RT (Eppendorf Centrifuge 5424, Germany). The supernatant was discarded and the pellets were washed in 1 ml MB medium or ASM supplemented with 300 µM DAP (9000 rpm for 2 min at RT). Both pellets were resuspended in 1 ml MB medium



or ASM supplemented with 300  $\mu\text{M}$  DAP and mixed. The mixed culture was spotted on a MB or ASM agar plate containing 300  $\mu\text{M}$  DAP and incubated overnight at 28°C. Cells were scraped from the plate, resuspended in 1 ml fresh MB medium or ASM, and pelleted by centrifugation (7000 rpm for 2 min at RT). They were washed twice in 1 ml medium without DAP (7000 rpm for 2 min at RT). Finally, the pellet was resuspended in 1 ml MB medium or ASM and a 1:10 dilution was made. 200  $\mu\text{l}$  of the undiluted cells and the 200  $\mu\text{l}$  of the 1:10 dilution were plated on MB or ASM agar plates supplemented with the corresponding antibiotic. Plates were incubated at 28°C for at least five days until single colonies appeared.

### 4.3 Microscopic methods

For visualizing bacterial cells via differential interference contrast (DIC), phase contrast (Ph3) or for fluorescence microscopy, 2  $\mu\text{l}$  cells were immobilized on agarose pads (1% [w/v] agarose in ddH<sub>2</sub>O). Microscopy was performed using a Zeiss Axio Imager.Z1 microscope (Zeiss, Germany) equipped with a Plan-Apochromat 100x/1.46 Oil DIC objective and a Plan-Apochromat 100x/1.40 Oil Ph3 M27 objective. Immersol<sup>®</sup> 518F was used as immersion oil. An X-Cite<sup>®</sup> 120PC metal halide lamp (EXFO, Canada) was used for fluorescence microscopy in combination with ET-DAPI (also for HADA), ET-YFP (Venus) or ET-TexasRed (mCherry) filter cubes (Chroma, USA). Pictures were taken with a pco.edge sCMOS camera, recorded with VisiView 4.0.0.5 (Visitron, Germany), and processed with MetaMorph<sup>®</sup> 7.7 (Universal Imaging, USA) and Adobe<sup>®</sup> Illustrator<sup>®</sup> CS6<sup>®</sup> (USA). Cell length measurements were made by utilizing the MetaMorph<sup>®</sup> 7.7 region measurement function.

#### 4.3.1 Nucleoid staining

In order to check the chromosome distribution in *H. neptunium* cells, their nucleoid was stained with DAPI (4',6-diamidino-2-phenylindole) which binds strongly to A-T-rich regions in DNA. A culture of interest was grown to exponential phase and incubated with 1.5  $\mu\text{g/ml}$  DAPI for 15 min at RT in the dark. Samples were analyzed by DIC and fluorescence microscopy.

#### 4.3.2 Visualization of nascent peptidoglycan

An *H. neptunium* culture of interest was grown to exponential phase ( $\text{OD}_{600} = 0.3 - 0.5$ ). 250  $\mu\text{l}$  of culture were pipetted into a tube and 1.25  $\mu\text{l}$  100 mM HADA (7-hydroxycoumarin-3-carboxylic acid-amino-D-alanine) were added. The sample was incubated at 28°C for 9 min with shaking, after which 100% ethanol was added to a final concentration of 70%. The cells were incubated at RT for 20 min in the dark. They were then washed three times by addition of 500  $\mu\text{l}$  sterile PBS (137 mM NaCl, 2.7 mM KCl, 10 mM Na<sub>2</sub>HPO<sub>4</sub>, 2 mM KH<sub>2</sub>PO<sub>4</sub>) and centrifugation at 9000 rpm for 2 min at RT (Eppendorf Centrifuge 5424, Germany). Finally, the cells were resuspended in 50 – 100  $\mu\text{l}$  sterile PBS, and samples were analyzed by fluorescence microscopy.

## 4.4 Molecular biology methods

### 4.4.1 Isolation of bacterial DNA

Chromosomal DNA of *H. neptunium* was isolated using the NucleoSpin® Microbial DNA kit (MACHEREY-NAGEL, Germany) following the manufacturer's instructions.

### 4.4.2 Polymerase chain reaction (PCR)

PCR for amplification of DNA products for cloning purposes was performed using the KOD Hot Start DNA-Polymerase Kit (Merck, Deutschland). All components of a standard reaction are listed in Table 3. A BioRad C1000™ Thermal Cycler (BioRad, USA) was used for amplification with the respective PCR program (Table 4). PCR products were purified using the GenElute™ PCR Clean-Up-Kit (Sigma, USA).

**Table 3:** Components of a standard PCR reaction mix.

Components	Volume
ddH <sub>2</sub> O	33 µl
10x KOD-PCR buffer	5.0 µl
dNTPs (2 mM)	5.0 µl
DMSO	2.5 µl
MgSO <sub>4</sub> (25 mM)	2.0 µl
template DNA	1.0 µl
Primer_for (100 µM)	0.25 µl
Primer_rev (100 µM)	0.25 µl
KOD-Polymerase (1 U/µl)	0.5 µl

**Table 4:** Thermo profile of a standard PCR reaction.

Step	Temperature [°C]	Time	Cycles
Initial denaturation	94	2 min	1
Denaturation	94	35 sec	} 30
Primer annealing	65	35 sec	
Elongation	72	30 sec per 1 kb	
Final elongation	72	5 min	1
Pause	12	∞	-

### 4.4.3 Colony PCR

To identify positive bacterial clones, colony PCR was performed. Single colonies of *E. coli* were picked and transferred into a PCR tube containing a 10 µl PCR reaction mixture. In the case of *H. neptunium* clones, the picked cells were transferred into 50 µl ddH<sub>2</sub>O and lysed at 95°C for 10 min. 2 µl of the supernatant were used as a template for the PCR reaction. BioMix™ Red (Bioline, Germany) was used for all colony PCR reactions (Table 5).

A BioRad C1000™ Thermal Cycler (BioRad, USA) was used for amplification with the respective PCR program (Table 6).

**Table 5:** Components of a standard colony PCR reaction mix.

Components	Volume
ddH <sub>2</sub> O	3.4 µl
2x Biomix™ Red	5.0 µl
DMSO	0.5 µl
Template DNA	colony or 2.0 µl
Primer_for (100 µM)	0.05 µl
Primer_rev (100 µM)	0.05 µl

**Table 6:** Thermo profile of a standard colony PCR reaction.

Step	Temperature [°C]	Time	Cycles
Initial denaturation	94	4 min	1
Denaturation	94	30 sec	} 28
Primer annealing	63	30 sec	
Elongation	72	15 sec per 1 kb	
Final elongation	72	4 min	1
Pause	12	∞	-

#### 4.4.4 Determination of the quality and purity of DNA

The concentration of DNA and the purity of PCR products and plasmids were determined photometrically using a NanoDrop® spektrophotometer ND-1000 (Thermo Scientific, USA). 1 µl samples were analyzed. If double-stranded DNA shows an absorption at 260 nm of 1, a concentration of 50 µg/ml was assumed. The purity was determined by the 260 nm/280 nm extinction ratio. Ideally, the ratio should have a value of 1.8 (Sambrook *et al.*, 1989).

#### 4.4.5 Agarose gel electrophoresis

DNA fragments were separated by agarose gel electrophoresis according to their size. 1% [w/v] agarose was dissolved via boiling in 0.5x TAE buffer (20 mM Tris-HCl, 0.175% acetic acid, 0.5 mM EDTA, pH 8) to prepare agarose gels. Ethidium bromide (50 µl/l) was added to the solution after cooling. The gels were poured into home-made chambers. After solidification, gels were loaded with samples and DNA separation occurred at a constant voltage of 160 V for 20 min in 0.5x TAE buffer. Samples were mixed with 6x DNA Loading Dye (Thermo Scientific, USA). GeneRuler™ 1 kb DNA Ladder (Fermentas, Germany) and NEB 100 bp DNA Ladder (NEB, USA) were used as DNA length standard. The separated DNA fragments were visualized at 254 nm on a UV-Transilluminator (UVP-BioDoc-IT™ Imaging System, UniEquip, Germany). DNA products of interest were purified using the GenElute™ Gel Extraction Kit (Sigma-Aldrich, Germany).

#### 4.4.6 Restriction and ligation of DNA fragments and Gibson assembly

Restrictions of vectors and DNA fragments (inserts) were performed according to the manufacturer's instructions using the recommended buffers. The standard restriction reaction is listed in Table 7. Samples were incubated at 37°C for a maximum of 2 h and purified using the PCR Clean-up Kit (Sigma, USA).

**Table 7:** Components of a standard restriction mix.

Components	Restriction of vector DNA	Restriction of insert
ddH <sub>2</sub> O	77 µl	38 µl
10x buffer	10 µl	10 µl
Template DNA	10 µl	50 µl
Restriction enzyme(s) (10 U/µl)	1 µl	1 µl
SAP (1 U/µl) optional	1 µl	-

Afterwards, DNA ligation reaction was performed using the T4 DNA ligase following the manufacturer's instructions. A standard ligation was incubated at RT up to 1 h (Table 8).

**Table 8:** Components for a standard ligation mix.

Components	Volume
ddH <sub>2</sub> O	9.75 µl
5x Rapid Ligation Buffer	4 µl
Insert DNA	4 µl
Vector DNA	2 µl
T4 DNA-Ligase (5 U/µl)	0.25 µl

Gibson assembly was performed as an alternative to classical cloning via restriction and ligation. Only restriction of the vector DNA was necessary. The corresponding DNA insert was generated via PCR using special PCR primers. The PCR reaction produced overlapping ends of the insert annealing to the linearized vector. Vector and insert were incubated in Gibson master mix (Table 9) in equimolar amounts at 50°C for 1 h. The reaction was performed in 5x isothermal reaction buffer (25% [w/v] PEG 8000, 500 mM Tris-HCL, pH 7.5, 50 mM MgCl<sub>2</sub>, 50 mM DTT, 5 mM NAD, 1 mM dNTP). *E. coli* cells were directly transformed with 10 µl of the reaction mix.

**Table 9:** Components of the Gibson master mix.

Components	Volume
5x isothermal reaction buffer	320 µl
T5 Exonuclease (10 U/µl)	0.64 µl
Phusion DNA Polymerase (2 U/µl)	20 µl
Taq DNA ligase (40 U/µl)	160 µl
ddH <sub>2</sub> O	699.36 µl

#### 4.4.7 Isolation of plasmid DNA and sequencing

Overnight cultures of *E. coli* TOP10 cells carrying the plasmid of interest were used for plasmid preparation using the GenElute™ Plasmid Miniprep Kit (Sigma, USA). The concentration of plasmid DNA was determined using a NanoDrop® spektrophotometer ND-1000 (Thermo Scientific, USA). Subsequently, the plasmids were sent to Eurofins MWG Operon (Germany) and sequenced. The company's instructions for preparing DNA sequence samples were followed. The results were analyzed using SnapGene® 3.2.1 (GSL Biotech LL, USA).

#### 4.4.8 Generation of markerless deletions and insertion in *H. neptunium*

To delete single genes in *H. neptunium*, the suicide vector pNPTS138 (M. R. K. Alley, unpublished) was used. In-frame deletions were generated by double-homologous recombination leaving 30 – 36 bp of the 5' and 3' end of the target gene in the chromosome. To this end, 550 – 750 bp long up- and downstream flanking regions of the target genes were cloned into the pNPTS138 vector. The resulting plasmids were used to transform *H. neptunium* by conjugation. Cells were plated on MB or ASM agar plates supplemented with kanamycin, which served as the selection marker for the first homologous recombination. Colony PCR was performed to test for the successful integration of the plasmid at one of the two flanking regions. Positive clones were inoculated in plain MB medium or ASM and grown at 28°C overnight. Subsequently, cells were plated in a 1:200 dilution on MB or ASM plates supplemented with 3% [w/v] sucrose to select for the second homologous recombination event. Plates were incubated at 28°C for at least five days until colonies appeared. Single colonies that arose from the second homologous recombination were re-streaked in parallel on MB/ASM-kanamycin and MB/ASM-sucrose plates to test for kanamycin-sensitive and sucrose-resistant clones. Deletion of the target region was verified by colony PCR, since the second homologous recombination gives rise to either deletion mutants of *H. neptunium* or wild type.

For the generation of markerless insertions, alleles encoding C-terminal fluorescent protein fusions were generated. Additionally, a 500 bp long downstream flanking region of the target gene was amplified and cloned together with the allele encoding the C-terminal fluorescent protein fusion (mCherry) in the pNPTS138 vector. The resulting plasmids were used to transform *H. neptunium* by conjugation, and markerless insertion mutants were generated as described above.

#### 4.4.9 Construction of plasmids

Plasmids were designed *in silico* using the program SnapGene® 3.2.1 (GSL Biotech LL, USA). Oligonucleotides used for the PCR amplification are listed in Table S6, those were for colony PCR can be found in Table S7 in the appendix. All constructed plasmid are given in Table S5 in the appendix.

### **Plasmids for the construction of markerless deletions or insertions in *H. neptunium***

**pSR50** was constructed by amplification of the upstream flanking region of *lmdB* from HNE EC36 chromosomal DNA using primer oSR120 and oEC89 (upstream). The vector pEC35 and the upstream fragment were digested with PstI and EcoRI. The fragment was ligated with pEC35.

**pSR55** was constructed by amplification of two fragments for overlap extension PCR using primer oSR135 and oSR136 (template pWS27) and oSR137 and oSR138 (HNE ATCC15444 chromosomal DNA). Both fragments were used as templates for overlap extension PCR to generate an *lmdA-mcherry*-downstream fragment using primer oSR135 and oSR138. The vector pNPTS138 was digested with HindIII and NheI. The linearized vector and PCR product were directly used for Gibson assembly.

**pSR56** was constructed by amplification of two fragments for overlap extension PCR using primer oSR139 and oSR140 (template pEC10) and oSR141 and oSR142 (HNE ATCC15444 chromosomal DNA). The two fragments were used as templates for overlap extension PCR to generate an *lmdD-mcherry*-downstream fragment using primer oSR139 and oSR142. The vector pNPTS138 was digested with HindIII and NheI. The linearized vector and PCR product were directly used for Gibson assembly.

**pSR57** was constructed by amplification of three fragments for overlap extension PCR using primer oSR143 and oSR144 (HNE ATCC15444 chromosomal DNA), oSR145 and oSR146 (template pSR47) and oSR147 and oSR148 (HNE ATCC15444 chromosomal DNA). All fragments were used as templates for overlap extension PCR to generate an *lmdE-mcherry*-downstream fragment using primer oSR143 and oSR148. The vector pNPTS138 was digested with BamHI and NheI. The linearized vector and PCR product were directly used for Gibson assembly.

**pSR65** was constructed by amplification of the flanking regions of *ftsEX* from HNE ATCC15444 chromosomal DNA using primer oSR182 and oSR183 (upstream) and oSR184 and oSR185 (downstream). The vector pNPTS138 was digested with HindIII and NheI. The linearized vector and PCR products were directly used for Gibson assembly.

### **Plasmids for complementation of in-frame deletion mutants of *H. neptunium***

**pSR54** was constructed by amplification of *lmdE* from HNE ATCC15444 chromosomal DNA using primer oSR135 and oSR136. The vector pCCHYC-2 was digested with NdeI and NheI. The linearized vector and PCR product were directly used for Gibson assembly.

**pSR77** was constructed by amplification of *ftsEX* from HNE ATCC15444 chromosomal DNA using primer oSR234 and oSR235. The vector pCCHYC-2 was digested with NdeI and NheI. The linearized vector and PCR product were directly used for Gibson assembly.

**pSR78** was constructed by amplification of *amiC*<sup>E370A</sup> from mutated pEC77\* using primer oSR236 and oSR237. The vector pCCHYC-2 was digested with NdeI and KpnI. The linearized vector and PCR product were directly used for Gibson assembly.

### Plasmids for localization analysis in *E. coli*

**pSR61** was constructed by amplification of *amiC-mCherry* from pEC115 using primer oSR162 and oSR163. The vector pBAD24 was digested with NheI and KpnI. The linearized vector and PCR product were directly used for Gibson assembly.

### Plasmids for expression in *E. coli*

**pSR68:** For the overexpression and purification of His<sub>6</sub>-SUMO-AmiC, pSR68 was constructed by amplification of *amiC* from HNE ATCC15444 chromosomal DNA using primer oSR200 and oSR201. The vector pTB146 was digested with SapI. The linearized vector and PCR product were directly used for Gibson assembly.

**pSR69:** For the overexpression and purification of His<sub>6</sub>-SUMO-LmdE, pSR69 was constructed by amplification of *lmdE* from HNE ATCC15444 chromosomal DNA using primer oSR202 and oSR203. The vector pTB146 was digested with SapI. The linearized vector and PCR product were directly used for Gibson assembly.

**pSR72:** For the overexpression and purification of His<sub>6</sub>-SUMO-AmiC<sup>E370A</sup>, pSR68 was amplified using primer oSR221 and oSR222 to insert the mutation. PCR product was digested with DpnI to digest the template vector. Restriction sample was directly used for transformation of *E. coli* TOP10.

**pSR73:** For the overexpression and purification of His<sub>6</sub>-SUMO-LmdA, pSR73 was constructed by amplification of *lmdA* from HNE ATCC15444 chromosomal DNA using primer oSR223 and oSR224. The vector pTB146 was digested with SapI. The linearized vector and PCR product were directly used for Gibson assembly.

**pSR74:** For the overexpression and purification of His<sub>6</sub>-SUMO-LmdE<sup>CC</sup>, pSR74 was constructed by amplification of *lmdE<sup>CC</sup>* from HNE ATCC15444 chromosomal DNA using primer oSR202 and oSR225. The vector pTB146 was digested with SapI. The linearized vector and PCR product were directly used for Gibson assembly.

**pSR75:** For the overexpression and purification of His<sub>6</sub>-SUMO-LmdE<sup>M23</sup>, pSR75 was constructed by amplification of *lmdE<sup>M23</sup>* from HNE ATCC15444 chromosomal DNA using primer oSR226 and oSR203. The vector pTB146 was digested with SapI. The linearized vector and PCR product were directly used for Gibson assembly.

**pSR76:** For the overexpression and purification of His<sub>6</sub>-SUMO-FtsX<sup>Loop1</sup>, pSR76 was constructed by amplification of *ftsX<sup>Loop1</sup>* from HNE ATCC15444 chromosomal DNA using primer oSR232 and oSR233. The vector pTB146 was digested with SapI. The linearized vector and PCR product were directly used for Gibson assembly.

### Plasmid for transposon mutagenesis in *H. neptunium*

**pSR51** was constructed by amplification of *P<sub>HNE\_0038</sub>* from HNE ATCC15444 chromosomal DNA using primer oSR122 and oSR123. The vector pSAM-RI and the PCR product *P<sub>HNE\_0038</sub>* was digested with BamHI and NdeI. PCR product was ligated with pSAM-RI.

## 4.5 Biochemical methods

### 4.5.1 SDS polyacrylamide gel electrophoresis (SDS-PAGE)

Proteins were separated by SDS-PAGE according to (Laemmli, 1970). First of all, a resolving gel (11%) was prepared followed by a stacking gel on top (Table 10). Glass plates, spacer and combs were cleaned with ethanol and assembled into a gel electrophoresis chambers (PerfectBlue™ Twin S system, Peqlab, USA).

**Table 10:** Components of the resolving and stacking gel.

Components	Resolving gel (11%)	Stacking gel
ddH <sub>2</sub> O	1.90 ml	1.43 ml
4x resolving gel buffer	1.25 ml	-
4x stacking gel buffer	-	625 µl
30% [v/v] Acrylamid (37, 5:1)	1.90 ml	417 µl
10% [w/v] APS	40 µl	25 µl
TEMED	3 µl	1.9 µl

To prepare samples for gel electrophoresis, cultures of interest were harvested by centrifugation (Eppendorf Centrifuge 5424, Germany) at 14,680 rpm for 1 min and resuspended in 2x SDS sample buffer (100 µl per 1 OD<sub>600</sub> unit). Samples were boiled at 95°C for 10 min in a heat block (VWR, USA). 15 µl of each sample was used for loading. PageRuler™ Prestained Protein Ladder (Fermentas, Germany) was used as a molecular weight standard. Gels were run at a constant 30 mA per gel in 1x SDS running buffer (Table 11).

After electrophoresis, proteins were stained with Coomassie blue solution (1 g/l Coomassie Brilliant Blue R250, 50% [v/v] methanol, 40% [v/v] ddH<sub>2</sub>O, 10% [v/v] acetic acid). Gels were incubated for 10 min on a rocker and destained with destaining solution (10% [v/v] acetic acid, 30% [v/v] methanol, 60% [v/v] ddH<sub>2</sub>O) for 40 min, followed by an overnight incubation in dH<sub>2</sub>O on a rocker (Stuart, UK).

**Table 11:** Used buffers and solutions for SDS-PAGE.

Components	2x SDS-sample buffer	10x SDS-running buffer	4x resolving gel buffer	4x stacking gel buffer
Tris base	125 mM	250 mM	1.5 M	500 mM
Glycerol	20% [v/v]	-	-	-
Glycine	-	1.92 M	-	-
SDS	2% [w/v]	1% [w/v]	0.4% [w/v]	0.4% [w/v]
DTT	200 mM	-	-	-
Bromphenol blue	0.001% [w/v]	-	-	-
pH value (adjust with HCl)	6.8	-	6.8	8.8



### 4.5.2 Immunoblot analysis

Separated proteins were transferred from SDS polyacrylamide gels onto a polyvinylidene fluoride membrane (Millipore Immobilon™-P Transfer Membrane, Millipore, USA) with a PerfectBlue™ Semi-Dry-Elektro blotter (Peqlab, USA). The membrane was activated in 100% methanol for 15 sec, washed with ddH<sub>2</sub>O and equilibrated in 1x Western transfer buffer. The gel, the membrane and blotting papers then were soaked in 1x Western transfer buffer (25 mM Tris-HCl, 0.192 M glycerol, 10% [v/v] methanol) for 5 min. The stack was assembled according to the manufacturer's instructions and the proteins were transferred at 2 mA/cm<sup>2</sup> for 1.5 h. Afterwards, the membrane was blocked in 2.5% [w/v] milk powder in TBST (10 mM Tris-HCl, 150 mM NaCl, 1% [v/v] Tween 20, pH 7.5) overnight at 4°C on a rocker. This blocking solution was discarded and the membrane was incubated with the primary antibody solution for protein detection. The primary antibody solution (antibody in adequate dilution in blocking solution) was incubated at RT for 2 h (Table 12). Subsequently, the membrane was washed three times for 5 – 10 min in 1x TBST. The secondary antibody solution (anti-rabbit IgG linked to horseradish peroxidase (HRP) in blocking solution) was applied to the membrane and incubated at RT for 1h. Solution was discarded and membrane was washed 3 – 5 times for 5 min in 1x TBST.

**Table 12:** Antibodies used in this study.

Antibody	Dilution	Reference
anti-GFP (for anti-YFP)	1:10000	Sigma-Aldrich, Germany
anti-mCherry	1:10000	BioVision, USA
anti-CtrA	1:10000	Eurogentec, Belgium
HRP-labelled anti rabbit IgG	1:20000	PerkinElmer, USA

For detection of proteins the Western Lightning™ Chemiluminescence Reagent Plus Kit (PerkinElmer, USA) was used according to the manufacturer's instructions. Chemiluminescence was detected with a ChemiDoc MP imaging system (Bio-Rad, USA). The membrane was incubated in amido black (0.1% [w/v] amido black 10B, 40% [v/v] methanol, 1% [v/v] acetic acid) at RT for 10 min to verify correct loading of protein samples. Finally, destaining occurred in dH<sub>2</sub>O until signals were visible.

### 4.5.3 Protein fractionation

Biochemical fractionation was performed using a modification of a previously published protocol (Chen *et al.*, 2005). An *H. neptunium* strain of interest was cultured in 80 ml ASM to an OD<sub>600</sub> of 0.6 and harvested by centrifugation at 9000 rpm for 10 min at 4°C in a SS34 rotor (Thermo Fisher, USA). The pelleted cells were washed once with 1 volume buffer A (200 mM Tris-HCl, pH 8) and finally resuspended in 1/10 volume buffer B (60 mM Tris-HCl, 200 mM sucrose, 0.2 mM EDTA, pH 8). This cell suspension was incubated with 100 µg/ml phenylmethylsulfonyl fluorid (PMSF), 5 µg/ml DNase I and 10 mg/ml lysozyme for 10 min on a rocker at RT. Cells were disrupted by three passages through a French Press at 16,000 psi. Remaining intact cells and cell debris were removed by centrifugation at 4.000 x g for 10 min at 4°C. Proteins were fractionated by three ultracentrifugation steps at 100,000 x g for 1 h at 4°C using a Beckman-Coulter Optima™ Max-XP ultracentrifuge. After the first centrifugation, the supernatant, containing soluble proteins, was removed and mixed with

an appropriate amount of 2x SDS sample buffer. The pellet was washed once with 1 volume buffer A. After the third centrifugation step, the pellet was resuspended in 1 volume buffer B and mixed with 2x SDS sample buffer. Protein samples were heated for 10 min at 95°C and analyzed by immunoblotting using antibodies against CtrA and mCherry as controls to confirm successful separation of soluble and membrane proteins.

### 4.5.4 Co-immunoprecipitation and mass-spectroscopy

For Co-IP of AmiC-mCherry, *H. neptunium* WT (negative control) and SR23 (*amiC-mCherry*) were grown in 200 ml ASM to an OD<sub>600</sub> 0.6. Cells were harvested by centrifugation (9000 rpm, 10 min, 4°C), washed in 200 ml 1x PBS and pelleted by centrifugation (9000 rpm, 10 min, 4°C). They were resuspended in 200 ml 1x PBS following the addition of *para*-formaldehyde to a final concentration of 0.6% to cross-link proteins for 5 min at 37°C. The reaction was quenched by the addition of glycine to a final concentration of 125 mM (in 1 x PBS) for 5 min at RT. Cells were pelleted by centrifugation (9000 rpm, 10 min, 4°C) and washed two times with 100 ml of wash buffer (50 mM NaPO<sub>4</sub>, pH 7.4, 5 mM MgCl<sub>2</sub>). The pellets were washed once in 40 ml of wash buffer (9000 rpm, 10 min, 4°C), resuspended in 100 ml Co-IP-Buffer (20 mM HEPES, pH 7.4, 100 mM NaCl, 20% glycerin, 0.5% Triton X-100) per 1 g cells and centrifuged (9000 rpm, 10 min, 4°C). The pellets were resuspended in 1/10 volume of Co-IP-Buffer supplemented with 10 mM MgCl<sub>2</sub>, 10 mg/ml lysozyme, 5 µg/ml DNaseI and 100 µg/ml PMSF, and incubated on ice for 30 min. Cells were disrupted by three passages through a French Press (16,000 psi). The cell debris were removed by centrifuge at 13,000 rpm for 10 min at 4°C.

10 µl RFP-Trap<sup>®</sup> sepharose beads (Chromotec, Germany) were added to the clear lysate and incubated for 1 h at 4°C on a rotator. The sepharose beads were centrifuged at 2,000 rpm for 30 sec (Eppendorf Centrifuge 5424, Germany). 700 µl 100 mM ammonium-bicarbonate was added to the beads and mixed. Beads were centrifuged at 2000 rpm for 1 min at 4°C following three washing steps. 200 µl elution buffer 1 (1 M urea, 100 mM ammonium-bicarbonate, 1 µg trypsin per sample) were added to the beads and incubated for 45 min on a thermomixer (Eppendorf, Germany) at 27°C at 1200 rpm. Beads were centrifuged to collect the supernatant following the addition of 80 µl elution buffer 2 (1 M urea, 100 mM ammonium-bicarbonate, 5 mM tris-2-carboxyethyl-phosphine), after centrifugation the supernatant was collected and combined with the first eluate. The wash was repeated using 80 µl elution buffer 2, the supernatant was collected and combined to the first eluate. The reaction was continued on a thermomixer at 27°C without shaking overnight. 2 µl 10 mM iodoacetamide was added, mixed and incubated for 30 min in the dark. Trifluoroacetic acid (TFA) was added to a final concentration of 1% and mixed.

Products were purified on a C18-microspin column. The column was conditioned with 300 µl Buffer 1 (0.1% [v/v] TFA; centrifugation at 1400 rpm, 30 sec) and equilibrated with 300 µl Buffer 2 (50% [v/v] acetonitrile, 50% [v/v] ddH<sub>2</sub>O, 0.1% [v/v] TFA; centrifugation at 1800 rpm, 30 sec). The sample was loaded and washed once with 300 µl Buffer 3 (5% [v/v] acetonitrile, 95% [v/v] ddH<sub>2</sub>O, 0.1% [v/v] TFA; centrifugation at 1800 rpm, 30 sec) and once with 150 µl Buffer 3 (centrifugation at 1600 rpm, 30 sec). Bound peptides were eluted into a new tube with 300 µl Buffer 4 (100% acetonitrile; centrifugation at 1200 rpm, 30 sec) and twice 150 µl Buffer 4 (centrifugation at 1200 rpm, 30 sec). Eluted peptides were concentrated under vacuum to dryness. Finally, they were dissolved in 100 µl reconstitution buffer (0.15% [v/v]

formic acid, 2% [v/v] acetonitrile), transferred into a LC vial and stored at -20°C until submission to mass spectroscopic analysis.

#### 4.5.5 Protein purification

Proteins were His<sub>6</sub>-SUMO-tagged and purified. In a second step, the His<sub>6</sub>-SUMO (small ubiquitin-related modifier) was successfully cleaved using the specific His<sub>6</sub>-Ulp1 (SUMO protease 1) (Malakhov *et al.*, 2004). To this end, *E. coli* Rosetta<sup>TM</sup> (DE3)pLysS was transformed with the corresponding plasmid. Cells were grown to an OD<sub>600</sub> of 0.6 – 0.8, induced with 0.5 mM IPTG and further incubated at 37°C for 3 h (for LmdE, LmdE<sup>CC</sup> and FtsX<sup>Loop1</sup>) or at 18°C overnight (for AmiC, AmiC<sup>E370A</sup>, LmdA, LmdE<sup>M23</sup>). Afterwards, cells were harvested by centrifugation at 6500 rpm for 10 min at 4°C. Pellet was washed in 1/10 volume of lysis buffer (Table 13) and frozen in liquid N<sub>2</sub>.

Cells were resuspended in buffer BZ3 (2 ml buffer per 1 g of wet cell extract) containing 100 µg/ml PMSF and 10 U/ml DNase I. Cells were disrupted by three passages through a French Press at 16,000 psi. Remaining intact cells and cell debris were removed by centrifugation at 30,000 x g for 1 h at 4°C. The cleared cell lysate was filtered (0.2 µm pore size, Sarstedt, Germany) and applied to a 5 ml HisTrap HP column (nickel sepharose) connected to an ÄKTA purifier 10 system (GE Healthcare, Germany). The column was washed and equilibrated with 5 column volume (CV) of BZ3. The filtered cell lysate was loaded onto the column and proteins were eluted by a linear gradient of imidazole (20 – 250 mM imidazole). The eluate was collected and all relevant fractions were analyzed by SDS-PAGE. Subsequently, fractions containing the protein of interest were pooled and dialyzed against 3 l of CB at 4°C overnight (Table 13). The next day, the sample was centrifuged at 30,000 x g for 20 min at 4°C to remove precipitates.

The protein concentration was determined by a modified Bradford assay (Bradford, 1976) using the Roti<sup>®</sup>-Nonyquant reagent (Carl Roth, Germany) following the manufacturer's instruction. To remove the His<sub>6</sub>-SUMO-tag, the protein was incubated with His<sub>6</sub>-Ulp1 at a molar ratio of 1000:1 (protein:protease) for 2 h at 4°C on a rocker. To separate cleaved His<sub>6</sub>-SUMO tag and His<sub>6</sub>-Ulp1, the protein solution was applied onto a 5 ml HisTrap HP column, which was equilibrated with CB. The flow-through (release of protein of interest) and wash fraction were collected, whereas the His<sub>6</sub>-SUMO tag and the His<sub>6</sub>-Ulp1 remained bound to the column. All relevant fractions were analyzed by SDS-PAGE. The protein of interest was aliquoted, snap-frozen in liquid N<sub>2</sub>, and stored at -80°C until further use.

For unknown reasons, two proteins (LmdE<sup>M23</sup> and FtsX<sup>Loop1</sup>) bound to the column after cleavage of the His<sub>6</sub>-SUMO-tag. Therefore, ion exchange chromatography was performed using the ÄKTA purifier 10 system (GE Healthcare, Germany). The protein solution was dialyzed against 2 l of IEX I buffer at 4°C overnight (Table 13). The next day, the sample was centrifuged at 30,000 x g for 20 min at 4°C to remove precipitates and filtered (0.2 µm pore size, Sarstedt, Germany). The sample was loaded onto a 1 ml Mono Q column (GE Healthcare). The column was washed and equilibrated with 5 CV of IEX I buffer. The protein was eluted by a linear gradient of NaCl (10 – 1000 mM NaCl). The eluate was collected and all relevant fractions were analyzed by SDS-PAGE. Subsequently, fractions containing the protein of interest were pooled and dialyzed against 3 l of storage buffer at 4°C overnight. Aliquots were made, snap-frozen in liquid N<sub>2</sub>, and stored at -80°C until further use.

Dilute protein solutions were concentrated by centrifugation in an Amicon Ultra centrifugal tube (Amicon, USA) at 20,000 x g and 4 °C. Afterwards, the protein concentration was determined as before.

**Table 13:** Components of used buffers.

Buffer	Components
Lysis buffer	50 mM NaH <sub>2</sub> PO <sub>4</sub> , pH 8.0 (NaOH), 300 mM NaCl, 10 mM imidazol
BZ3	50 mM Tris-HCl, pH 7.5, 300 mM NaCl, 20 mM imidazol, 10% [v/v] glycerol
BZ4	50 mM Tris-HCl, pH 7.5, 300 mM NaCl, 250 mM imidazol, 10% [v/v] glycerol
CB (cleavage buffer)	50 mM Tris-HCl, pH 7.5, 150 mM NaCl, 10% [v/v] glycerol
IEX I	25 mM Tris-HCl, pH 7.5, 10 mM NaCl
IEX II	25 mM Tris-HCl, pH 7.5, 1 M NaCl
Storage buffer	50 mM Tris-HCl, pH 7.5, 150 – 300 mM NaCl, 10% [v/v] glycerol

#### 4.5.6 Dye-release assay for PG hydrolysis

The ability of PG remodeling enzymes to hydrolyze PG was tested by performing the dye-release assay as previously described (Uehara *et al.*, 2010; Yang *et al.*, 2012; Zhou *et al.*, 1988). In a first step, purified PG sacculi of wild-type *C. crescentus* CB15N were labelled with Remazol Brilliant Blue (RBB). 1 ml of PG sacculi was incubated with 20 mM RBB in 0.25 M NaOH overnight at 37°C. The preparation was neutralized with 0.5 M HCl (final concentration: 0.25 M). RBB-labelled PG sacculi were pelleted by centrifugation at 21,000 x g for 20 min at RT (Eppendorf Centrifuge 5424, Germany). The PG sacculi were resuspended and washed in ddH<sub>2</sub>O until the supernatant was clear. Finally, the pellet was resuspended in 1 ml ddH<sub>2</sub>O containing 0.02% [v/v] sodium azide and stored at 4°C.

In a second step, 10 µl of RBB-labelled PG sacculi were incubated with 4 µM of purified protein of interest in 100 µl of reaction buffer (25 mM HEPES/NaOH, pH 7.5, 150 mM NaCl, 10% [v/v] glycerol) at 37°C for 2 h. RBB-labelled PG sacculi incubated with reaction buffer alone was used as a negative control and reactions with 4 µM of lysozyme were used as a positive control. The reactions were terminated by incubation at 95°C for 5 min, followed by a centrifugation step (21,000 x g, 20 min at RT). The supernatants were transferred into a fresh tube, and the absorbance was measured at 595 nm using an Ultrospec™ 2100 pro UV/Visible spectrophotometer (GE Healthcare, Germany).

#### 4.5.7 Bio-layer interferometry (BLI)

Interaction analyses of proteins of interest were performed in real time by bio-layer interferometry using a BLItz™ System Package (PALL Life Sciences, USA). The protein of interest was biotinylated for 2 h on ice using a 2-fold molar excess of NHS-PEG<sub>4</sub>-Biotin (Thermo Scientific, USA), followed by an overnight dialysis against 2 x 1 l reaction buffer (25 mM HEPES/NaOH, pH 7.5, 150 mM NaCl, 10% [v/v] glycerol) to remove non-reacted biotin. The biotinylated protein was captured on a high precision streptavidin biosensor (PALL Life Sciences, USA). For AmiC-LmdE binding, the immobilized LmdE (30 µM) was probed with AmiC (0 – 150 µM) in reaction buffer (25 mM HEPES/NaOH, pH 7.5, 150 mM

NaCl, 10% [v/v] glycerol, 10  $\mu$ M BSA, 0.01% [v/v] Triton X-100). The association step was followed by a washing step with reaction buffer to dissociate AmiC from the immobilized LmdE. The association and dissociation traces were recorded.

## 4.6 Transposon mutagenesis in *H. neptunium*

A modified conjugation protocol was used to transform *H. neptunium* in order to create a transposon library. The *H. neptunium* ATCC15444 wild type was grown to stationary phase in 10 ml MB medium at 28°C for 2 days. The preculture was used to inoculate 400 ml MB medium in a 5 L flask and incubated at 28°C for at least 24 h. *E. coli* WM3064 + pSAM-RI (SR74) or *E. coli* WM3064 + pSAM-HNE (pSR51) was inoculated in 10 ml LB medium + 200  $\mu$ g/ $\mu$ l ampicillin + 300  $\mu$ M DAP in the morning and incubated at 37°C. At the end of the day the preculture was used to inoculate 200 ml LB medium + 200  $\mu$ g/ $\mu$ l ampicillin + 300  $\mu$ M DAP and incubated at 37°C over night. Cells were harvested by centrifugation at 7300 rpm for 15 min at RT (rotor: JLA-16.250, Thermo Fisher, USA). Each cell pellet was washed in 200 ml plain MB medium (+ 300  $\mu$ M of DAP for *E. coli* WM3064) by centrifugation at 7300 rpm for 15 min at RT (rotor: JLA-16.250). Cells were resuspended in a total amount of 20 ml MB medium + 100  $\mu$ l of 60 mM DAP and 250  $\mu$ l were spotted on extra dry MB plates + 300  $\mu$ M DAP. Plates were incubated at 28°C for 12h.

Cells were scraped from the plates and transferred into a 50 ml-Falcon tube containing plain MB medium. Cells were pelleted by centrifugation at 5000 g for 15 min at RT and washed three times with 40 ml plain MB medium (5000 g for 15 min at RT). Cells were resuspended in a final volume of 80 ml plain MB medium. 0.25 ml of the cell suspension was plated on well-dried MB + 200  $\mu$ g/ $\mu$ l kanamycin + 50  $\mu$ g/ $\mu$ l gentamycin Petri dishes (92 x 16 mm, Sarstedt, Germany). All plates were incubated at 28°C for 7 days until colony formation was visible.

Colonies were scraped from the plates, transferred into a 50 ml-Falcon tube and centrifuged at 8000 g for 15 min at RT. Pellet was washed three times with 40 ml plain MB medium (centrifugation at 8000 g for 15 min at RT), followed by the resuspension in a final volume of 47  $\mu$ l of plain MB per Petri dish (92 x 16 mm, Sarstedt, Germany). Up to 3 ml of suspension were transferred into a fresh 15 ml-Falcon tubes to make aliquots and snap-froze in liquid N<sub>2</sub>. Aliquots were stored at -80°C until DNA isolation.

TnSeq was performed using the Nextera™ DNA Library Preparation Kit FC-121-1030 (Illumina, USA) and a modified protocol (A. Camilli, unpublished). All oligonucleotides are summarized in Table S8. Genomic DNA was prepared using the NucleoSpin® Microbial DNA (MACHEREY-NAGEL, Germany). The DNA concentration was measured using a NanoDrop® spektrophotometer ND-1000 (Thermo Scientific, USA). From the Nextera™ DNA Library Preparation Kit, 5  $\mu$ l of Tagment DNA buffer, 4  $\mu$ l of genomic DNA at 20 ng/ $\mu$ l, and 1  $\mu$ l of Tagment DNA enzyme were combined in a PCR tube. The sample was mixed and heated for 10 min at 55°C, followed by the addition of 27.5  $\mu$ l ddH<sub>2</sub>O, 5  $\mu$ l 10x KOD-PCR buffer, 5  $\mu$ l 2 mM dNTPs, 2  $\mu$ l MgSO<sub>4</sub>, 1  $\mu$ l of 30  $\mu$ M Nextera 2A-R (oSR230), 1  $\mu$ l of 30  $\mu$ M Tn\_HNE (oSR227), and 0.5  $\mu$ l KOD-Polymerase. After mixing, the following PCR program was run: preheat at 98°C for 1 min, 30 cycles of 98°C for 10 sec followed by 65°C for 20 sec followed by 72°C for 1 min. The run finished with a final 2 min extension at 72°C.

0.5 µl from the first PCR were taken and transferred into a new PCR tube. 37 µl ddH<sub>2</sub>O, 5 µl 10x KOD-PCR buffer, 5 µl 2 mM dNTPs, 2 µl MgSO<sub>4</sub>, 1 µl of 30 µM N701 index (oSR231), 1 µl of 30 µM Tn\_HNE\_N502 index (oSR228), and 0.5 µl KOD-Polymerase were added. After mixing, the following PCR program was run: preheat at 98°C for 1 min, 15 cycles of 98°C for 10 sec followed by 65°C for 20 sec followed by 72°C for 1 min. run was finished with a final 2 min extension at 72°C. Each sample was tested by agarose gel electrophoresis to confirm a smear of products ranging from ~150 – 1500 bp. PCR products were purified using a GenElute™ PCR Clean-Up Kit (Sigma, USA).

Samples were submitted to our collaboration partner Dr. J. Serrania (Dept. of Biology, FB17, Philipps-Universität and LOEWE Center for Synthetic Microbiology, Germany) for TnSeq analysis, together with the sequencing primer Tn\_HNE\_Seq (oSR229). Data were analyzed with the CLC Genomics Workbench 11.0.1 (Qiagen, Germany).

## 4.7 Bioinformatic methods

DNA and protein sequences were obtained from either the database National Centers for Biotechnology Information (NCBI; <http://www.ncbi.nlm.nih.gov/>) (Geer *et al.*, 2010) or the KEGG database (<http://www.genome.jp/kegg/>). Functional domains of proteins were identified by SMART (Simple Modular Architecture Research Tool) analysis (<http://smart.embl-heidelberg.de/>) (Letunic *et al.*, 2009; Schultz *et al.*, 1998) or Pfam analysis (<http://pfam.sanger.ac.uk/>) (Bateman *et al.*, 2004; Sonnhammer *et al.*, 1997). The prediction of signal peptides or transmembrane domains in proteins were done using SignalP (<http://www.cbs.dtu.dk/services/SignalP/>) and TMHMM (<http://www.cbs.dtu.dk/services/TMHMM-2.0/>). Protein structures were modeled with I-TASSER (Iterative Threading ASSEmbly Refinement, <https://zhanglab.ccmb.med.umich.edu/I-TASSER/>) and processed with Pymol 1.8 (DeLano Scientific LLC.). Sequence alignments were generated with Clustal Omega (<https://www.ebi.ac.uk/Tools/msa/clustalo/>) and edited with GeneDoc (Nicholas & Nicholas, 1997). The molecular weight and isoelectric point of proteins were calculated using the ExPASy protparam server (<http://web.expasy.org/protparam/>). Box plots were generated using QtiPlot 0.9.9 and demographs were made with Fiji and R x64 3.1.1.

## 5. APPENDIX

### 5.1 Supplement figures

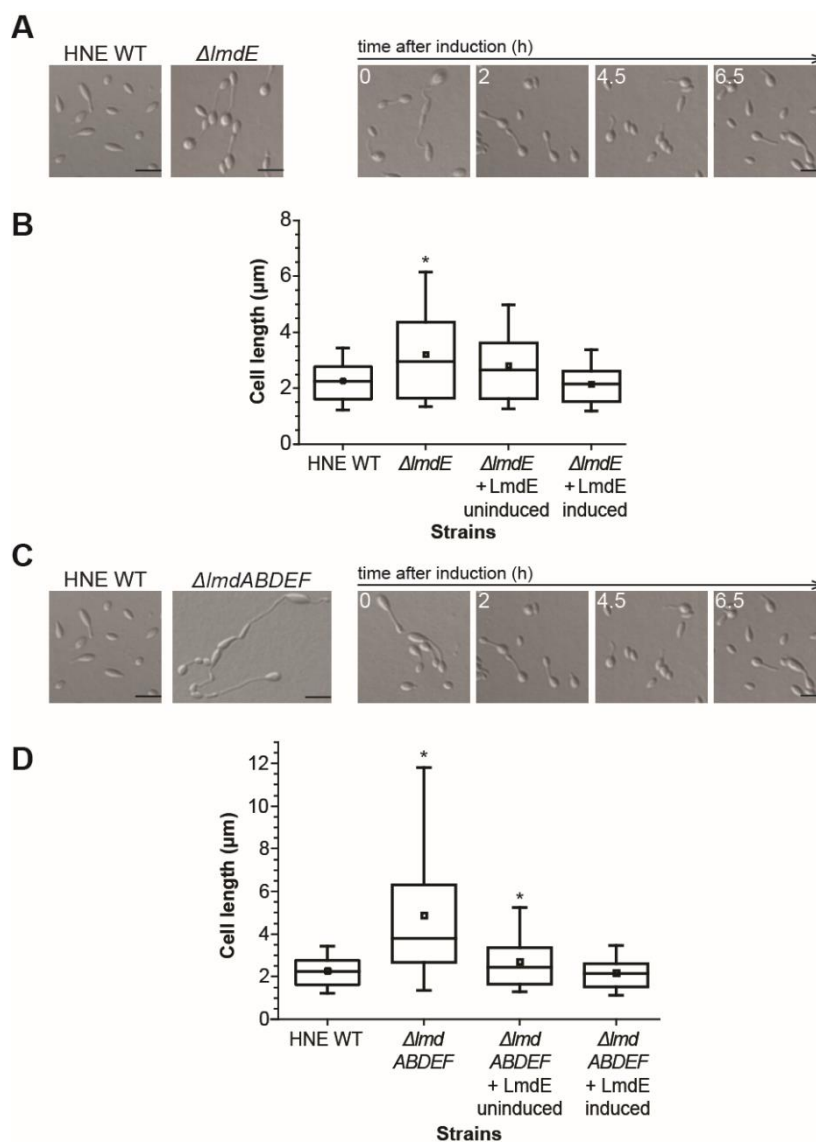


**Figure S1: The *lmdE* gene is responsible for the aberrant phenotypes.** (A) Phenotype of the wild type (HNE WT) and the deletion strain EC39 ( $\Delta lmdE$ ). Complementation of the  $\Delta lmdE$  mutant with native LmdE restores the wild-type morphology. SR44 ( $\Delta lmdE P_{Cu}::P_{Cu}-lmdE$ ) was grown to exponential phase in ASM, induced for 6.5 h with 300  $\mu\text{M}$   $\text{CuSO}_4$  and imaged by DIC microscopy. Scale bar: 3  $\mu\text{m}$ . (B) Cell lengths of the indicated strains. Cells were grown as described in (A). The distribution of cell lengths is shown as a box plot (explanation see Figure 7). Asterisk indicates a  $p$ -value of  $< 0.0001$  ( $t$ -test). (C) Phenotype of the wild type (HNE WT) and the deletion strain SR51 ( $\Delta lmdABDEF$ ). Complementation of the  $\Delta lmdABDEF$  mutant with native LmdE restores the wild-type morphology. SR56 ( $\Delta lmdABDEF P_{Cu}::P_{Cu}-lmdE$ ) was grown to exponential phase in ASM, induced for 6.5 h with 300  $\mu\text{M}$   $\text{CuSO}_4$  and imaged by DIC microscopy. Scale bar: 3  $\mu\text{m}$ . (D) Cell lengths of the indicated strains. Cells were grown as described in (C). The distribution of cell lengths is shown as a box plot (explanation see Figure 7). Asterisks indicate a  $p$ -value of  $< 0.0001$  ( $t$ -test).

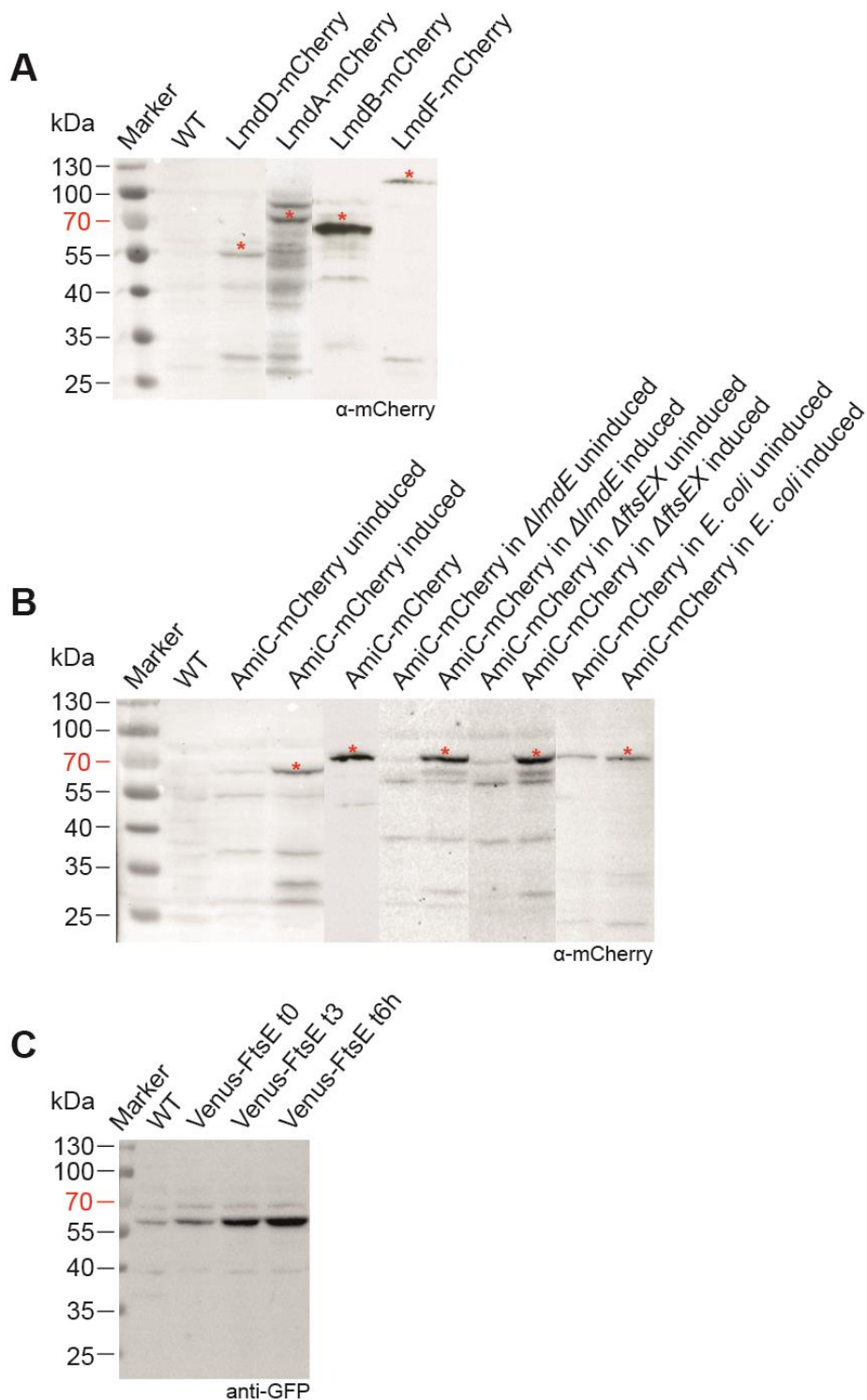


**Figure S2: Stability of fusion proteins.** (A) Wild type cells of *H. neptunium* and strains SR24 (*lmdB-mCherry*), SR26 (*lmdF-mCherry*), SR58 (*lmdD-mCherry*), SR61 (*lmdA-mCherry*) were grown in ASM at 28°C to the exponential phase and analyzed microscopically. An anti-mCherry antibody was used for immunodetection. (B) Strain EC70 (*P<sub>Cu</sub>::P<sub>Cu</sub>-amiC-mCherry*), SR23 (*amiC-mCherry*), SR59 (*P<sub>ara</sub>-amiC-mCherry*), SR71 (*ΔlmdE P<sub>Cu</sub>::P<sub>Cu</sub>-amiC-mCherry*), SR72 (*ΔftsEX P<sub>Cu</sub>::P<sub>Cu</sub>-amiC-mCherry*) were grown to exponential phase in ASM or LB, induced with 300 μM CuSO<sub>4</sub> or 0.02% arabinose and analyzed microscopically. An anti-mCherry antibody was used for immunodetection. (C) Strain JZ12 (*P<sub>Zn</sub>::P<sub>Zn</sub>-venus-ftsE*) was grown to exponential phase in ASM, induced for 6 h with 300 μM ZnSO<sub>4</sub> and analyzed microscopically. An anti-GFP antibody was used for immunodetection.



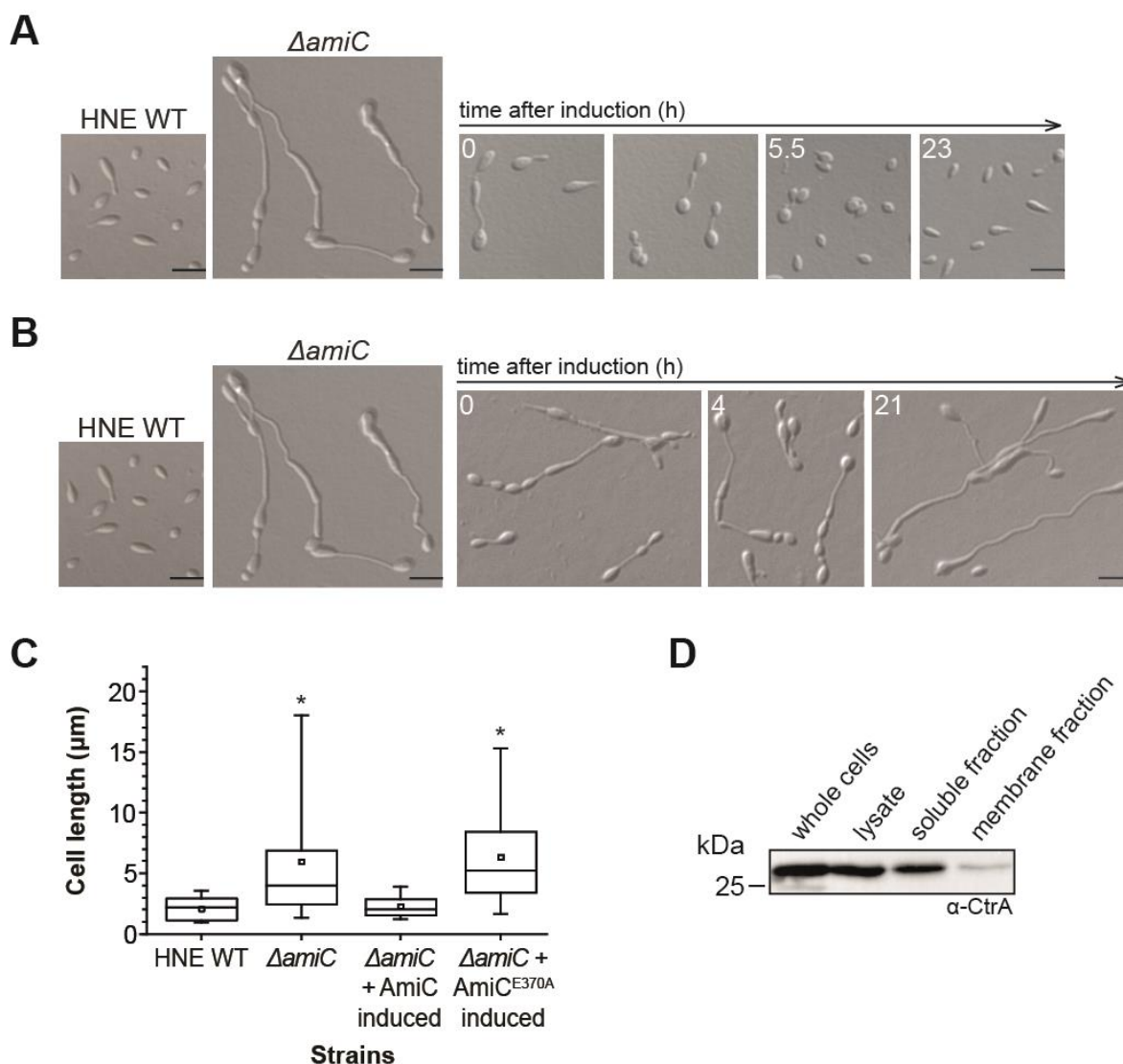


**Figure S3: AmiC is needed for the complementation of the  $\Delta amiC$  mutant.** (A) Phenotype of the wild type (HNE WT) and the deletion strain SR18 ( $\Delta amiC$ ). Cells were grown in ASM at 28°C (shaking at 210 rpm) to the exponential phase and analyzed microscopically. SR21 ( $\Delta amiC P_{Cu}::P_{Cu}-amiC$ ) was grown to exponential phase in MB medium, induced for 23 h with 300  $\mu M$   $CuSO_4$  and imaged by DIC microscopy. Scale bar: 3  $\mu m$ . (B) Complementation of the  $\Delta amiC$  mutant with mutated  $AmiC^{E370A}$  does not restore the wild type phenotype. SR75 ( $\Delta amiC P_{Cu}::P_{Cu}-amiC^{E370A}$ ) was grown to exponential phase in ASM, induced for 21 h with 300  $\mu M$   $CuSO_4$  and imaged by DIC microscopy. Scale bar: 3  $\mu m$ . (C) Cell lengths of the indicated strains. Cells were grown as described in (A and B). The distribution of cell lengths is shown as box plots (explanation see Figure 7). Asterisks indicate a  $p$ -value of  $< 0.0001$  ( $t$ -test). (D) **Control experiment for the protein fractionation of AmiC.** A whole cell lysate of *H. neptunium* wild type was fractionated by ultracentrifugation into the membrane and soluble fractions, followed by immunoblot analysis with anti-CtrA antibody.

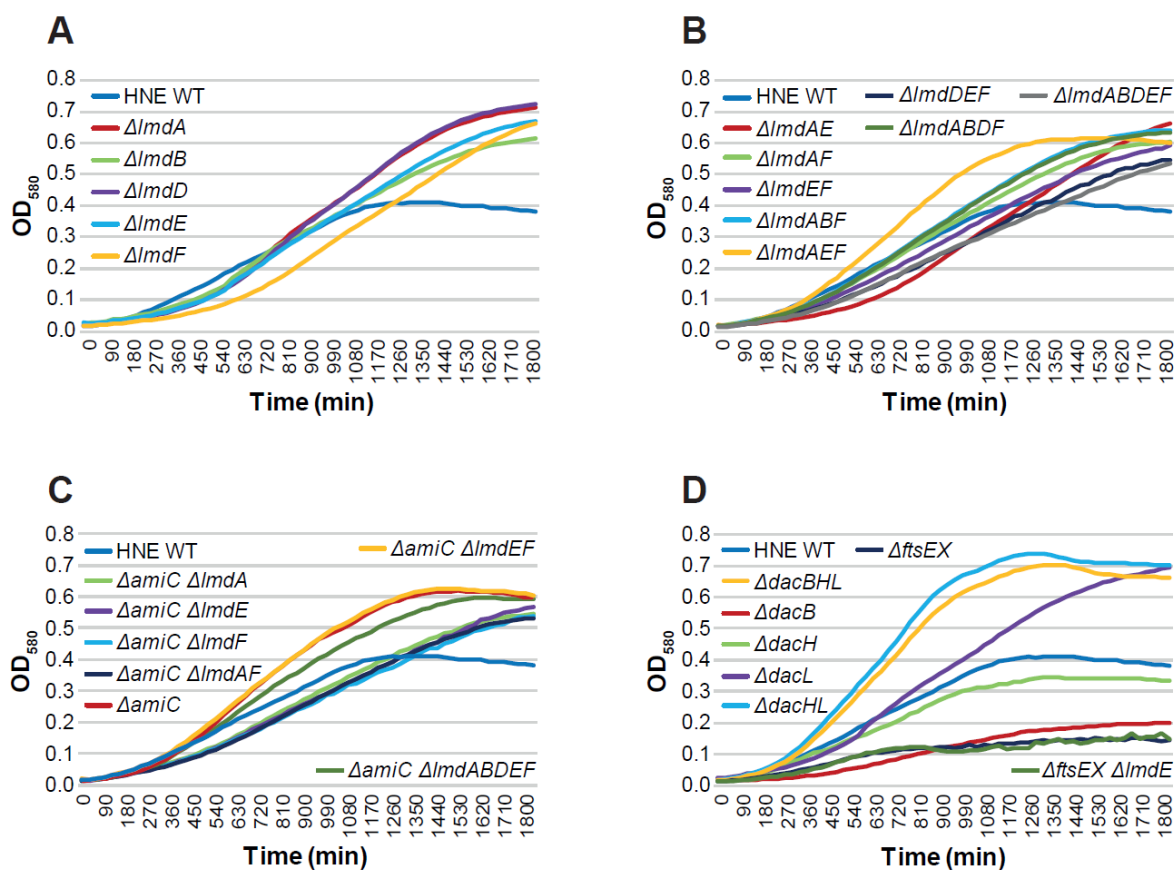


**Figure S4: Effect of deletions in PG remodeling enzymes for the growth of *H. neptunium*.** (A) Deletions of single endopeptidase-encoding genes. Cells were grown in ASM at 28°C (shaking at 210 rpm) to the exponential phase, diluted, inoculated into a 24-well plate, and incubated at 31 – 33°C shaking while cell growth was monitored at OD<sub>580</sub> for 31 h. For details see Material and Methods 4.2.5. (B) Deletions of multiple endopeptidase-encoding genes. Cells were grown as in (A). (C) Deletion of the amidase-encoding gene in combination with specific endopeptidase-encoding genes. Cells were grown as in (A). (D) Deletions of carboxypeptidase-encoding genes and the *ftsEX* genes. Cells were grown as in (A). A list of all strains is given in Table S1 (including doubling times and biofilm production). Growth of strains and measurement of the growth curves see.

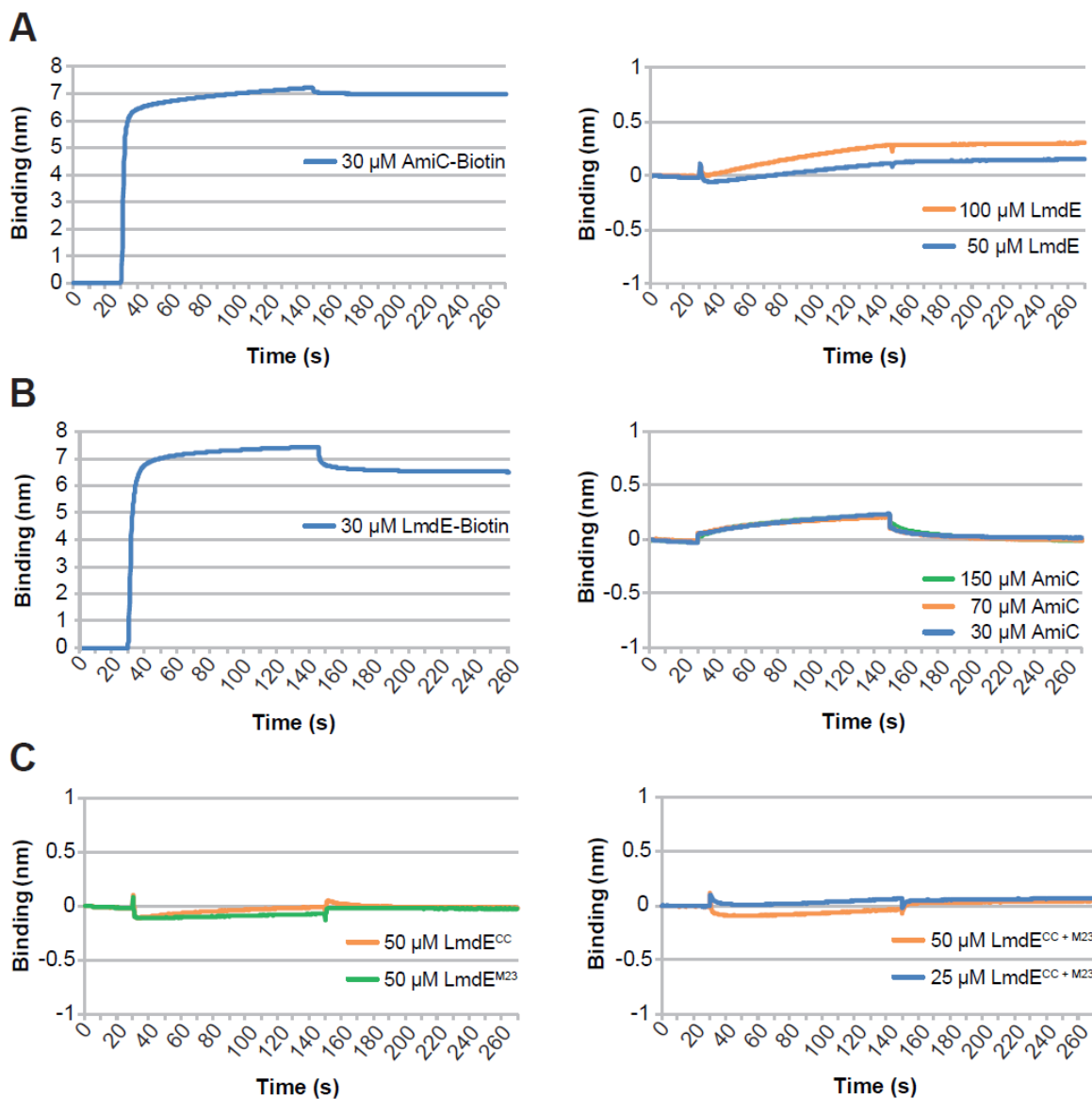


**Figure S5: Control experiments for BLI. (A)** AmiC-Biotin binds strongly to the streptavidin biosensor, whereas non-tagged LmdE shows very weak non-specific binding. **(B)** LmdE-Biotin binds strongly to the streptavidin biosensor, whereas non-tagged AmiC shows very weak non-specific binding. **(C)** LmdE<sup>CC/M23</sup> or LmdE<sup>CC + M23</sup> do not bind to the streptavidin biosensor.

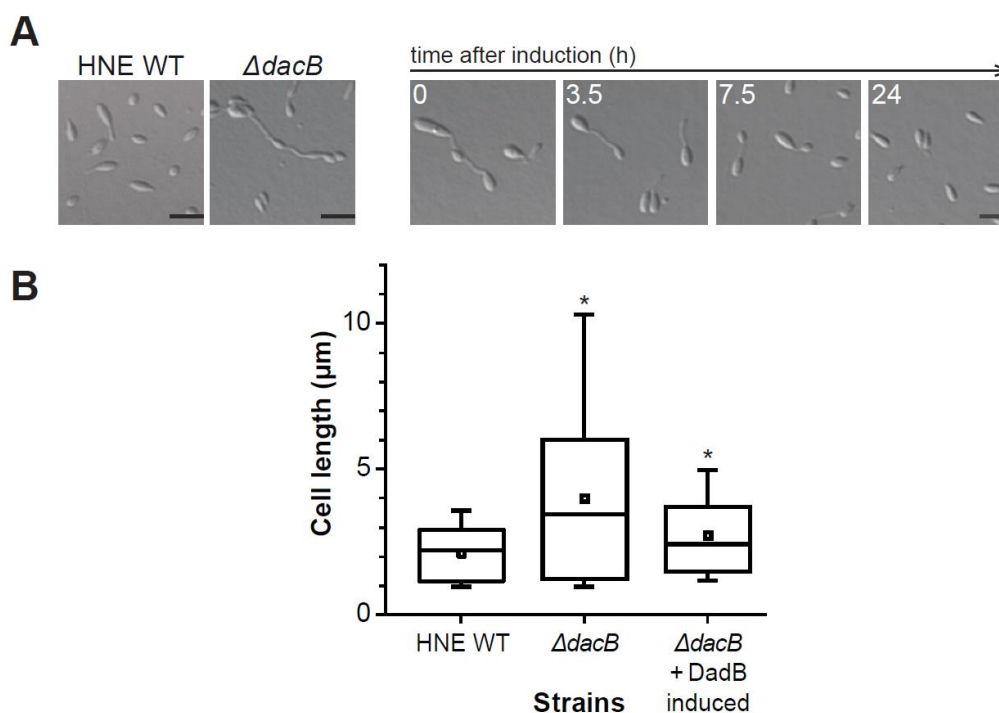


**Figure S6: The *dacB* gene is responsible for the aberrant phenotypes.** (A) Phenotype of the wild type (HNE WT) and the deletion strain SR11 ( $\Delta dacB$ ). Cells were grown in MB medium at 28°C (shaking at 210 rpm) to the exponential phase and analyzed microscopically. Complementation of the  $\Delta dacB$  mutant with native DacB restores the wild type morphology. SR15 ( $\Delta dacB P_{Cu}::P_{Cu}-dacB$ ) was grown to exponential phase in MB medium, induced for 24 h with 300  $\mu\text{M}$   $\text{CuSO}_4$  and imaged by DIC microscopy. Scale bar: 3  $\mu\text{m}$ . (B) Cell lengths of the indicated strains. Cells were grown as described in (A). The distribution of cell lengths is shown as box plots (explanation see Figure 7). Asterisks indicate a  $p$ -value of < 0.0001 ( $t$ -test). Adapted from Roskopf (2014).

## 5.2 Supplemental tables

**Table S1: Characterization of deletion strains generated in this study.** Growth rates were calculated from the represent growth experiments shown in Figure S4. Biofilm production was determined by a biofilm assay using crystal violet. The cell lengths given the mean value and the standard deviation generated from cell length measurements.

Genotype	Strain	Growth rate to WT (%)	Biofilm (%)	Cell length ( $\mu\text{m}$ )
HNE wild type	LE670	100	100	2.01 $\pm$ 0.66
$\Delta amiC$	SR18	89	0	3.73 $\pm$ 2.31
$\Delta lmdA$	EC36	120	0	2.01 $\pm$ 0.75
$\Delta lmdB$	EC53	101	0	2.05 $\pm$ 0.82
$\Delta lmdD$	EC38	125	0	2.10 $\pm$ 0.89
$\Delta lmdE$	EC39	108	0	3.00 $\pm$ 1.33
$\Delta lmdF$	EC90	85	103	2.04 $\pm$ 0.70
$\Delta lmdAE$	EC56	93	0	4.32 $\pm$ 2.74
$\Delta lmdAF$	SR34	92	0	1.99 $\pm$ 0.67
$\Delta lmdEF$	SR35	93	0	3.35 $\pm$ 2.09
$\Delta amiC \Delta lmdA$	SR47	96	0	3.83 $\pm$ 2.79
$\Delta amiC \Delta lmdE$	SR36	95	0	3.60 $\pm$ 2.36
$\Delta amiC \Delta lmdF$	SR37	94	0	3.83 $\pm$ 2.79

**Table S1: Characterization of deletion strains generated in this study.** (continued)

$\Delta$ lmdABF	SR41	95	0	2.13 ± 0.77
$\Delta$ lmdAEF	SR78	92	0	4.66 ± 3.62
$\Delta$ lmdDEF	SR40	94	0	5.93 ± 4.41
$\Delta$ amiC $\Delta$ lmdAF	SR42	100	0	8.48 ± 7.13
$\Delta$ amiC $\Delta$ lmdEF	SR55	87	0	3.07 ± 2.41
$\Delta$ lmdABDF	SR45	96	0	1.98 ± 0.69
$\Delta$ lmdABDEF	SR51	96	0	5.66 ± 3.95
$\Delta$ amiC $\Delta$ lmdABDEF	SR60	87	0	5.82 ± 5.29
$\Delta$ ftsEX	SR64	86	333	6.67 ± 7.35
$\Delta$ ftsEX $\Delta$ lmdE	SR80	85	385	6.84 ± 6.62
$\Delta$ dacB	SR11	98	189	2.87 ± 1.18
$\Delta$ dachH	SR08	92	129	2.12 ± 0.77
$\Delta$ dacL	EC46	80	0	2.25 ± 0.87
$\Delta$ dachL	SR50	102	0	2.13 ± 0.75
$\Delta$ dacBHL	SR54	102	0	1.98 ± 0.69

**Table S2: Significantly enriched genes with a putative interaction with AmiC.** Co-IP was performed using AmiC-mCherry as bait. The experiment was performed in triplicates. Light orange indicate the input proteins, green very interesting and light green interesting candidates for future investigations. Index values display the relative protein abundance in comparison to the HNE WT (control sample). Abbreviation: MW: molecular weight; SP: signal peptide; TM: transmembrane helix; CCRP: coiled-coil rich protein; TPR: tetratricopeptide repeat.

Locus	Predicted proteins	MW	SP/TM	Index
-	mCherry	20 kDa	-	3794176
HNE_0392	Cell division protein FtsQ	32 kDa	1 TM	3391433
HNE_0156	Conserved hypothetical protein, CpoB	33 kDa	SP	3298654
HNE_1815	Rare lipoprotein A, RlpA	42 kDa	SP	3083167
HNE_0427	Conserved hypothetical protein	89 kDa	SP	2312967
HNE_0177	CHAD domain protein	32 kDa	No	2301524
HNE_2697	Outer membrane protein	27 kDa	SP	1868212
HNE_0737	Uncharacterized protein	16 kDa	2 TM	1788527
HNE_2936	Rod shape-determining protein MreC	36 kDa	1 TM	1692700
HNE_0816	Efflux transporter, RND family	39 kDa	1 TM	1542733
HNE_2916	Uncharacterized protein, T6SS_HCP	19 kDa	SP	1234500
HNE_0885	Putative membrane protein	24 kDa	4 TM	1134220
HNE_2474	Uncharacterized protein	136 kDa	SP	961808
HNE_1822	Conserved domain protein	63 kDa	1 TM	891774
HNE_1954	Conserved hypothetical protein	30 kDa	SP	863349
HNE_2317	Uncharacterized protein	27 kDa	SP	844415
HNE_2262	Uncharacterized protein	36 kDa	SP	480906
HNE_3490	Uncharacterized protein, CCRP	69 kDa	No	464267
HNE_0768	Penicillin-binding protein, 1A family, PBP1X	76 kDa	1 TM	464267
HNE_0766	Glycosyl transferase, group 2	42 kDa	No	464267
HNE_3361	Putative lipoprotein	16 kDa	SP	363487
HNE_0674	N-acetylmuramoyl-L-alanine amidase, AmiC	45 kDa	SP	20096
HNE_1179	Uncharacterized protein, TPR	53 kDa	1 TM	150

Table S3: *H. neptunium* strains used in this study.

Strain	Genotype	Reference
LE670	<i>H. neptunium</i> wild type (ATCC15444)	E. Leifson, 1964
SR08	$\Delta dacH$	Rosskopf, 2014
SR11	$\Delta dacB$	Rosskopf, 2014
SR15	$\Delta dacB P_{Cu}::P_{Cu}-dacB$	Rosskopf, 2014
SR18	$\Delta amiC$	Rosskopf, 2014
SR21	$\Delta amiC P_{Cu}::P_{Cu}-amiC$	Rosskopf, 2014
SR23	<i>amiC-mCherry</i>	Rosskopf, 2014
SR24	<i>ImdB-mCherry</i>	Rosskopf, 2014
SR26	<i>ImdF-mCherry</i>	Rosskopf, 2014
SR28	<i>dacL-mCherry</i>	Rosskopf, 2014
SR34	$\Delta ImdAF$	This study
SR35	$\Delta ImdEF$	This study
SR36	$\Delta amiC \Delta ImdE$	This study
SR37	$\Delta amiC \Delta ImdF$	This study
SR40	$\Delta ImdDEF$	This study
SR41	$\Delta ImdABF$	This study
SR42	$\Delta amiC \Delta ImdAF$	This study
SR44	$\Delta ImdE P_{Cu}::P_{Cu}-ImdE$	This study
SR45	$\Delta ImdABDF$	This study
SR47	$\Delta amiC \Delta ImdA$	This study
SR50	$\Delta dacHL$	This study
SR51	$\Delta ImdABDEF$	This study
SR54	$\Delta dacBHL$	This study
SR55	$\Delta amiC \Delta ImdEF$	This study
SR56	$\Delta ImdABDEF P_{Cu}::P_{Cu}-ImdE$	This study
SR57	<i>ImdE-mCherry</i>	This study
SR58	<i>ImdD-mCherry</i>	This study
SR60	$\Delta amiC \Delta ImdABDEF$	This study
SR61	<i>ImdA-mCherry</i>	This study
SR64	$\Delta ftsEX$	This study
SR71	$\Delta ImdE P_{Cu}::P_{Cu}-amiC-mCherry$	This study
SR72	$\Delta ftsEX P_{Cu}::P_{Cu}-amiC-mCherry$	This study
SR73	$P_{Cu}::P_{Cu}-ImdC^N-mCherry$	This study
SR75	$\Delta amiC P_{Cu}::P_{Cu}-amiC^{E370A}$	This study
SR76	$\Delta ftsEX P_{Cu}::P_{Cu}-ftsEX$	This study
SR78	$\Delta ImdAEF$	This study
SR80	$\Delta ftsEX \Delta ImdE$	This study
EC36	$\Delta ImdA$	Cserti <i>et al.</i> , 2017
EC38	$\Delta ImdD$	Cserti <i>et al.</i> , 2017
EC39	$\Delta ImdE$	Cserti <i>et al.</i> , 2017
EC46	$\Delta dacL$	Cserti <i>et al.</i> , 2017
EC53	$\Delta ImdB$	Cserti <i>et al.</i> , 2017

EC56	$\Delta lmdAE$	Roskopf, 2014
EC90	$\Delta lmdF$	Cserti <i>et al.</i> , 2017
JZ12	$P_{Zn}::P_{Zn}\text{-venus-ftsE}$	Zimmer, 2013

**Table S4: *E. coli* strains used in this study.**

Strain	Genotype	Reference
TOP10	$F^- mcrA \Delta(mrr\text{-}hsdRMS\text{-}mcrBC) \Phi 80 lacZ \Delta M15 \Delta lacX74 recA1 araD139 \Delta(araleu) 7697 galU galK rpsL (Str^R) endA1 nupG$	Invitrogen
WM3064	Donor strain for conjugation: <i>thrB1004 pro thi rpsL hsdS lacZ</i> $\Delta M15$ RP4–1360 $\Delta(arabad)567 \Delta dapA1341::[erm pir(wt)]$	W. Metcalf (unpublished)
BL21 (DE3)	Expression strain: $F^- ompT, hsdS_B(r_B^- m_B^-) gal dcm$ (DE3)	Novagen
Rosetta <sup>TM</sup> (DE3)pLysS	Protein overproduction strain: $F^- ompT hsdS_B(r_B^- m_B^-) gal dcm$ (DE3) pLysSRARE (Cam <sup>R</sup> )	Merck Milipore
SR59	pBAD24- $P_{BAD}$ - <i>amiC-mCherry</i>	This study
SR62	pTB146- $P_{T7}$ - <i>amiC</i>	This study
SR63	pTB146- $P_{T7}$ - <i>lmdE</i>	This study
SR66	pTB146- $P_{T7}$ - <i>amiC</i> <sup>E370A</sup>	This study
SR67	pTB146- $P_{T7}$ - <i>lmdA</i>	This study
SR68	pTB146- $P_{T7}$ - <i>lmdE</i> <sup>M23</sup>	This study
SR69	pTB146- $P_{T7}$ - <i>lmdE</i> <sup>CC</sup>	This study
SR70	pTB146- $P_{T7}$ - <i>ftsX</i> <sup>Loop1</sup>	This study

**Table S5: Plasmids used in this study.**

Plasmid	Description	Reference
pSR01	pNPTS138- $\Delta dacB$ , Kan <sup>R</sup>	Roskopf, 2014
pSR03	pNPTS138- $\Delta dacH$ , Kan <sup>R</sup>	Roskopf, 2014
pSR17	pNPTS138- <i>lmdF-mCherry</i> , Kan <sup>R</sup>	Roskopf, 2014
pSR22	pNPTS138- $\Delta amiC$ , Kan <sup>R</sup>	Roskopf, 2014
pSR23	pNPTS138- <i>amiC-mCherry</i> , Kan <sup>R</sup>	Roskopf, 2014
pSR35	pCCHYC-2- <i>dacB</i> , Kan <sup>R</sup>	Roskopf, 2014
pSR38	pCCHYC-2- <i>dacL</i> , Kan <sup>R</sup>	Roskopf, 2014
pSR47	pCHYC-2- <i>HNE_1815</i> , Kan <sup>R</sup>	This study
pSR50	pNPTS138- $\Delta lmdB$ , Kan <sup>R</sup>	This study
pSR54	pCCHYC-2- <i>lmdE</i> , Kan <sup>R</sup>	This study
pSR55	pNPTS138- <i>lmdA</i> , Kan <sup>R</sup>	This study
pSR56	pNPTS138- <i>lmdD</i> , Kan <sup>R</sup>	This study
pSR57	pNPTS138- <i>lmdE</i> , Kan <sup>R</sup>	This study
pSR61	pBAD24- <i>amiC-mCherry</i> , Amp <sup>R</sup>	This study
pSR65	pNPTS138- $\Delta ftsEX$ , Kan <sup>R</sup>	This study
pSR68	pTB146- <i>amiC</i> , Amp <sup>R</sup>	This study
pSR69	pTB146- <i>lmdE</i> , Amp <sup>R</sup>	This study

pSR71	pCCHYC-2- <i>lmdC<sup>N</sup></i> , Kan <sup>R</sup>	This study
pSR72	pTB146- <i>amiC<sup>E370A</sup></i> , Amp <sup>R</sup>	This study
pSR73	pTB146- <i>lmdA</i> , Amp <sup>R</sup>	This study
pSR74	pTB146- <i>lmdE<sup>CC</sup></i> , Amp <sup>R</sup>	This study
pSR75	pTB146- <i>lmdE<sup>M23</sup></i> , Amp <sup>R</sup>	This study
pSR76	pTB146- <i>ftsX<sup>Loop1</sup></i> , Amp <sup>R</sup>	This study
pSR77	pCCHYC-2- <i>ftsEX</i> , Kan <sup>R</sup>	This study
pSR78	pCCHYC-2- <i>amiC<sup>E370A</sup></i> , Kan <sup>R</sup>	This study
pNPTS148	sacB-containing suicide vector used for double homologous recombination, Kan <sup>R</sup>	M. R. K. Alley, unpublished
pCHYC-2	Integration plasmid for generation of C-terminal mCherry fusions at the site of interest, Kan <sup>R</sup>	Jung <i>et al.</i> , 2014
pCCHYC-2	Integration plasmid for generation of C-terminal mCherry fusions under control of P <sub>Cu</sub> , Kan <sup>R</sup>	Jung <i>et al.</i> , 2014
pBAD24	Plasmid for the generation of expression constructs under control of P <sub>BAD</sub> , Amp <sup>R</sup>	Guzman <i>et al.</i> , 1995
pTB146	Plasmid for the generation of N-terminal His <sub>6</sub> -SUMO overexpression constructs under control of P <sub>T7</sub> , Amp <sup>R</sup>	Bendezú <i>et al.</i> , 2008
pEC10	pCCHYC-2- <i>lmdD</i> , Kan <sup>R</sup>	Rosskopf, 2014
pEC34	pNPTS138- $\Delta$ <i>lmdA</i> , Kan <sup>R</sup>	Rosskopf, 2014
pEC35	pNPTS138- $\Delta$ <i>lmdB</i> , Kan <sup>R</sup>	Rosskopf, 2014
pEC38	pNPTS138- $\Delta$ <i>lmdD</i> , Kan <sup>R</sup>	Rosskopf, 2014
pEC39	pNPTS138- $\Delta$ <i>lmdE</i> , Kan <sup>R</sup>	Rosskopf, 2014
pEC64	pNPTS138- $\Delta$ <i>dacL</i> , Kan <sup>R</sup>	Rosskopf, 2014
pEC77	pCVENC-3- <i>amiC</i> , Rif <sup>R</sup>	Rosskopf, 2014
pEC115	pCCHYC-2- <i>amiC</i> , Kan <sup>R</sup>	Cserti <i>et al.</i> , 2017
pEC126	pNPTS138- $\Delta$ <i>lmdF</i> , Kan <sup>R</sup>	Rosskopf, 2014
pWS27	pCHYC-2- <i>lmdA</i> , Kan <sup>R</sup>	Strobel, 2010
pSAM-RI	RP4- <i>oriT</i> , <i>oriR6K</i> , <i>mariner himar1C9</i> transposase, with <i>B. thetaiotamicron rpoD</i> promoter replaced with <i>R. leguminosarum</i> 3841 <i>rpoD</i> promoter region, Amp <sup>R</sup> , Kan <sup>R</sup>	Perry and Yost, 2014
pSAM-HNE (pSR51)	pSAM_RI with <i>H. neptunium HNE_0038</i> promoter region, Amp <sup>R</sup> , Kan <sup>R</sup>	This study

**Table S6: Oligonucleotides used in this study.** Restriction sites are indicated in boldface.

Name	Designation	Sequence (5'–3')
oSR120	HNE_0633_del1_new	aca <b>CTGCAG</b> gacccgctgccccggctgct
oSR121	0633_delcheck_for_new	ctgaaggaccggaagatgaag
oSR131	HNE_3210_for	cacaggaactctt <b>CATATG</b> gcgcatttccgcgcatg
oSR132	HNE_3210_rev	ccgggctgca <b>GCATAT</b> gtcagccgccacgcgacaacca
oSR135	0632_int_for1	ggctggcgcc <b>AAGCTT</b> ccaggacgcttcgggcagctg
oSR136	0632_int_rev2	attaaatcgctcggcgcccttactgtacagctctcca
oSR137	0632_int_for3	tggcagagctgtacaagtaagggcgccgagggcgattaat



oSR138	0632_int_rev4	cacggccgaa <b>GCTAGC</b> cgatggccagggccgcacggt
oSR139	2982_int_for1	ggctggcgcc <b>AAGCTT</b> gcctgcgctcatgcccgcg
oSR140	2982_int_rev2	ttccctccgctgtgacagattactgtacagctcgtcca
oSR141	2982_int_for3	tggacgagctgtacaagtaatctgtcacacgcgaggaa
oSR142	2982_int_rev4	acggccgaa <b>GCTAGC</b> gcgacacggatgaggatgaggagg
oSR143	3210_int_for1	caggatatct <b>GGATCC</b> ggaaattgagcgttggccgcgac
oSR144	3210_int_rev2	gctcgagatcttaaggtaccgcccacgcgacaaccact
oSR145	3210_int_for3	agtggttgtcgcgtggcggcggtaccttaagatctcgagc
oSR146	3210_int_rev4	cttcacctcacacggcggattactgtacagctcgtcca
oSR147	3210_int_for5	tggacgagctgtacaagtaatccgccgtgtgaggatgaag
oSR148	3210_int_rev6	cacggccgaa <b>GCTAGC</b> cggatataggcaatgtcgtttgcc
oSR161	0632_delcheck_rev	atgtcggctatgatgaaggcgggg
oSR162	0674-mCherry_for	ctccatacccgttttttgggatgggcactcaacgccgtct
oSR163	0674-mCherry_rev	ctagaggatccccgggtactactgtacagctcgtccatgc
oSR182	FtsEX_del1	tgaagccggctggcgccatctcgaccggggtggctcga
oSR183	FtsEX_del2	gcgcccgcacaccgtgatcgcttcgtaaaatgtccggctg
oSR184	FtsEX_del3	cggacatttcgacgaagcgatcacggtgatgcgggcgctt
oSR185	FtsEX_del4	gacgcgtcacggccgaaggaaggatttcgtagatgatcttc
oSR186	FtsEX_check_for	ccgtaggcggcaaaggcggag
oSR187	FtsEX_check_rev	gctttccttctgcacggcg
oSR188	3210_ups_for1	ttgaagccggctggcgccactcgaagccgcccttgaggcg
oSR189	3210_N-int_rev2	ctcgcccttgctcaccatgtccggccccgagccgtcag
oSR191	3210_mChy_for3	acggctgcggggccggacatggtgagcaagggcgaggag
oSR192	3210_mChy_rev4	atcctggcgcgtataggtagccgggtgcaccagacttga
oSR193	3210_N-int_for5	acaagtctggtgcaccgggtacctatacgcgccaggatctt
oSR194	3210_N-int_rev6	gacgcgtcacggccgaagggcctctttgccagtttctgggc
oSR200	0674noTM-for	cagagaacagattggtggtgtgcacaaatccgcttgcggt
oSR201	0674exp-rev	acggagctctgctcttctattgggacgcgaggcggag
oSR202	3210noSP-for	cacagagaacagattggtggtgcggggccggacacctatacg
oSR203	3210exp-rev	acggagctctgctcttctcagccgccacgcgacaacca
oSR219	2628N_for	cattcacaggaactctccacatggcgaagtggagtccaac
oSR220	2628N_rev	agctcgagatcttaaggtaccgcccgcgcaggtcctgga
oSR221	mutAmiC_for	cgcagtgctgctgcacttggcttctga
oSR222	mutAmiC_rev	tcaggaagccaagtgcgagcagcactgcg
oSR223	0632noTM-for	ctcacagagaacagattggtggtgccgagccggaagccct
oSR224	0632exp-rev	gacggagctctgctcttctcaaggcgcggggcgctt
oSR225	3210CCexp-rev	ggagctctgctcttcttaggcgggcgcgctggattcc
oSR226	3210M23-for	gagaacagattggtggtgtagcattgcagaatgggtcag
oSR232	FtsX_Loop1_for	ctcacagagaacagattggtggtgaagtccacctatggcgc
oSR233	FtsX_Loop1_rev	cgacggagctctgctcttctacgcggtgccagcatgc
oSR234	FtsEX_for	cattcacaggaactcttccatgatgaccagatacaccggac
oSR235	FtsEX_rev	tggatccccgggctgcagctagcctacatcacggacttaagcgc
oSR236	AmiC_m_for	cattcacaggaactcttccataggcactcaacgcccg
oSR237	AmiC_m_rev	ggagctcgagatcttaaggtaccctattgggacgcgaggc
oEC23	HNE_3409_for	aaa <b>CATAT</b> gctgaaaagacgcttatccgcc

oEC24	HNE_3409_rev	ttt <b>GGTACC</b> ttcgatgatctcgtagccttcggg
oEC25	HNE_2982_for	ttt <b>CATAT</b> gagggtacgggcgattgctcttg
oEC26	HNE_2982_rev	tat <b>GGTACC</b> gtatccggcctgcaacgccccttc
oEC84	HNE_0632_del1	tat <b>AAGCTT</b> ggtgtccgagcaggcccgcgagcat
oEC87	HNE_0632_del4	ttt <b>GCTAGC</b> gacaccgcctatgccacctctcgc
oEC89	HNE_0633_del2	tat <b>GAATTC</b> ccgctgaagcaacgccccgtaagcc
oEC91	HNE_0633_del4	ttt <b>GCTAGC</b> ccttctggcctctgcgggcacatc
oEC92	HNE_2982_del1	tat <b>CTGCAG</b> tctatcaggaagacggcaaggtttg
oEC95	HNE_2982_del4	ttt <b>GCTAGC</b> cattctccaagcccggcattgac
oEC96	HNE_3210_del1	tat <b>GAATTC</b> ggccgtgatctcggtgatatagtc
oEC99	HNE_3210_del4	ttt <b>GCTAGC</b> gggctgtggcgttgggtggcgcttg
oEC111	0632_delcheck_for	cagggccgcacggttgattt
oEC112	0632_delcheck_rev	ctgactttgccgccccacc
oEC114	0633_delcheck_rev	cgtgccgcgcatctccagac
oEC115	2982_delcheck_for	tgatggcgagggtgcagcgtg
oEC116	2982_delcheck_rev	gccaaagccagaccatgagc
oEC117	3210_delcheck_for	gacctggaatggatcaacgc
oEC118	3210_delcheck_rev	ccgaccggaaaccggtatc
oEC120	3409_delcheck_rev	gcccaaactcgttgaagacc
oEC165	HNE_0674_for	tata <b>CATAT</b> gggcactcaacgcccgtctc
oEC166	HNE_0674_rev	tata <b>GGTACC</b> ctattgggacgcgaggcggagatc
oEC289	HNE_3409_del1new	ttt <b>AAGCTT</b> cccggccagaaggacacaaaatgag
oEC292	HNE_3409_del4new	tata <b>GCTAGC</b> cgcgctgtatatgccgcccggc
oEC293	3409_delcheck_f_new	ctgtccggcgccagctattcgggc
oEC294	3409_delcheck_r_new	gcgggcctctggtcgcgcgccacg
oEC295	HNE_3102_del1new	ttt <b>AAGCTT</b> gggcccacacaaaacctcgtcagc

Table S7: Common oligonucleotides used for colony PCR and sequencing.

Name	Designation	Sequence (5'–3')
3	IntSpec-1 (RecUni-1)	atgccgtttgtgatggcttccatgtcg
5	M13for	gccagggtttcccagtcacga
6	M13rev	gagcggataacaatttcacacagg
8	pBAD24-rev	accgcttctgcttctgatttaatc
9	pBAD24-uni	cctacctgacgcttttatcgcaac
14	T7 rev	gctagtattgctcagcgg
15	pET-for	cacgatgcgtccggcgtagaggatc
20	mCherry-up	ctcgccctcgccctcgatctcgaac
21	mCherry-down	ggcgcctacaacgtcaacatcaagttgg
22	REV-uni	ggggatgtgctgcaaggcggattaagttg
24	pET-rev	cctttcagcaaaaaaccctcaagaccgg
38	pCop1486_out_for	cgaagtcgcccgtggccgag
39	pCop1486_check_for	ccccttatcatccagaccagctacg
40	pCop1486_check_rev	ggcttttgatttttgacgtcag

**Table S8: Oligonucleotides for transposon mutagenesis and TnSeq.** Restriction sites are indicated in boldface.

<b>Name</b>	<b>Designation</b>	<b>Sequence (5'–3')</b>
oSR122	P_HNE_0038_for	aac <b>GGATCC</b> cggaagtcaccccatcacg
oSR123	P_HNE_0038_rev	aca <b>CATATG</b> gggggggtctcctgtaagtct
oSR124	P_HNE_0038_check_for	tggccttttgcgtttctacc
oSR125	P_HNE_0038_check_rev	tcaagccaagttttgcttcc
oSR133	KanRs_for	gttccttgcgcagctgtgctcgacgtt
oSR134	KanRs_rev	ccaacgctatgtcctgatagcgggccg
oSR227	Tn_HNE	ttcgcttgctgtccataaaaccgcccagtc
oSR228	Tn_HNE_N502 index	aatgatacggcgaccaccgagatctacacctctatccggggg cggggacttatcatccaacctgtta
oSR229	Tn_HNE_Seq	ccgggggcggggacttatcatccaacctgtta
oSR230	Nextera 2A-R	gtctcgtgggctcgggagatgtgtataagagacag
oSR231	N701 index	caagcagaagacggcatacagagattcgccttagtctcgtgggct cggagatgtg

## 6. REFERENCES

- Aaron, M., Charbon, G., Lam, H., Schwarz, H., Vollmer, W. & Jacobs-Wagner, C. (2007) The tubulin homologue FtsZ contributes to cell elongation by guiding cell wall precursor synthesis in *Caulobacter crescentus*. *Mol Microbiol* **64**, 938-952
- Aarsman, M. E., Piette, A., Fraipont, C., Vinkenvleugel, T. M., Nguyen-Disteche, M. & den Blaauwen, T. (2005) Maturation of the *Escherichia coli* divisome occurs in two steps. *Mol Microbiol* **55**, 1631-1645
- Ackermann, M., Stearns, S. C. & Jenal, U. (2003) Senescence in a bacterium with asymmetric division. *Science* **300**, 1920-1920
- Alyahya, S. A., Alexander, R., Costa, T., Henriques, A. O., Emonet, T. & Jacobs-Wagner, C. (2009) RodZ, a component of the bacterial core morphogenic apparatus. *Proc Natl Acad Sci USA* **106**, 1239-1244
- Arends, S. J., Kustusch, R. J. & Weiss, D. S. (2009) ATP-binding site lesions in FtsE impair cell division. *J Bacteriol* **191**, 3772-3784
- Ausubel, F. M. (1988) Current protocols in molecular biology. *Greene Pub Associates, Wiley-Interscience, New York*
- Babudieri, B. (1950) [Nature of the so-called S-formen of *Leptospira*; their identification with *Hyphomicrobium vulgare* Stutzer & Hartleb; study of the latter]. *Rend Ist Sup Sanit* **13**, 580-591
- Badger, J. H., Eisen, J. A. & Ward, N. L. (2005) Genomic analysis of *Hyphomonas neptunium* contradicts 16S rRNA gene-based phylogenetic analysis: implications for the taxonomy of the orders 'Rhodobacterales' and Caulobacterales. *Int J Syst Evol Microbiol* **55**, 1021-1026
- Badger, J. H., Hoover, T. R., Brun, Y. V., Weiner, R. M., Laub, M. T., Alexandre, G., Mrazek, J., Ren, Q., Paulsen, I. T., Nelson, K. E., Khouri, H. M., Radune, D., Sosa, J., Dodson, R. J., Sullivan, S. A., Rosovitz, M. J., Madupu, R., Brinkac, L. M., Durkin, A. S., Daugherty, S. C., Kothari, S. P., Giglio, M. G., Zhou, L., Haft, D. H., Selengut, J. D., Davidsen, T. M., Yang, Q., Zafar, N. & Ward, N. L. (2006) Comparative genomic evidence for a close relationship between the dimorphic prosthecate bacteria *Hyphomonas neptunium* and *Caulobacter crescentus*. *J Bacteriol* **188**, 6841-6850
- Baier, R. E., Meyer, A. E., Depalma, V. A., King, R. W. & Fornalik, M. S. (1983) Surface microfouling during the induction period. *J Heat Transfer* **105**, 618-624
- Bajaj, R., Bruce, K. E., Davidson, A. L., Rued, B. E., Stauffacher, C. V. & Winkler, M. E. (2016) Biochemical characterization of essential cell division proteins FtsX and FtsE that mediate peptidoglycan hydrolysis by PcsB in *Streptococcus pneumoniae*. *Microbiologyopen* **5**, 738-752
- Barton, A. A. (1950) Some aspects of cell division in *Saccharomyces cerevisiae*. *J Gen Microbiol* **4**, 84-86
- Bartual, S. G., Straume, D., Stamsas, G. A., Munoz, I. G., Alfonso, C., Martinez-Ripoll, M., Havarstein, L. S. & Hermoso, J. A. (2014) Structural basis of PcsB-mediated cell separation in *Streptococcus pneumoniae*. *Nat Commun* **5**, 3842
- Bateman, A. & Bycroft, M. (2000) The structure of a LysM domain from *E. coli* membrane-bound lytic murein transglycosylase D (MltD). *J Mol Biol* **299**, 1113-1119
- Bateman, A., Coin, L., Durbin, R., Finn, R. D., Hollich, V., Griffiths-Jones, S., Khanna, A., Marshall, M., Moxon, S., Sonnhammer, E. L. L., Studholme, D. J., Yeats, C. & Eddy, S. R. (2004) The Pfam protein families database. *Nucleic Acids Res* **32**, D138-141
- Bendezu, F. O., Hale, C. A., Bernhardt, T. G. & de Boer, P. A. (2009) RodZ (YfgA) is required for proper assembly of the MreB actin cytoskeleton and cell shape in *E. coli*. *EMBO J* **28**, 193-204
- Berendt, S., Lehner, J., Zhang, Y. V., Rasse, T. M., Forchhammer, K. & Maldener, I. (2012) Cell wall amidase AmiC1 is required for cellular communication and heterocyst development in the Cyanobacterium *Anabaena* PCC 7120 but not for filament integrity. *J Bacteriol* **194**, 5218-5227

- Bernhardt, T. G. & de Boer, P. A. (2003)** The *Escherichia coli* amidase AmiC is a periplasmic septal ring component exported via the twin-arginine transport pathway. *Mol Microbiol* **48**, 1171-1182
- Bisson-Filho, A. W., Hsu, Y. P., Squyres, G. R., Kuru, E., Wu, F., Jukes, C., Sun, Y., Dekker, C., Holden, S., VanNieuwenhze, M. S., Brun, Y. V. & Garner, E. C. (2017)** Treadmilling by FtsZ filaments drives peptidoglycan synthesis and bacterial cell division. *Science* **355**, 739-743
- Bochtler, M., Odintsov, S. G., Marcyjaniak, M. & Sabala, I. (2004)** Similar active sites in lysostaphins and D-Ala-D-Ala metallopeptidases. *Protein Sci* **13**, 854-861
- Bornikoel, J., Staiger, J., Madlung, J., Forchhammer, K. & Maldener, I. (2018)** LytM factor Alr3353 affects filament morphology and cell-cell communication in the multicellular cyanobacterium *Anabaena* sp. PCC 7120. *Mol Microbiol* **108**, 187-203
- Boutte, C. C., Baer, C. E., Papavinasasundaram, K., Liu, W., Chase, M. R., Meniche, X., Fortune, S. M., Sassetti, C. M., Ioerger, T. R. & Rubin, E. J. (2016)** A cytoplasmic peptidoglycan amidase homologue controls mycobacterial cell wall synthesis. *Elife* **5**
- Bradford, M. M. (1976)** A rapid and sensitive method for the quantitation of microgram quantities of protein utilizing the principle of protein-dye binding. *Anal Biochem* **72**, 248-254
- Braun, V. & Wolff, H. (1970)** The murein-lipoprotein linkage in the cell wall of *Escherichia coli*. *Eur J Biochem* **14**, 387-391
- Browder, H. P., Zygmunt, W. A., Young, J. R. & Tavormina, P. A. (1965)** Lysostaphin: enzymatic mode of action. *Biochem Biophys Res Commun* **19**, 383-389
- Brown, P. J., Kysela, D. T. & Brun, Y. V. (2011)** Polarity and the diversity of growth mechanisms in bacteria. *Semin Cell Dev Biol* **22**, 790-798
- Brown, P. J., de Pedro, M. A., Kysela, D. T., Van der Henst, C., Kim, J., De Bolle, X., Fuqua, C. & Brun, Y. V. (2012)** Polar growth in the Alphaproteobacterial order Rhizobiales. *Proc Natl Acad Sci USA* **109**, 1697-1701
- Brun, Y. V. & Janakiraman, R. (2000)** The dimorphic life cycle of *Caulobacter crescentus* and stalked bacteria. In *Prokaryotic Development, Washington, DC: American Society for Microbiology*, pp. 297-317
- Cameron, T. A., Anderson-Furgeson, J., Zupan, J. R., Zik, J. J. & Zambryski, P. C. (2014)** Peptidoglycan synthesis machinery in *Agrobacterium tumefaciens* during unipolar growth and cell division. *MBio* **5**, e01219-01214
- Cameron, T. A., Zupan, J. R. & Zambryski, P. C. (2015)** The essential features and modes of bacterial polar growth. *Trends Microbiol* **23**, 347-353
- Cascales, E., Lloubes, R. & Sturgis, J. N. (2001)** The TolQ-TolR proteins energize TolA and share homologies with the flagellar motor proteins MotA-MotB. *Mol Microbiol* **42**, 795-807
- Cascales, E. & Lloubes, R. (2004)** Deletion analyses of the peptidoglycan-associated lipoprotein Pal reveals three independent binding sequences including a TolA box. *Mol Microbiol* **51**, 873-885
- Chen, J. C., Viollier, P. H. & Shapiro, L. (2005)** A membrane metalloprotease participates in the sequential degradation of a *Caulobacter* polarity determinant. *Mol Microbiol* **55**, 1085-1103
- Cho, H., Wivagg, C. N., Kapoor, M., Barry, Z., Rohs, P. D., Suh, H., Marto, J. A., Garner, E. C. & Bernhardt, T. G. (2016)** Bacterial cell wall biogenesis is mediated by SEDS and PBP polymerase families functioning semi-autonomously. *Nat Microbiol*, 16172
- Christianson, D. W., Mangani, S., Shoham, G. & Lipscomb, W. N. (1989)** Binding of D-phenylalanine and D-tyrosine to carboxypeptidase A. *J Biol Chem* **264**, 12849-12853
- Cleverley, R. & Lewis, R. (2015)** EzrA: a spectrin-like scaffold in the bacterial cell division machinery. *Microb Cell* **2**, 59-61
- Cohen, S. N., Chang, A. C. & Hsu, L. (1972)** Nonchromosomal antibiotic resistance in bacteria: genetic transformation of *Escherichia coli* by R-factor DNA. *Proc Natl Acad Sci USA* **69**, 2110-2114
- Conti, S. F. & Hirsch, P. (1965)** Biology of budding bacteria. 3. Fine structure of *Rhodocyclidium* and *Hypomicrobium* spp. *J Bacteriol* **89**, 503-512

- Corbin, B. D., Wang, Y., Beuria, T. K. & Margolin, W. (2007)** Interaction between cell division proteins FtsE and FtsZ. *J Bacteriol* **189**, 3026-3035
- Costa, T., Priyadarshini, R. & Jacobs-Wagner, C. (2008)** Localization of PBP3 in *Caulobacter crescentus* is highly dynamic and largely relies on its functional transpeptidase domain. *Mol Microbiol* **70**, 634-651
- Cserti, E. (2016)** Control of morphogenesis in the budding Alphaproteobacterium *Hyphomonas neptunium*. *PhD thesis* Philipps-Universität Marburg, Germany
- Cserti, E., Roskopf, S., Chang, Y. W., Eisheuer, S., Selter, L., Shi, J., Regh, C., Koert, U., Jensen, G. J. & Thanbichler, M. (2017)** Dynamics of the peptidoglycan biosynthetic machinery in the stalked budding bacterium *Hyphomonas neptunium*. *Mol Microbiol* **103**, 875-895
- Curtis, P. D. & Brun, Y. V. (2010)** Getting in the loop: regulation of development in *Caulobacter crescentus*. *Microbiol Mol Biol Rev* **74**, 13-41
- Curtis, P. D. & Brun, Y. V. (2014)** Identification of essential alphaproteobacterial genes reveals operational variability in conserved developmental and cell cycle systems. *Mol Microbiol* **93**, 713-735
- Daniel, R. A. & Errington, J. (2003)** Control of cell morphogenesis in bacteria: two distinct ways to make a rod-shaped cell. *Cell* **113**, 767-776
- Davies, C., White, S. W. & Nicholas, R. A. (2001)** Crystal structure of a deacylation-defective mutant of penicillin-binding protein 5 at 2.3-Å resolution. *J Biol Chem* **276**, 616-623
- de Leeuw, E., Graham, B., Phillips, G. J., ten Hagen-Jongman, C. M., Oudega, B. & Luirink, J. (1999)** Molecular characterization of *Escherichia coli* FtsE and FtsX. *Mol Microbiol* **31**, 983-993
- de Pedro, M. A., Quintela, J. C., Holtje, J. V. & Schwarz, H. (1997)** Murein segregation in *Escherichia coli*. *J Bacteriol* **179**, 2823-2834
- de Pedro, M. A., Donachie, W. D., Holtje, J. V. & Schwarz, H. (2001)** Constitutive septal murein synthesis in *Escherichia coli* with impaired activity of the morphogenetic proteins RodA and penicillin-binding protein 2. *J Bacteriol* **183**, 4115-4126
- de Souza, R. F., Anantharaman, V., de Souza, S. J., Aravind, L. & Gueiros-Filho, F. J. (2008)** AMIN domains have a predicted role in localization of diverse periplasmic protein complexes. *Bioinformatics* **24**, 2423-2426
- Delcour, A. H. (2009)** Outer membrane permeability and antibiotic resistance. *Biochim Biophys Acta* **1794**, 808-816
- Demchick, P. & Koch, A. L. (1996)** The permeability of the wall fabric of *Escherichia coli* and *Bacillus subtilis*. *J Bacteriol* **178**, 768-773
- Derouaux, A., Wolf, B., Fraipont, C., Breukink, E., Nguyen-Disteche, M. & Terrak, M. (2008)** The monofunctional glycosyltransferase of *Escherichia coli* localizes to the cell division site and interacts with penicillin-binding protein 3, FtsW, and FtsN. *J Bacteriol* **190**, 1831-1834
- Dominguez-Cuevas, P., Porcelli, I., Daniel, R. A. & Errington, J. (2013)** Differentiated roles for MreB-actin isologues and autolytic enzymes in *Bacillus subtilis* morphogenesis. *Mol Microbiol* **89**, 1084-1098
- Dominguez-Escobar, J., Chastanet, A., Crevenna, A. H., Fromion, V., Wedlich-Soldner, R. & Carballido-Lopez, R. (2011)** Processive movement of MreB-associated cell wall biosynthetic complexes in bacteria. *Science* **333**, 225-228
- Du, S., Pichoff, S. & Lutkenhaus, J. (2016)** FtsEX acts on FtsA to regulate divisome assembly and activity. *Proc Natl Acad Sci USA* **113**, E5052-5061
- Dubey, A. & Priyadarshini, R. (2018)** Amidase activity is essential for medial localization of AmiC in *Caulobacter crescentus*. *Curr Genet* **64**, 661-675
- Duchow, E. & Douglas, H. C. (1949)** *Rhodomicrobium Vanniellii*, a new photoheterotrophic Bacterium. *J Bacteriol* **58**, 409-416
- Egan, A. J., Jean, N. L., Koumoutsi, A., Bougault, C. M., Biboy, J., Sassine, J., Solovyova, A. S., Breukink, E., Typas, A., Vollmer, W. & Simorre, J. P. (2014)** Outer-membrane lipoprotein LpoB spans the periplasm to stimulate the peptidoglycan synthase PBP1B. *Proc Natl Acad Sci USA* **111**, 8197-8202

- Egan, A. J., Cleverley, R. M., Peters, K., Lewis, R. J. & Vollmer, W. (2017) Regulation of bacterial cell wall growth. *FEBS J* **284**, 851-867
- Eisheuer, S. (2016) Characterization of the division apparatus in the budding bacterium *Hyphomonas neptunium*. *PhD thesis* Philipps-Universität Marburg, Germany
- Ercoli, G., Tani, C., Pezzicoli, A., Vacca, I., Martinelli, M., Pecetta, S., Petracca, R., Rappuoli, R., Pizza, M., Norais, N., Soriani, M. & Arico, B. (2015) LytM proteins play a crucial role in cell separation, outer membrane composition, and pathogenesis in nontypeable *Haemophilus influenzae*. *MBio* **6**, e02575
- Errington, J. (2015) Bacterial morphogenesis and the enigmatic MreB helix. *Nat Rev Microbiol* **13**, 241-248
- Figge, R. M., Divakaruni, A. V. & Gober, J. W. (2004) MreB, the cell shape-determining bacterial actin homologue, co-ordinates cell wall morphogenesis in *Caulobacter crescentus*. *Mol Microbiol* **51**, 1321-1332
- Finn, R. D., Mistry, J., Tate, J., Coggill, P., Heger, A., Pollington, J. E., Gavin, O. L., Gunasekaran, P., Ceric, G., Forslund, K., Holm, L., Sonnhammer, E. L. L., Eddy, S. R. & Bateman, A. (2010) The Pfam protein families database. *Nucleic Acids Res* **38**, D211-222
- Firczuk, M. & Bochtler, M. (2007) Folds and activities of peptidoglycan amidases. *FEMS Microbiol Rev* **31**, 676-691
- Flardh, K. (2003) Essential role of DivIVA in polar growth and morphogenesis in *Streptomyces coelicolor* A3(2). *Mol Microbiol* **49**, 1523-1536
- Geer, L. Y., Marchler-Bauer, A., Geer, R. C., Han, L., He, J., He, S., Liu, C., Shi, W. & Bryant, S. H. (2010) The NCBI BioSystems database. *Nucleic Acids Res* **38**, D492-496
- Gerding, M. A., Ogata, Y., Pecora, N. D., Niki, H. & de Boer, P. A. (2007) The trans-envelope Tol-Pal complex is part of the cell division machinery and required for proper outer-membrane invagination during cell constriction in *E. coli*. *Mol Microbiol* **63**, 1008-1025
- Glauner, B., Höltje, J. V. & Schwarz, U. (1988) The composition of the murein of *Escherichia coli*. *J Biol Chem* **263**, 10088-10095
- Glauner, B. & Holtje, J. V. (1990) Growth pattern of the murein sacculus of *Escherichia coli*. *J Biol Chem* **265**, 18988-18996
- Goley, E. D., Yeh, Y. C., Hong, S. H., Fero, M. J., Abeliuk, E., McAdams, H. H. & Shapiro, L. (2011) Assembly of the *Caulobacter* cell division machine. *Mol Microbiol* **80**, 1680-1698
- Goodman, A. L., McNulty, N. P., Zhao, Y., Leip, D., Mitra, R. D., Lozupone, C. A., Knight, R. & Gordon, J. I. (2009) Identifying genetic determinants needed to establish a human gut symbiont in its habitat. *Cell Host Microbe* **6**, 279-289
- Goodman, A. L., Wu, M. & Gordon, J. I. (2011) Identifying microbial fitness determinants by insertion sequencing using genome-wide transposon mutant libraries. *Nat Protoc* **6**, 1969-1980
- Grangeon, R., Zupan, J. R., Anderson-Furgeson, J. & Zambryski, P. C. (2015) PopZ identifies the new pole, and PodJ identifies the old pole during polar growth in *Agrobacterium tumefaciens*. *Proc Natl Acad Sci USA* **112**, 11666-11671
- Gray, A. N., Egan, A. J., Van't Veer, I. L., Verheul, J., Colavin, A., Koumoutsis, A., Biboy, J., Altelaar, A. F., Damen, M. J., Huang, K. C., Simorre, J. P., Breukink, E., den Blaauwen, T., Typas, A., Gross, C. A. & Vollmer, W. (2015) Coordination of peptidoglycan synthesis and outer membrane constriction during *Escherichia coli* cell division. *Elife* **4**, e07118
- Greene, N. G., Fumeaux, C. & Bernhardt, T. G. (2018) Conserved mechanism of cell-wall synthase regulation revealed by the identification of a new PBP activator in *Pseudomonas aeruginosa*. *Proc Natl Acad Sci USA* **115**, 3150-3155
- Guzman, L. M., Belin, D., Carson, M. J. & Beckwith, J. (1995) Tight regulation, modulation, and high-level expression by vectors containing the arabinose P<sub>BAD</sub> promoter. *J Bacteriol* **177**, 4121-4130
- Haney, S. A., Glasfeld, E., Hale, C., Keeney, D., He, Z. Z. & de Boer, P. (2001) Genetic analysis of the *Escherichia coli* FtsZ center dot ZipA interaction in the yeast two-hybrid system - Characterization of FtsZ residues essential for the interactions with ZipA and with FtsA. *J Biol Chem* **276**, 11980-11987

- Harberding, H. (2018)** Etablierung von CRISPRi in *Hyphomonas neptunium*. *Bachelor thesis* Philipps-Universität Marburg, Germany
- Havenner, J. A., McCardell, B. A. & Weiner, R. M. (1979)** Development of defined, minimal, and complete media for the growth of *Hyphomicrobium neptunium*. *Appl Environ Microbiol* **38**, 18-23
- Heidrich, C., Templin, M. F., Ursinus, A., Merdanovic, M., Berger, J., Schwarz, H., de Pedro, M. A. & Höltje, J. V. (2001)** Involvement of N-acetylmuramyl-L-alanine amidases in cell separation and antibiotic-induced autolysis of *Escherichia coli*. *Mol Microbiol* **41**, 167-178
- Henrici, A. T. & Johnson, D. E. (1935)** Studies of freshwater Bacteria: II. Stalked Bacteria, a new order of *Schizomycetes*. *J Bacteriol* **30**, 61-93
- Hirsch, P. (1974)** Budding bacteria. *Annu Rev Microbiol* **28**, 391-444
- Hocking, J., Priyadarshini, R., Takacs, C. N., Costa, T., Dye, N. A., Shapiro, L., Vollmer, W. & Jacobs-Wagner, C. (2012)** Osmolality-dependent relocation of penicillin-binding protein PBP2 to the division site in *Caulobacter crescentus*. *J Bacteriol* **194**, 3116-3127
- Höltje, J. V., Mirelman, D., Sharon, N. & Schwarz, U. (1975)** Novel type of murein transglycosylase in *Escherichia coli*. *J Bacteriol* **124**, 1067-1076
- Höltje, J. V. (1995)** From growth to autolysis: the murein hydrolases in *Escherichia coli*. *Arch Microbiol* **164**, 243-254
- Höltje, J. V. (1998)** Growth of the stress-bearing and shape-maintaining murein sacculus of *Escherichia coli*. *Microbiol Mol Biol Rev* **62**, 181-203
- Huang, L. (2011)** A new mechanistic growth model for simultaneous determination of lag phase duration and exponential growth rate and a new Belehrádek-type model for evaluating the effect of temperature on growth rate. *Food Microbiol* **28**, 770-776
- Iba, H., Fukuda, A. & Okada, Y. (1977)** Chromosome replication in *Caulobacter crescentus* growing in a nutrient broth. *J Bacteriol* **129**, 1192-1197
- Ikeda, M., Sato, T., Wachi, M., Jung, H. K., Ishino, F., Kobayashi, Y. & Matsubashi, M. (1989)** Structural similarity among *Escherichia coli* FtsW and RodA proteins and *Bacillus subtilis* SpoVE protein, which function in cell division, cell elongation, and spore formation, respectively. *J Bacteriol* **171**, 6375-6378
- Ireland, M. M., Karty, J. A., Quardokus, E. M., Reilly, J. P. & Brun, Y. V. (2002)** Proteomic analysis of the *Caulobacter crescentus* stalk indicates competence for nutrient uptake. *Mol Microbiol* **45**, 1029-1041
- Ishino, F., Park, W., Tomioka, S., Tamaki, S., Takase, I., Kunugita, K., Matsuzawa, H., Asoh, S., Ohta, T., Spratt, B. G. & et al. (1986)** Peptidoglycan synthetic activities in membranes of *Escherichia coli* caused by overproduction of penicillin-binding protein 2 and RodA protein. *J Biol Chem* **261**, 7024-7031
- Jacobs, C., Joris, B., Jamin, M., Klarsov, K., Van Beeumen, J., Mengin-Lecreux, D., van Heijenoort, J., Park, J. T., Normark, S. & Frere, J. M. (1995)** AmpD, essential for both beta-lactamase regulation and cell wall recycling, is a novel cytosolic N-acetylmuramyl-L-alanine amidase. *Mol Microbiol* **15**, 553-559
- Jacobson, J. W., Medhora, M. M. & Hartl, D. L. (1986)** Molecular structure of a somatically unstable transposable element in *Drosophila*. *Proc Natl Acad Sci USA* **83**, 8684-8688
- Jean, N. L., Bougault, C. M., Lodge, A., Derouaux, A., Callens, G., Egan, A. J., Ayala, I., Lewis, R. J., Vollmer, W. & Simorre, J. P. (2014)** Elongated structure of the outer-membrane activator of peptidoglycan synthesis LpoA: implications for PBP1A stimulation. *Structure* **22**, 1047-1054
- Jiang, C., Brown, P. J., Ducret, A. & Brun, Y. V. (2014)** Sequential evolution of bacterial morphology by co-option of a developmental regulator. *Nature* **506**, 489-493
- Jones, H. C. & Schmidt, J. M. (1973)** Ultrastructural study of crossbands occurring in the stalks of *Caulobacter crescentus*. *J Bacteriol* **116**, 466-470
- Jones, L. J., Carballido-Lopez, R. & Errington, J. (2001)** Control of cell shape in bacteria: helical, actin-like filaments in *Bacillus subtilis*. *Cell* **104**, 913-922
- Jorgenson, M. A., Chen, Y., Yahashiri, A., Popham, D. L. & Weiss, D. S. (2014)** The bacterial septal ring protein RlpA is a lytic transglycosylase that contributes to rod shape and daughter cell separation in *Pseudomonas aeruginosa*. *Mol Microbiol* **93**, 113-128



- Joyce, G., Williams, K. J., Robb, M., Noens, E., Tizzano, B., Shahrezaei, V. & Robertson, B. D. (2012) Cell division site placement and asymmetric growth in Mycobacteria. *PLoS One* **7**, e44582
- Jung, A., Eisheuer, S., Cserti, E., Leicht, O., Strobel, W., Möll, A., Schlimpert, S., Kühn, J. & Thanbichler, M. (2015) Molecular toolbox for genetic manipulation of the stalked budding bacterium *Hyphomonas neptunium*. *Appl Environ Microbiol* **81**, 736-744
- Jung, A. (2016) Chromosome arrangement and dynamics in the budding bacterium *Hyphomonas neptunium*. *PhD thesis* Philipps-Universität Marburg, Germany
- Kamio, Y. & Nikaido, H. (1976) Outer membrane of *Salmonella typhimurium*: accessibility of phospholipid head groups to phospholipase c and cyanogen bromide activated dextran in the external medium. *Biochem* **15**, 2561-2570
- Kanngießner, S. (2016) Die Rolle der M23-Metallopeptidase LmdC in *Hyphomonas neptunium*. *Bachelor thesis* Philipps-Universität Marburg, Germany
- Kishida, H., Unzai, S., Roper, D. I., Lloyd, A., Park, S. Y. & Tame, J. R. (2006) Crystal structure of penicillin binding protein 4 (*dacB*) from *Escherichia coli*, both in the native form and covalently linked to various antibiotics. *Biochem* **45**, 783-792
- Korat, B., Mottl, H. & Keck, W. (1991) Penicillin-binding protein 4 of *Escherichia coli*: molecular cloning of the *dacB* gene, controlled overexpression, and alterations in murein composition. *Mol Microbiol* **5**, 675-684
- Korndörfer, I. P., Danzer, J., Schmelcher, M., Zimmer, M., Skerra, A. & Loessner, M. J. (2006) The crystal structure of the bacteriophage PSA endolysin reveals a unique fold responsible for specific recognition of *Listeria* cell walls. *J Mol Biol* **364**, 678-689
- Kruse, T., Bork-Jensen, J. & Gerdes, K. (2005) The morphogenetic MreBCD proteins of *Escherichia coli* form an essential membrane-bound complex. *Mol Microbiol* **55**, 78-89
- Kühn, J., Briegel, A., Morschel, E., Kahnt, J., Leser, K., Wick, S., Jensen, G. J. & Thanbichler, M. (2010) Bactofilins, a ubiquitous class of cytoskeletal proteins mediating polar localization of a cell wall synthase in *Caulobacter crescentus*. *EMBO J* **29**, 327-339
- Kuru, E., Hughes, H. V., Brown, P. J., Hall, E., Tekkam, S., Cava, F., de Pedro, M. A., Brun, Y. V. & VanNieuwenhze, M. S. (2012) In Situ probing of newly synthesized peptidoglycan in live bacteria with fluorescent D-amino acids. *Angew Chem Int Ed Engl* **51**, 12519-12523
- Kysela, D. T., Brown, P. J., Huang, K. C. & Brun, Y. V. (2013) Biological consequences and advantages of asymmetric bacterial growth. *Annu Rev Microbiol* **67**, 417-435
- Kysela, D. T., Randich, A. M., Caccamo, P. D. & Brun, Y. V. (2016) Diversity takes shape: understanding the mechanistic and adaptive basis of bacterial morphology. *PLoS Biol* **14**, e1002565
- Laemmli, U. K. (1970) Cleavage of structural proteins during assembly of head of bacteriophage-T4. *Nature* **227**, 680-685
- Lampe, D. J., Akerley, B. J., Rubin, E. J., Mekalanos, J. J. & Robertson, H. M. (1999) Hyperactive transposase mutants of the *Himar1* mariner transposon. *Proc Natl Acad Sci USA* **96**, 11428-11433
- Langridge, G. C., Phan, M. D., Turner, D. J., Perkins, T. T., Parts, L., Haase, J., Charles, I., Maskell, D. J., Peters, S. E., Dougan, G., Wain, J., Parkhill, J. & Turner, A. K. (2009) Simultaneous assay of every *Salmonella* Typhi gene using one million transposon mutants. *Genome Res* **19**, 2308-2316
- Lazzaroni, J. C., Germon, P., Ray, M. C. & Vianney, A. (1999) The Tol proteins of *Escherichia coli* and their involvement in the uptake of biomolecules and outer membrane stability. *FEMS Microbiol Lett* **177**, 191-197
- Leclercq, S., Derouaux, A., Olatunji, S., Fraipont, C., Egan, A. J., Vollmer, W., Breukink, E. & Terrak, M. (2017) Interplay between penicillin-binding proteins and SEDS proteins promotes bacterial cell wall synthesis. *Sci Rep* **7**, 43306
- Leicht, O. (2016) Zellzyklusregulation in einem strikt dimorphen Vertreter der  $\alpha$ -Proteobakterien. *PhD thesis* Philipps-Universität Marburg, Germany
- Leifson, E. (1964) *Hyphomicrobium neptunium* sp. n. *Antonie Van Leeuwenhoek* **30**, 249-256

- Leisch, N., Verheul, J., Heindl, N. R., Gruber-Vodicka, H. R., Pende, N., den Blaauwen, T. & Bulgheresi, S. (2012)** Growth in width and FtsZ ring longitudinal positioning in a gammaproteobacterial symbiont. *Curr Biol* **22**, R831-832
- Lenarcic, R., Halbedel, S., Visser, L., Shaw, M., Wu, L. J., Errington, J., Marenduzzo, D. & Hamoen, L. W. (2009)** Localisation of DivIVA by targeting to negatively curved membranes. *EMBO J* **28**, 2272-2282
- Letek, M., Fiuza, M., Ordonez, E., Villadangos, A. F., Flardh, K., Mateos, L. M. & Gil, J. A. (2009)** DivIVA uses an N-terminal conserved region and two coiled-coil domains to localize and sustain the polar growth in *Corynebacterium glutamicum*. *FEMS Microbiol Lett* **297**, 110-116
- Letunic, I., Doerks, T. & Bork, P. (2009)** SMART 6: recent updates and new developments. *Nucleic Acids Res* **37**, D229-232
- Lupas, A. (1996)** Coiled coils: new structures and new functions. *Trends Biochem Sci* **21**, 375-382
- Lutkenhaus, J., Pichoff, S. & Du, S. (2012)** Bacterial cytokinesis: From Z ring to divisome. *Cytoskeleton (Hoboken)* **69**, 778-790
- Magnet, S., Dubost, L., Marie, A., Arthur, M. & Gutmann, L. (2008)** Identification of the L,D-transpeptidases for peptidoglycan cross-linking in *Escherichia coli*. *J Bacteriol* **190**, 4782-4785
- Malakhov, M. P., Mattern, M. R., Malakhova, O. A., Drinker, M., Weeks, S. D. & Butt, T. R. (2004)** SUMO fusions and SUMO-specific protease for efficient expression and purification of proteins. *J Struct Funct Genomics* **5**, 75-86
- Mattei, P. J., Neves, D. & Dessen, A. (2010)** Bridging cell wall biosynthesis and bacterial morphogenesis. *Curr Opin Struct Biol* **20**, 749-755
- Meeske, A. J., Sham, L. T., Kimsey, H., Koo, B. M., Gross, C. A., Bernhardt, T. G. & Rudner, D. Z. (2015)** MurJ and a novel lipid II flippase are required for cell wall biogenesis in *Bacillus subtilis*. *Proc Natl Acad Sci USA* **112**, 6437-6442
- Meeske, A. J., Riley, E. P., Robins, W. P., Uehara, T., Mekalanos, J. J., Kahne, D., Walker, S., Kruse, A. C., Bernhardt, T. G. & Rudner, D. Z. (2016)** SEDS proteins are a widespread family of bacterial cell wall polymerases. *Nature* **537**, 634-638
- Meier, E. L., Razavi, S., Inoue, T. & Goley, E. D. (2016)** A novel membrane anchor for FtsZ is linked to cell wall hydrolysis in *Caulobacter crescentus*. *Mol Microbiol* **101**, 265-280
- Meier, E. L., Daitch, A. K., Yao, Q., Bhargava, A., Jensen, G. J. & Goley, E. D. (2017)** FtsEX-mediated regulation of the final stages of cell division reveals morphogenetic plasticity in *Caulobacter crescentus*. *PLoS Genet* **13**, e1006999
- Meisner, J., Montero Llopis, P., Sham, L. T., Garner, E., Bernhardt, T. G. & Rudner, D. Z. (2013)** FtsEX is required for CwIO peptidoglycan hydrolase activity during cell wall elongation in *Bacillus subtilis*. *Mol Microbiol* **89**, 1069-1083
- Miller, J. (1972)**. Experiments in molecular genetics. Cold Spring Harbor Laboratory, Cold Spring Harbor, New York.
- Miller, S. I., Ernst, R. K. & Bader, M. W. (2005)** LPS, TLR4 and infectious disease diversity. *Nat Rev Microbiol* **3**, 36-46
- Mohammadi, T., Karczmarek, A., Crouvoisier, M., Bouhss, A., Mengin-Lecreux, D. & den Blaauwen, T. (2007)** The essential peptidoglycan glycosyltransferase MurG forms a complex with proteins involved in lateral envelope growth as well as with proteins involved in cell division in *Escherichia coli*. *Mol Microbiol* **65**, 1106-1121
- Mohammadi, T., van Dam, V., Sijbrandi, R., Vernet, T., Zapun, A., Bouhss, A., Diepeveen-de Bruin, M., Nguyen-Disteche, M., de Kruijff, B. & Breukink, E. (2011)** Identification of FtsW as a transporter of lipid-linked cell wall precursors across the membrane. *EMBO J* **30**, 1425-1432
- Möll, A., Schlimpert, S., Briegel, A., Jensen, G. J. & Thanbichler, M. (2010)** DipM, a new factor required for peptidoglycan remodelling during cell division in *Caulobacter crescentus*. *Mol Microbiol* **77**, 90-107
- Möll, A., Dörr, T., Alvarez, L., Chao, M. C., Davis, B. M., Cava, F. & Waldor, M. K. (2014)** Cell separation in *Vibrio cholerae* is mediated by a single amidase whose action is modulated by two nonredundant activators. *J Bacteriol* **196**, 3937-3948

- Monahan, L. G., Liew, A. T., Bottomley, A. L. & Harry, E. J. (2014)** Division site positioning in bacteria: one size does not fit all. *Front Microbiol* **5**, 19
- Moore, R. L. (1981)** The biology of *Hyphomicrobium* and other prosthecate, budding bacteria. *Annu Rev Microbiol* **35**, 567-594
- Moore, R. L., Weiner, R. M. & Gebers, R. (1984)** Genus *Hyphomonas* pongratz 1957 nom-rev emend, *Hyphomonas-polymorpha* pongratz 1957 nom-rev emend, and *Hyphomonas-neptunium* (Leifson 1964) comb-nov emend (*Hyphomicrobium-neptunium*). *Int J Syst Bacteriol* **34**, 71-73
- Morgenstein, R. M., Bratton, B. P., Nguyen, J. P., Ouzounov, N., Shaevitz, J. W. & Gitai, Z. (2015)** RodZ links MreB to cell wall synthesis to mediate MreB rotation and robust morphogenesis. *Proc Natl Acad Sci USA* **112**, 12510-12515
- Neuhaus, F. C. & Baddiley, J. (2003)** A continuum of anionic charge: structures and functions of D-alanyl-teichoic acids in gram-positive bacteria. *Microbiol Mol Biol Rev* **67**, 686-723
- Nicholas, K. & Nicholas, H. (1997)** GeneDoc: a tool for editing and annotating multiple sequence alignments. *Distributed by the author*
- Ong, C. J., Wong, M. L. & Smit, J. (1990)** Attachment of the adhesive holdfast organelle to the cellular stalk of *Caulobacter crescentus*. *J Bacteriol* **172**, 1448-1456
- Paradis-Bleau, C., Markovski, M., Uehara, T., Lupoli, T. J., Walker, S., Kahne, D. E. & Bernhardt, T. G. (2010)** Lipoprotein cofactors located in the outer membrane activate bacterial cell wall polymerases. *Cell* **143**, 1110-1120
- Pende, N., Wang, J., Weber, P. M., Verheul, J., Kuru, E., Rittmann, S. K. R., Leisch, N., VanNieuwenhze, M. S., Brun, Y. V., den Blaauwen, T. & Bulgheresi, S. (2018)** Host-polarized cell growth in animal symbionts. *Curr Biol* **28**, 1039-1051 e1035
- Perry, B. J. & Yost, C. K. (2014)** Construction of a mariner-based transposon vector for use in insertion sequence mutagenesis in selected members of the *Rhizobiaceae*. *BMC Microbiol* **14**, 298
- Peters, K., Kannan, S., Rao, V. A., Biboy, J., Vollmer, D., Erickson, S. W., Lewis, R. J., Young, K. D. & Vollmer, W. (2016)** The redundancy of peptidoglycan carboxypeptidases ensures robust cell shape maintenance in *Escherichia coli*. *Mbio* **7**, e00819-00816
- Peters, N. T., Dinh, T. & Bernhardt, T. G. (2011)** A fail-safe mechanism in the septal ring assembly pathway generated by the sequential recruitment of cell separation amidases and their activators. *J Bacteriol* **193**, 4973-4983
- Peters, N. T., Morlot, C., Yang, D. C., Uehara, T., Vernet, T. & Bernhardt, T. G. (2013)** Structure-function analysis of the LytM domain of EnvC, an activator of cell wall remodelling at the *Escherichia coli* division site. *Mol Microbiol* **89**, 690-701
- Pichoff, S. & Lutkenhaus, J. (2002)** Unique and overlapping roles for ZipA and FtsA in septal ring assembly in *Escherichia coli*. *EMBO J* **21**, 685-693
- Pichoff, S. & Lutkenhaus, J. (2005)** Tethering the Z ring to the membrane through a conserved membrane targeting sequence in FtsA. *Mol Microbiol* **55**, 1722-1734
- Pinho, M. G., Kjos, M. & Veening, J. W. (2013)** How to get (a)round: mechanisms controlling growth and division of coccoid bacteria. *Nat Rev Microbiol* **11**, 601-614
- Poindexter, J. L. S. & Cohenbazire, G. (1964)** Fine structure of stalked bacteria belonging to family *Caulobacteraceae*. *J Cell Biol* **23**, 587-607
- Potluri, L. P., de Pedro, M. A. & Young, K. D. (2012)** *Escherichia coli* low-molecular-weight penicillin-binding proteins help orient septal FtsZ, and their absence leads to asymmetric cell division and branching. *Mol Microbiol* **84**, 203-224
- Punta, M., Coghill, P. C., Eberhardt, R. Y., Mistry, J., Tate, J., Boursnell, C., Pang, N., Forslund, K., Ceric, G., Clements, J., Heger, A., Holm, L., Sonnhammer, E. L., Eddy, S. R., Bateman, A. & Finn, R. D. (2012)** The Pfam protein families database. *Nucleic Acids Res* **40**, 290-301
- Qi, L. S., Larson, M. H., Gilbert, L. A., Doudna, J. A., Weissman, J. S., Arkin, A. P. & Lim, W. A. (2013)** Repurposing CRISPR as an RNA-guided platform for sequence-specific control of gene expression. *Cell* **152**, 1173-1183

## References

---

- Quintela, J. C., Caparros, M. & de Pedro, M. A. (1995)** Variability of peptidoglycan structural parameters in Gram-negative bacteria. *FEMS Microbiol Lett* **125**, 95-100
- Randich, A. M. & Brun, Y. V. (2015)** Molecular mechanisms for the evolution of bacterial morphologies and growth modes. *Front Microbiol* **6**, 580
- Rocaboy, M., Herman, R., Sauvage, E., Remaut, H., Moonens, K., Terrak, M., Charlier, P. & Kerff, F. (2013)** The crystal structure of the cell division amidase AmiC reveals the fold of the AMIN domain, a new peptidoglycan binding domain. *Mol Microbiol* **90**, 267-277
- Romeis, T. & Holtje, J. V. (1994)** Specific interaction of penicillin-binding proteins 3 and 7/8 with soluble lytic transglycosylase in *Escherichia coli*. *J Biol Chem* **269**, 21603-21607
- Roskopf, S. (2014)** Analyse der Peptidoglycan-Biosynthese in *Hyphomonas neptunium*. *Master thesis* Philipps-Universität Marburg, Germany
- Royet, J. & Dziarski, R. (2007)** Peptidoglycan recognition proteins: pleiotropic sensors and effectors of antimicrobial defences. *Nat Rev Microbiol* **5**, 264-277
- Rued, B. E., Zheng, J. J., Mura, A., Tsui, H. T., Boersma, M. J., Mazny, J. L., Corona, F., Perez, A. J., Fadda, D., Doubravova, L., Buriankova, K., Branny, P., Massidda, O. & Winkler, M. E. (2017)** Suppression and synthetic-lethal genetic relationships of  $\Delta gpsB$  mutations indicate that GpsB mediates protein phosphorylation and penicillin-binding protein interactions in *Streptococcus pneumoniae* D39. *Mol Microbiol* **103**, 931-957
- Ruiz, N. (2008)** Bioinformatics identification of MurJ (MviN) as the peptidoglycan lipid II flippase in *Escherichia coli*. *Proc Natl Acad Sci USA* **105**, 15553-15557
- Ruiz, N., Kahne, D. & Silhavy, T. J. (2009)** Transport of lipopolysaccharide across the cell envelope: the long road of discovery. *Nat Rev Microbiol* **7**, 677-683
- Sambrook, J., Fritsch, E. F. & Maniatis, T. (1989)** Molecular cloning: a laboratory manual. *Cold Spring Harbor Laboratory Press, Cold Spring Harbor, New York*
- Scheurwater, E. M., Pfeffer, J. M. & Clarke, A. J. (2007)** Production and purification of the bacterial autolysin N-acetylmuramoyl-L-alanine amidase B from *Pseudomonas aeruginosa*. *Protein Expr Purif* **56**, 128-137
- Schleifer, K. H. & Kandler, O. (1972)** Peptidoglycan types of bacterial cell walls and their taxonomic implications. *Bacteriol Rev* **36**, 407-477
- Schlimpert, S., Klein, E. A., Briegel, A., Hughes, V., Kahnt, J., Bolte, K., Maier, U. G., Brun, Y. V., Jensen, G. J., Gitai, Z. & Thanbichler, M. (2012)** General protein diffusion barriers create compartments within bacterial cells. *Cell* **151**, 1270-1282
- Schmidt, J. M. (1973)** Effect of lysozyme on crossbands in stalks of *Caulobacter crescentus*. *Archiv Fur Mikrobiologie* **89**, 33-40
- Schmidt, K. L., Peterson, N. D., Kustus, R. J., Wissel, M. C., Graham, B., Phillips, G. J. & Weiss, D. S. (2004)** A predicted ABC transporter, FtsEX, is needed for cell division in *Escherichia coli*. *J Bacteriol* **186**, 785-793
- Schultz, J., Milpetz, F., Bork, P. & Ponting, C. P. (1998)** SMART, a simple modular architecture research tool: Identification of signaling domains. *Proc Natl Acad Sci USA* **95**, 5857-5864
- Sham, L. T., Barendt, S. M., Kopecky, K. E. & Winkler, M. E. (2011)** Essential PcsB putative peptidoglycan hydrolase interacts with the essential FtsX<sub>spn</sub> cell division protein in *Streptococcus pneumoniae* D39. *Proc Natl Acad Sci USA* **108**, E1061-1069
- Sham, L. T., Jensen, K. R., Bruce, K. E. & Winkler, M. E. (2013)** Involvement of FtsE ATPase and FtsX extracellular loops 1 and 2 in FtsEX-PcsB complex function in cell division of *Streptococcus pneumoniae* D39. *MBio* **4**, e00431-00413
- Sham, L. T., Butler, E. K., Lebar, M. D., Kahne, D., Bernhardt, T. G. & Ruiz, N. (2014)** Bacterial cell wall. MurJ is the flippase of lipid-linked precursors for peptidoglycan biogenesis. *Science* **345**, 220-222
- Shiomi, D., Sakai, M. & Niki, H. (2008)** Determination of bacterial rod shape by a novel cytoskeletal membrane protein. *EMBO J* **27**, 3081-3091

- Silhavy, T. J., Kahne, D. & Walker, S. (2010)** The bacterial cell envelope. *Cold Spring Harb Perspect Biol* **2**, a000414
- Singh, J. K., Makde, R. D., Kumar, V. & Panda, D. (2007)** A membrane protein, EzrA, regulates assembly dynamics of FtsZ by interacting with the C-terminal tail of FtsZ. *Biochem* **46**, 11013-11022
- Singh, S. K., SaiSree, L., Amrutha, R. N. & Reddy, M. (2012)** Three redundant murein endopeptidases catalyse an essential cleavage step in peptidoglycan synthesis of *Escherichia coli* K12. *Mol Microbiol* **86**, 1036-1051
- Singh, S. K., Parveen, S., SaiSree, L. & Reddy, M. (2015)** Regulated proteolysis of a cross-link-specific peptidoglycan hydrolase contributes to bacterial morphogenesis. *Proc Natl Acad Sci USA* **112**, 10956-10961
- Smith, T. J., Blackman, S. A. & Foster, S. J. (2000)** Autolysins of *Bacillus subtilis*: multiple enzymes with multiple functions. *Microbiology* **146** ( Pt 2), 249-262
- Söderström, B., Mirzadeh, K., Toddo, S., von Heijne, G., Skoglund, U. & Daley, D. O. (2016)** Coordinated disassembly of the divisome complex in *Escherichia coli*. *Mol Microbiol* **101**, 425-438
- Sonnhammer, E. L., Eddy, S. R. & Durbin, R. (1997)** Pfam: a comprehensive database of protein domain families based on seed alignments. *Proteins* **28**, 405-420
- Spratt, B. G. (1975)** Distinct penicillin binding proteins involved in the division, elongation, and shape of *Escherichia coli* K12. *Proc Natl Acad Sci USA* **72**, 2999-3003
- Stamm, O. A. (1963)** Zur Reaktion von Reaktivfarbstoffen mit Cellulose. 2. Natur der Bindung. *Helvetica Chimica Acta* **46**, 3008-3019
- Stewart, E. J., Madden, R., Paul, G. & Taddei, F. (2005)** Aging and death in an organism that reproduces by morphologically symmetric division. *PLoS Biol* **3**, e45
- Stohl, E. A., Lenz, J. D., Dillard, J. P. & Seifert, H. S. (2016)** The gonococcal NlpD protein facilitates cell separation by activating peptidoglycan cleavage by AmiC. *J Bacteriol* **198**, 615-622
- Strobel, W., Möll, A., Kiekebusch, D., Klein, K. E. & Thanbichler, M. (2014)** Function and localization dynamics of bifunctional penicillin-binding proteins in *Caulobacter crescentus*. *J Bacteriol* **196**, 1627-1639
- Sturgis, J. N. (2001)** Organisation and evolution of the *tol-pal* gene cluster. *J Mol Microbiol Biotechnol* **3**, 113-122
- Suginaka, H., Blumberg, P. M. & Strominger, J. L. (1972)** Multiple penicillin-binding components in *Bacillus subtilis*, *Bacillus cereus*, *Staphylococcus aureus*, and *Escherichia coli*. *J Biol Chem* **247**, 5279-5288
- Sycuro, L. K., Pincus, Z., Gutierrez, K. D., Biboy, J., Stern, C. A., Vollmer, W. & Salama, N. R. (2010)** Peptidoglycan crosslinking promotes *Helicobacter pylori*'s helical shape and stomach colonization. *Cell* **141**, 822-833
- Sycuro, L. K., Wyckoff, T. J., Biboy, J., Born, P., Pincus, Z., Vollmer, W. & Salama, N. R. (2012)** Multiple peptidoglycan modification networks modulate *Helicobacter pylori*'s cell shape, motility, and colonization potential. *PLoS Pathog* **8**, e1002603
- Terrak, M., Ghosh, T. K., van Heijenoort, J., Van Beeumen, J., Lampilas, M., Aszodi, J., Ayala, J. A., Ghuysen, J. M. & Nguyen-Disteche, M. (1999)** The catalytic, glycosyl transferase and acyl transferase modules of the cell wall peptidoglycan-polymerizing penicillin-binding protein 1b of *Escherichia coli*. *Mol Microbiol* **34**, 350-364
- Tipper, D. J. & Strominger, J. L. (1965)** Mechanism of action of penicillins: a proposal based on their structural similarity to acyl-D-alanyl-D-alanine. *Proc Natl Acad Sci USA* **54**, 1133-1141
- Tsang, P. H., Li, G., Brun, Y. V., Freund, L. B. & Tang, J. X. (2006)** Adhesion of single bacterial cells in the micronewton range. *Proc Natl Acad Sci USA* **103**, 5764-5768
- Typas, A., Banzhaf, M., van den Berg van Saparoea, B., Verheul, J., Biboy, J., Nichols, R. J., Zietek, M., Beilharz, K., Kannenberg, K., von Rechenberg, M., Breukink, E., den Blaauwen, T., Gross, C. A. & Vollmer, W. (2010)** Regulation of peptidoglycan synthesis by outer-membrane proteins. *Cell* **143**, 1097-1109
- Typas, A., Banzhaf, M., Gross, C. A. & Vollmer, W. (2012)** From the regulation of peptidoglycan synthesis to bacterial growth and morphology. *Nat Rev Microbiol* **10**, 123-136

- Uehara, T. & Park, J. T. (2007)** An anhydro-N-acetylmuramyl-L-alanine amidase with broad specificity tethered to the outer membrane of *Escherichia coli*. *J Bacteriol* **189**, 5634-5641
- Uehara, T., Dinh, T. & Bernhardt, T. G. (2009)** LytM-domain factors are required for daughter cell separation and rapid ampicillin-induced lysis in *Escherichia coli*. *J Bacteriol* **191**, 5094-5107
- Uehara, T., Parzych, K. R., Dinh, T. & Bernhardt, T. G. (2010)** Daughter cell separation is controlled by cytokinetic ring-activated cell wall hydrolysis. *EMBO J* **29**, 1412-1422
- van den Ent, F., Amos, L. A. & Lowe, J. (2001)** Prokaryotic origin of the actin cytoskeleton. *Nature* **413**, 39-44
- van den Ent, F., Leaver, M., Bendezu, F., Errington, J., de Boer, P. & Lowe, J. (2006)** Dimeric structure of the cell shape protein MreC and its functional implications. *Mol Microbiol* **62**, 1631-1642
- van der Ploeg, R., Verheul, J., Vischer, N. O., Alexeeva, S., Hoogendoorn, E., Postma, M., Banzhaf, M., Vollmer, W. & den Blaauwen, T. (2013)** Colocalization and interaction between elongasome and divisome during a preparative cell division phase in *Escherichia coli*. *Mol Microbiol* **87**, 1074-1087
- van Heijenoort, J. (2001)** Formation of the glycan chains in the synthesis of bacterial peptidoglycan. *Glycobiology* **11**, 25R-36R
- van Teeffelen, S., Wang, S. Y., Furchtgott, L., Huang, K. C., Wingreen, N. S., Shaevitz, J. W. & Gitai, Z. (2011)** The bacterial actin MreB rotates, and rotation depends on cell-wall assembly. *Proc Natl Acad Sci USA* **108**, 15822-15827
- Vazquez-Laslop, N., Lee, H., Hu, R. & Neyfakh, A. A. (2001)** Molecular sieve mechanism of selective release of cytoplasmic proteins by osmotically shocked *Escherichia coli*. *J Bacteriol* **183**, 2399-2404
- Vollmer, W., von Rechenberg, M. & Holtje, J. V. (1999)** Demonstration of molecular interactions between the murein polymerase PBP1B, the lytic transglycosylase MltA, and the scaffolding protein MipA of *Escherichia coli*. *J Biol Chem* **274**, 6726-6734
- Vollmer, W. & Bertsche, U. (2008)** Murein (peptidoglycan) structure, architecture and biosynthesis in *Escherichia coli*. *Biochim Biophys Acta* **1778**, 1714-1734
- Vollmer, W., Joris, B., Charlier, P. & Foster, S. (2008)** Bacterial peptidoglycan (murein) hydrolases. *FEMS Microbiol Rev* **32**, 259-286
- von Olshausen, P., Soufo, N. J. D., Wicker, K., Heintzmann, R., Graumann, P. L. & Rohrbach, A. (2013)** Superresolution imaging of dynamic MreB filaments in *B. subtilis*—A multiple-motor-driven transport? *Biophysical Journal* **105**, 1171-1181
- Wagner, J. K. & Brun, Y. V. (2007)** Out on a limb: how the *Caulobacter* stalk can boost the study of bacterial cell shape. *Mol Microbiol* **64**, 28-33
- Wali, T. M., Hudson, G. R., Danald, D. A. & Weiner, R. M. (1980)** Timing of swarmer cell-cycle morphogenesis and macromolecular-synthesis by *Hyphomicrobium neptunium* in synchronous culture. *J Bacteriol* **144**, 406-412
- Ward, J. B. & Perkins, H. R. (1973)** The direction of glycan synthesis in a bacterial peptidoglycan. *Biochem J* **135**, 721-728
- Weiner, R. M. & Blackman, M. A. (1973)** Inhibition of deoxyribonucleic acid synthesis and bud formation by nalidixic acid in *Hyphomicrobium neptunium*. *J Bacteriol* **116**, 1398-1404
- Weiss, D. S., Chen, J. C., Ghigo, J. M., Boyd, D. & Beckwith, J. (1999)** Localization of FtsI (PBP3) to the septal ring requires its membrane anchor, the Z ring, FtsA, FtsQ, and FtsL. *J Bacteriol* **181**, 508-520
- Weiss, D. S. (2015)** Last but not least: new insights into how FtsN triggers constriction during *Escherichia coli* cell division. *Mol Microbiol* **95**, 903-909
- Whittenbury, R. & Dow, C. S. (1977)** Morphogenesis and differentiation in *Rhodospirillum rubrum* and other budding and prosthecate bacteria. *Bacteriol Rev* **41**, 754-808
- Wiles, T. J., Norton, J. P., Russell, C. W., Dalley, B. K., Fischer, K. F. & Mulvey, M. A. (2013)** Combining quantitative genetic footprinting and trait enrichment analysis to identify fitness determinants of a bacterial pathogen. *PLoS Genet* **9**, e1003716

- Yahashiri, A., Jorgenson, M. A. & Weiss, D. S. (2015)** Bacterial SPOR domains are recruited to septal peptidoglycan by binding to glycan strands that lack stem peptides. *Proc Natl Acad Sci USA* **112**, 11347-11352
- Yakhnina, A. A. & Gitai, Z. (2013)** Diverse functions for six glycosyltransferases in *Caulobacter crescentus* cell wall assembly. *J Bacteriol* **195**, 4527-4535
- Yakhnina, A. A., McManus, H. R. & Bernhardt, T. G. (2015)** The cell wall amidase AmiB is essential for *Pseudomonas aeruginosa* cell division, drug resistance and viability. *Mol Microbiol* **97**, 957-973
- Yang, D. C., Peters, N. T., Parzych, K. R., Uehara, T., Markovski, M. & Bernhardt, T. G. (2011)** An ATP-binding cassette transporter-like complex governs cell-wall hydrolysis at the bacterial cytokinetic ring. *Proc Natl Acad Sci USA* **108**, E1052-1060
- Yang, D. C., Tan, K., Joachimiak, A. & Bernhardt, T. G. (2012)** A conformational switch controls cell wall-remodelling enzymes required for bacterial cell division. *Mol Microbiol* **85**, 768-781
- Yang, X., Lyu, Z., Miguel, A., McQuillen, R., Huang, K. C. & Xiao, J. (2017)** GTPase activity-coupled treadmilling of the bacterial tubulin FtsZ organizes septal cell wall synthesis. *Science* **355**, 744-747
- Yeh, Y. C., Comolli, L. R., Downing, K. H., Shapiro, L. & McAdams, H. H. (2010)** The caulobacter Tol-Pal complex is essential for outer membrane integrity and the positioning of a polar localization factor. *J Bacteriol* **192**, 4847-4858
- Zhou, R., Chen, S. & Recsei, P. (1988)** A dye release assay for determination of lysostaphin activity. *Anal Biochem* **171**, 141-144
- Zielińska, A., Billini, M., Möll, A., Kremer, K., Briegel, A., Izquierdo Martinez, A., Jensen, G. J. & Thanbichler, M. (2017)** LytM factors affect the recruitment of autolysins to the cell division site in *Caulobacter crescentus*. *Mol Microbiol* **106**, 419-438
- Zimmer, J. (2013)** Analyse der Zellteilung in *Hyphomonas neptunium*. *Bachelor thesis* Philipps-Universität Marburg, Germany

## Acknowledgements

First, I would like to thank my thesis advisor Prof. Dr. Martin Thanbichler for the opportunity to work in his group on such a fascinating organism. Thanks for your positive thinking in all situations, exchange of ideas and discussions.

I would also like to thank my IMPRS thesis advisory committee and my thesis committee: Prof. Dr. Peter Graumann, Prof. Dr. Torsten Waldminghaus, and Prof. Dr. Anke Becker. Additional thanks goes to Prof. Dr. Peter Graumann in his role as my second supervisor.

A very big thank you goes to all members of the Thanbichler lab for creating such a wonderful and productive working atmosphere. You were always helpful, supportive and took your time for discussions (sometimes non-scientific ones). It was great how we stood together after the fire affected our lab work. We tried to take the problems and concerns with humor and made the best out of it.

Thank you Tanja for being such a wonderful and assertive secretary. Your good mood and funny stories made every working day amusing.

Julia, I want to thank you for being the best and nicest technician I can imagine. You deserve it to be our true lab manager since you know everything about the lab and its equipment. Furthermore, for the amusing lunch times we spent together in our kitchen and the many laughter we shared.

Emöke, you supervised me from the first moment I entered the Thanbichler lab as an intern back at the MPI, during my Master thesis and even at the beginning of my own PhD project. You helped me getting started, shared your knowledge and were always helpful when I needed advice. Thank you so much for everything!

I had the opportunity to supervise two Bachelor students during my PhD. Jannik Harberding was a very pleasant and motivated student, who was always helpful. He never avoided the general lab duties and succeeded with his project.

I am thankful that I could work together with former members of the Thanbichler lab, namely Alex, Dani, Wollé, Sabrina and Oliver. Thanks for the pleasant time we had together.

Mein letzter und größter Dank geht an meine Freunde und meine Familie, besonders an meine Eltern. Ihr habt mir alles ermöglicht, mich immer unterstützt und mir stets freie Wahl in meinen eigenen Entscheidungen gelassen.



---

## Curriculum Vitae

### Personal data:

Name: Sabine Rosskopf  
Date/place of birth: 06.04.1989, Offenbach am Main

### Education and professional experience:

- 06/2015 – 10/2018 PhD student at the Philipps-Universität Marburg,  
Prokaryotic Cell Biology group (Prof. Dr. M. Thanbichler)
- 11/2014 – 03/2015 Internship at the Centre for Bacterial Cell Biology  
Bacterial Biochemistry, laboratory of Prof. Dr. Waldemar Vollmer,  
Newcastle University, Newcastle upon Tyne, UK  
Research project: "Regulation of PG synthesis during cell division"
- 10/2012 – 09/2014 Philipps-Universität Marburg, Germany  
Master studies "Molecular and Cellular Biology"  
Master thesis at the Max-Planck-Institute for Terrestrial Microbiology,  
Prokaryotic Cell Biology, laboratory of Prof. Dr. Martin Thanbichler:  
"Analysis of peptidoglycan biosynthesis in *Hyphomonas neptunium*"
- 10/2009 – 09/2012 Goethe Universität, Frankfurt am Main, Germany  
Bachelor studies "Biological Sciences"  
Bachelor thesis at the Institute of Molecular Biological Science,  
Molecular Microbiology, laboratory of Prof. Dr. Volker Müller  
"Cloning, production and characterization of electron-transfer  
proteins in *Acetobacterium woodii*"
- 09/2006 – 06/2009 Abitur (Higher Education Entrance Qualification),  
Claus-von-Stauffenberg-Schule, Rodgau, Germany

## Einverständniserklärung

Ich versichere, dass ich meine Dissertation:

**„Regulation of peptidoglycan biosynthesis in *Hyphomonas neptunium*“**

selbstständig, ohne unerlaubte Hilfe angefertigt und mich dabei keiner anderen als der von mir ausdrücklich bezeichneten Quellen und Hilfen bedient habe. Die Dissertation wurde in der jetzigen oder einer ähnlichen Form noch bei keiner anderen Hochschule eingereicht und hat noch keinen sonstigen Prüfungszwecken gedient.

Marburg, den .....

.....

Sabine Rosskopf